YEAR-END TECHNICAL REPORT
May 18, 2012 to August 17, 2013

Rapid Deployment of Engineered Solutions for Environmental Problems at Hanford

Date submitted:

August 17, 2013

Principal Investigator:

Leonel E. Lagos, Ph.D., PMP®

FIU Applied Research Center Collaborators:

Leonel E. Lagos, Ph.D., PMP® (Project Manager)
Yelena Katsenovich, Ph.D.
Ravi Gudavalli, Ph.D.
Claudia Cardona, M.S., DOE Fellow
Vishal Musaramthota, Ph.D. candidate
Paola Sepulveda, MS candidate, DOE Fellow
Robert Lapierre, B.S., DOE Fellow
Valentina Padilla, B.S., DOE Fellow

PNNL Collaborator:

Dawn Wellman, Ph.D.

Submitted to:
U.S. Department of Energy
Office of Environmental Management
Under Grant No. DE-EM0000598

FIU | Applied Research Center
FLORIDA INTERNATIONAL UNIVERSITY

Addendum:

This document represents one (1) of five (5) reports that comprise the Year End Reports for the period of May 18, 2012 to July 17, 2013 prepared by the Applied Research Center at Florida International University for the U.S. Department of Energy Office of Environmental Management (DOE-EM) under Cooperative Agreement No. DE-EM0000598.

The planned period of performance for FIU Year 3 under the Cooperative Agreement was May 18, 2012 to May 17, 2013. However, two no-cost extensions have been executed by DOE-EM. The first no-cost extension was received from DOE on 05/17/13 to extend the end of the period of performance for a period of two months (until 07/17/13). Another two months no-cost extension was received from DOE on 07/10/13 to extend the end of the period of performance to 9/16/13. The activities described in this report are for the FIU Year 3 period of performance from May 18, 2012 to August 17, 2013.

The complete set of FIU's Year End Reports for this reporting period includes the following documents:

1. Chemical Process Alternatives for Radioactive Waste
   Document number: FIU-ARC-2013-800000393-04b-213
2. Rapid Deployment of Engineered Solutions for Environmental Problems at Hanford
   Document number: FIU-ARC-2013-800000438-04b-217
3. Remediation and Treatment Technology Development and Support
   Document number: FIU-ARC-2013-800000439-04b-219
4. Waste and D&D Engineering and Technology Development
   Document number: FIU-ARC-2013-800000440-04b-216
5. DOE-FIU Science & Technology Workforce Development Initiative
   Document number: FIU-ARC-2013-800000394-04b-072

Each document will be submitted to OSTI separately under the respective project title and document number as shown above.

DISCLAIMER

This report was prepared as an account of work sponsored by an agency of the United States government. Neither the United States government nor any agency thereof, nor any of their employees, nor any of its contractors, subcontractors, nor their employees makes any warranty, express or implied, or assumes any legal liability or responsibility for the accuracy, completeness, or usefulness of any information, apparatus, product, or process disclosed, or represents that its use would not infringe upon privately owned rights. Reference herein to any specific commercial product, process, or service by trade name, trademark, manufacturer, or otherwise does not necessarily constitute or imply its endorsement, recommendation, or favoring by the United States government or any other agency thereof. The views and opinions of authors expressed herein do not necessarily state or reflect those of the United States government or any agency thereof.

Table of Contents

List of Figures

List of Tables

EXECUTIVE SUMMARY

The reprocessing of irradiated fuel at Hanford's 200 Area to obtain plutonium for atomic weapons has left about 202,703 kg of legacy uranium contamination in the vadose zone (VZ). This uranium is a potential source for groundwater contamination and a risk to receptors through water uptake from contaminated wells or discharges to surface water. Uranium is present in the VZ sediment at concentrations ranging from medium to high as uranyl-carbonates (liebigite and rutherfordine), co-precipitated with carbonates and hydrous silicates and Na-boltwoodite. However, uranium is also present in mobile forms such as aqueous and adsorbed phases (Szecsody et al. 2012). The investigation under task 1.1 of this project targets uranium (U) contamination in the VZ of the 200 Area that may affect potential discharges to the Columbia River via groundwater migration. Injection of reactive gases such as NH_3 is an innovative technology that targets U contamination in the VZ to reduce the potential for radionuclides mobility in the subsurface. This technology is aiming to decrease the mobility of the uranium species without water addition causing undesired downward contaminants migration. The vadose zone at Hanford is composed of sediments quartz, plagioclase, orthoclase, muscovite, biotite, hornblende, illite, calcite, montmorillonite, chlorite, kaolinite, smectite and kaolinite (Szecsody et al. 2012). All of these mineral phases may undergo dissolution reactions in the hyperalkaline conditions. The 200 Area sediment composition analyses showed that silica is the predominant element, found in much higher quantities than any other constituent, followed by aluminum. The injection of ammonia gas in the vadose zone causes the formation of NH_4OH, followed by a subsequent increase in pH. The alkaline conditions can greatly enhance the solubility rates of most Si-containing minerals. In addition, the dissolution of silicate containing quartz and feldspars at high pH is promoted in the presence of different cations, like Na^+, which accelerates the release of Si from their structure (Blum and Stillings 1995). The following decrease in pH as the system stabilizes and reaches natural equilibrium will cause uranium co-precipitation during the recrystallization of minerals. There is a need for a better understanding of the effects of Si, Al, Ca and bicarbonate ions on the U co-precipitation process. This research was conducted to improve our understanding of possible mechanisms of U removal from the solution mixture by replicating the pore water composition found at the Hanford Site. This study involved a series of batch experiments to evaluate the effect of various concentration ratios of silicon and aluminum, in the presence of several bicarbonate and Ca concentrations. For simplicity, the early stage of experiments was limited to only four elements: Si, Al, U, and inorganic C in the form of bicarbonate. This year, the focus shifted to the addition of Ca and Mg into the solution mixture.

Research under task 1.2 investigated the potential role of bicarbonate, which is an integral complexing ligand for U (VI) and a major ion in groundwater compositions. More specifically, the objectives were to: (1) Investigate the effect of bicarbonate on the microbial dissolution of the autunite mineral and U (VI) adsorption by *Arthrobacter* G968; (2) Make a comparison between G975 and G968 strains; (3) Inspect bacterial surface in the presence of bicarbonate and uranium in the solution using atomic-force microscopy (AFM); (4) Determine the difference between microbial dissolution of synthetic autunite versus natural autunite.

ACRONYMS

AFM	atomic force microscope
µg/L	parts per billion (ppb)
atm	atmosphere
BEC	backscatter electron capture
bgs	below ground surface
C	Celsius
CFU	colony forming units
DIW	deionized water
DOE	U.S. Department of Energy
EDS	energy-dispersive spectroscopy
HEPES	Na-2-(2-hydroxyethyl)-1-piperazine ethanesulfonic acid sodium salt hydrate
HMDS	hexamethyldisilazane
ICP-OES	inductively coupled plasma optical emission spectroscopy
KPA	Kinetic Phosphorescence Analyzer
mg/L	parts per million (ppm)
NH_3	ammonia gas
SEM	scanning electron microscopy
SGW	synthetic groundwater
SMCC	subsurface microbial culture collection
SPW	synthetic pore water
VZ	vadose zone
XRD	X-ray diffraction

INTRODUCTION

The Hanford Site was the first nuclear production facility in the world serving a key role in the nation's defense for over 40 years. Located on the Columbia Plateau of southeastern Washington State, the site was originally built in 1943 as part of the Manhattan Project for the production of plutonium for the first atomic weapons and remained in production throughout the cold war. Now, the Hanford Site has become the second largest cleanup project in the United States. Large amounts of radioactive waste containing uranium, among other constituents, were generated to obtain plutonium and other useful radioisotopes by the fabrication of natural and slightly enriched uranium into fuel elements for nuclear reactors in Hanford's 300 Area, and the reprocessing of irradiated fuel in Hanford's 200 Area. This waste was stored in underground storage tanks (USTs). There are 149 underground single-shell tanks (SST) used to store radioactive mixed waste; sixty-seven of these SSTs have been classified as assumed/confirmed leakers. Uranium from these tanks leaked into the surrounding soil, specifically at the 200 East and 200 West Areas, producing waste streams depositing into the subsurface. These leakages into the vadose zone represent a potential future source for groundwater contamination and risk to possible receptors through water uptake from contaminated wells or discharge to surface water. Despite extensive remediation efforts initiated in the early 1990s, uranium groundwater plumes identified in multiple locations around the site have persisted for many years. A key element of the overall Hanford cleanup program is the protection of water resources from contaminated groundwater resulting from operations at the Hanford Site.

Due to the complex chemistry of uranium, a predictive understanding of its mobility in the subsurface is limited. In neutral or basic pH conditions, uranium undergoes hydrolysis in aqueous solution and can readily complex with a wide variety of ligands (Grenthe et al. 1992, Langmuir 1997). These complexation reactions often result in the formation of mobile aqueous species or precipitation of U-bearing minerals. Environmental factors, such as pore water ion composition have a tremendous effect on both uranium and its mineral phases. Additional research is necessary to understand the effect of these factors on the behavior of U(VI) in groundwater and sediments.

Pore water in the vadose zone is under the influence of carbon dioxide partial pressures that exceed atmospheric ($P_{CO2}=10^{-3.5}$atm) (Karberg et al. 2005). In the oxidized carbonate-buffered environments, the behavior of uranium is greatly affected by the presence of carbonates since U(VI) tends to form complexes with carbonate ions. Their mobility in aquifers under circumneutral pH conditions is explained by the formation of highly soluble and stable ternary uranyl-carbonato complexes, $UO_2CO_3^0$, $UO_2(CO_3)_2^{2-}$ and $UO_2(CO_3)_3^{4-}$ (Langmuir 1978, Guillaumont et al. 2003). At a high pH between 9 and 11, most actinides reside as negatively charged hydroxide or carbonate (CO_3^{2-}) species, such as $(UO_2)_2(OH)_5^-$ and the tris(carbonato) complex $UO_2(CO_3)_3^{4-}$. The structure of the latter mononuclear complex exhibits the hexagonal uranyl coordination where the three carbonate ligands in a bidentate coordination are located in the equatorial plane of the uranyl moiety (Schlosser 2010) (Figure 1). The surfaces of most solids are negatively charged at these pH values and are unlikely to adsorb ionic species, which

can explain why the formation of negatively-charged, highly soluble U(VI)-carbonate species typically suppress U(VI) sorption in circumneutral and alkaline conditions (Um et al. 2007).

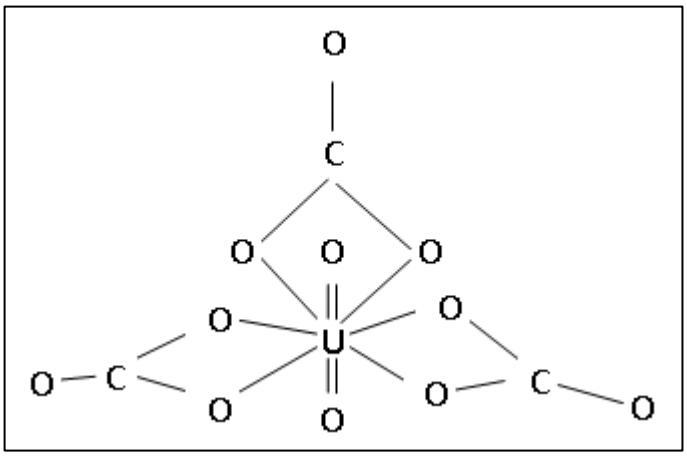

Figure 1. The structures of uranyl carbonate complexes $[UO_2(CO_3)_3]^{4-}$.

Calcium (Ca) is a common aqueous cation found in equilibrium with calcite in porewater and groundwater at many sites contaminated with U. Ca can complex with U(VI) in bicarbonate solutions to form calcium-uranyl-carbonate species such as $Ca_2UO_2(CO_3)_3^{o}(aq)$ and $CaUO_2(CO_3)_3^{2-}$. Their large complexation constants (Guillaumont et al. 2003) suggest that Ca can affect U(VI) fate and transport due to the formation of soluble and stable calcium-uranyl-carbonate complexes in aqueous solution. Generally, high soil pH and increased potential for complexation with carbonate and calcium indicate a high possibility for U(VI) mobility in the soil. Zachara et al. (2007) reported relatively high mobility of U in groundwater based on the low distribution coefficient K_d ranging from 0.2 to 4 L/kg and averaging 0.8 L/kg at natural conditions of pH 8. So, remediation of U(VI) using ammonia gas injection can decrease U(VI) mobility without water addition, which would avoid the downward contaminant migration (Szecsody et al., 2012).

During FIU Year 3, FIU ARC conducted two subtasks under Task 1 of this project: Task 1.1, Sequestering Uranium at the Hanford 200 Area by In-Situ Subsurface pH Manipulation Using Ammonia (NH_3) Gas Injection, and Task 1.2, Investigation on Microbial-Meta-Autunite Interaction: the Effects of Bicarbonate and Calcium Ions. Results on the effect of bicarbonate and Ca ions on the biosorption of uranium by G968 cells, previously summarized in the progress report, are included in the Task 1.2 Results and Discussion section.

Based on the results of this investigation, the following three publications have been published in peer-reviewed journals in 2012-2013:

- Gudavalli, R., Katsenovich, Y. Wellman, D., Idarraga, M., Lagos, L., Tansel, B. "Comparison of the Kinetic Rate Law Parameters for the Dissolution of Natural and Synthetic Autunite in the Presence of Aqueous Bicarbonate Ions." Chemical Geology, volume 351, August 2013, p. 299-309.

- Carvajal, D., Katsenovich, Y., Lagos, L. “The Effects of Aqueous Bicarbonate and Calcium Ions on Uranium Biosorption by *Arthrobacter* G975 Strain." Chemical Geology, volumes 330–331, November 2012, p. 51–59.
- Katsenovich, Y, Carvajal, D., Guduru, R., Lagos, L., Li, C. (2013): Assessment of the Resistance to Uranium (VI) Exposure by *Arthrobacter* sp. Isolated from Hanford Site Soil, Geomicrobiology Journal, 30:2, 120-130.

Project results were presented at the Waste Management 2013 conference. DOE Fellow Paola Sepulveda gave an oral presentation and results were published in a proceeding paper. Two students, Claudia Cordona and Robert Lapierre, presented posters in the students’ poster competition session.

Ravi Gudavalli completed his Ph.D. from this research. Claudia Cardona has been accepted to the Ph.D. program. Three students are currently performing master level research based on this research.

TASK 1.1 SEQUESTERING URANIUM AT THE 200 AREA BY IN SITU SUBSURFACE PH MANIPULATION USING NH_3 GAS

TASK 1.1 BACKGROUND

Deep vadose zone contamination of radionuclides requires in-situ stabilization to convert aqueous U-carbonates mobile phases to lower solubility precipitates that are stable in the natural environment. In Ca-rich carbonate-bearing subsurface environments, U(VI) is present primarily as calcium-uranyl-carbonate species such as $Ca_2UO_2(CO_3)_3^o(aq)$ and $CaUO_2(CO_3)_3^{2-}$ (Kalmykov and Choppin 2000). Wellman et al. (2006) investigated the U(VI) stabilization through polyphosphate injection in the groundwater with the formation of the synthetic autunite mineral. However, polyphosphate treatment via injection of amendment solutions can cause undesirable U and co-contaminants downward migration. Injection of reactive gases such as NH_3 to create alkaline conditions in the vadose zone is an innovative technology used to decrease uranium mobility in the subsurface contaminated with radionuclides. Previous short-term laboratory evaluation showed a decrease in U mobility after ammonia gas injection in the low water content sediments (Szecsody et al. 2010a). This task investigates the mechanisms and effectiveness of NH_3 gas injection on the removal of uranium (VI) in the synthetic groundwater solutions mimicking 200-Area pore water. Evidently, an understanding of the role of pore water constituencies on the removal of U(VI) is needed to predict the mineralogical changes and the formation of precipitates that would be created in the treated vadose zone soil. Ammonia is a highly soluble gas and its injection in the vadose zone causes the formation of NH_4OH followed by a subsequent increase in pH. Partitioning of NH_3 gas into liquid and the aqueous speciation reactions for NH_3 are written as (Szecsody et al. 2012):

$$NH_3\ (g) \leftrightarrow NH3\ (aq) \quad K_h = 6.58 * 10^{-4}\ N \qquad [1]$$

$$NH_3\ (aq) + H^+ \leftrightarrow NH_4^+,\ pK = 9.4 \qquad [2]$$

Where K_h is the dimensionless Henry's Law partition coefficient and pK is the negative logarithm of the dissociation constant.

Partitioning of 5% NH_3 and 95% N_2 gas mixture to liquid can increase pH up to 11.8 (3.1 mol/L NH_3 (aq)). Changes in pore-water pH can profoundly affect the dominant soil minerals such as calcite, feldspar, iron oxides, and quartz present in the Hanford Site vadose zone. Chou and Wollast (1984) previously illustrated that the rate of feldspar dissolution has been shown to increase by two to three orders of magnitude with an increase in pH from 8 to 12 at 23ºC. These dissolution reactions potentially induce the release of cations such as Si, Al, Ca, Mg, Na, and K from soil minerals to pore water. The subsequent decrease in pH to natural conditions would lead to precipitation of magnesium silicate and aluminosilicates that could possibly sequester contaminants in a process called co-precipitation (Szecsody et al. 2010a/b). Another possible mechanism that can decrease U mobility is coating by a low solubility, non-U precipitate, such as cancrinite (Bickmore et al. 2001), sodalite, hydrobiotite, brucite, and goethite, as observed in water-saturated systems (Qafoku et al. 2004, Qafoku and Icenhower 2008). This technology has significant uncertainty at the 200 Area vadose zone specific conditions and requires additional testing in the laboratory to understand the effect of various

environmental factors on the formation and precipitation of uranium-bearing mineral phases. Particularly, what requires clarification is the role of major pore water constituents and the time on the formation of precipitates after the NH_3 injection. This task also involves the characterization studies of silica-aluminum-carbonate precipitates created after NH_3 gas injection.

Silicate Chemistry and Its Interaction with Metals

Silicates are one of the most abundant natural compounds found in the earth's crust that can occur in amorphous and crystalline forms. The presence of dissolved silica in the aqueous solution can result in the complexation of metals and radionuclides and the precipitation of silica-containing phases. The basic chemistry of silica is complex due to the variety of species in aqueous solution that depend on pH, ionic strength and temperature. Forms of silica that are soluble and stable for a long period in solutions with low dissolved concentrations of less than 0.007-0.1% are monomeric [H_4SiO_4(aq), $H_3SiO_4^-$, and $H_2SiO_4^{2-}$]. However, when the solution is supersaturated with respect to amorphous silica, extensive polymerization occurs due to the condensation of the silanol Si-OH group. It proceeds with formation of polymeric species that includes dimeric, trimer, tetrameric, and hexameric species and amorphous silica precipitates (Busey and Mesmer 1977, Choppin et al. 1994, Felmy et al. 2001).

Having two valence electrons, oxygen can form an additional bond with another metal atom or a bond with a second silicon atom. This possibility leads to polymerization reactions by the linkage of SiO_4^- tetrahedra through Si – O – Si (siloxane) bonds. Therefore, silica can be regarded as a polymer of silicic acid, consisting of interlinked SiO_4 tetrahedral:

$$\text{Si-OH} + \text{Si-OH} \leftrightarrow H_2O + \text{- Si – O – Si -} \qquad [3]$$

These reactions produce the hydrated silica polymers with molecular weights of up to ~100,000 consisting of dense spherical particles less than about 50A in diameter. The highly polymerized species form colloidal particles with sizes larger than 50A.

Electrolyte concentrations greater than 1.00M in the pH range of 7 to 10 lead to coagulation of silicic acid with the particles linked together by acid-base inter-particle bonding rather than by Si-O-Si bonds. The observed increase in polymerization with increased ionic strength >1M is due to the closer approach of the particles through Si-O..M^{n+}…O-Si bond formation (Choppin et al. 1994).

The polymerization of $Si(OH)_4$ involves some aspects of the theory of nucleation. Nucleation implies the formation of critical clusters called nuclei after which crystal growth occurs spontaneously (Stumm and Morgan 1996). It is well known that thermodynamically nucleation or seeding of some chemical reactions can result in a lowering of the activation energy associated with the reaction (Mattus et al. 2002). The presence of impurities such as alkali metal ions and aluminum, which precipitates because of reacting with silicate, can accelerate polymerization reactions and the rate of silica precipitation (Iler 1979, Gallup 1997). In alkaline conditions, Al(III) is present in the tetrahedral $Al(OH)_4^-$ form. The reaction between the uncharged silica species $Si(OH)_4$ and the charged alumina species $Al(OH)_4^-$ will form aluminosilicate chains joined by shared oxygen atoms as follows:

$$\begin{array}{ccccc} OH & & OH & & OH \quad OH \\ | & & | & & | \quad | \\ HO-Si-OH & + & HO-Al-OH & \rightarrow & HO-Si-O-Al-OH + H_2O \\ | & & | & & | \quad | \\ OH & & OH & & OH \quad OH \end{array}$$

The silica species $Si(OH)_4$ is considered to be the important species for this reaction given that the other two Si species, $SiO(OH)_3^-$ or $SiO_2(OH)_2^{2-}$, are negatively charged, preventing them from coming into contact with $Al(OH)_4^-$.

Aluminate ions make important modifications to the silica surface. Geometrically, the aluminate ion $Al(OH)_4^-$ is depicted by a regular tetrahedron, with the aluminum atom located in the center and the hydroxide ions forming the corner points (Gasteiger et al. 1992). Polymerization reactions of aluminum and silicon tetrahedra create an alumino-silicate anion; excess silica must be present at the reaction (Iler 1979). The alumina- modified colloidal silica are negatively charged in a wide range of pH down to 3, compared to pure silica, which is negatively charged by the adsorption of hydroxyl ions above pH 7 but loses the charge in acidic solutions. Iler (1969) observed that surface aluminosilicate complexes reduce silica solubility and dissolution. Previous estimates of the reduction in silica dissolution rate by aluminum range from three to five orders of magnitude (Hurd 1973, Iler 1975). Negatively charged colloidal silica particles can also flocculate through reaction with alkaline earth metals. Divalent ions, such as Ca, interact with silica surfaces through displacement of a proton such as:

$$>SiOH + Ca^{2+} \rightarrow \quad >SiCaO^{+} \qquad [4]$$

This can cause Si aggregation reactions to convert it to calcium silicate nuclei. As nucleus mass continues to grow, it results in flocculation and precipitation reactions (Dove and Nix 1997).

TASK 1.1 OBJECTIVES

The objective of this task is to assess the role of major pore water constituents and time on the formation of precipitates after NH_3 injection to the vadose zone of the Hanford Site 200 Area. This task examined the effect of concentration ratios of silicon and aluminum, in the presence of various bicarbonate concentrations and divalent ions such as calcium and magnesium, on the co-precipitation process of U(VI) under conditions imitating the pore water composition of the 200 Area vadose zone. These experiments can identify the geochemical changes that would occur with U(VI) after NH_3 gas treatment of contaminated vadose zone sediments. Manipulations with porewater constituencies can simulate the conditions occurring in the subsurface and explain changes in the removal of elements through co-precipitation with silica and calcium carbonate. Parallel studies have focused on the detailed characterization of the uranium-bearing precipitates created after ammonia gas injection. Mineralogical and morphological characterization experiments of U(VI)-bearing precipitates were carried out by means of scanning electron microscope energy-dispersive spectroscopy (SEM-EDS) and Micro-Raman spectroscopy (MRS). Future studies will examine the mineralogy of precipitates via XRD analysis and evaluate uranium precipitates for the solubility over the pH range of 6 to

11 in the presence of bicarbonate/carbonate ions to evaluate the migration potential of radionuclides that still reside in the vadose zone.

TASK 1.1 MATERIALS AND METHODS

The natural groundwater is $CaCO_3$ and $MgCO_3$ saturated. The composition of pore water has been previously characterized in terms of concentrations of major cations (Ca^{2+}, Na^{+}, K^{+}, Mg^{2+}, Fe^{2+}, Al^{3+}, and Si^{4+}), anions (F^{-}, Cl^{-}, NO_2^{-}, Br^{-}, SO_4^{-}, and NO_3^{-}), and pH (Szecsody et al. 2012). The average concentrations of ions and uranium for different sediment layers were presented in the FY2010 report. For the initial experiments, the complicated pore water composition was simplified to have only four components in the test solutions: uranium, silica, aluminum, and bicarbonate. In this year's experiments, calcium was added to the pore water composition in concentrations of 5 mM and 10 mM. In addition to Ca, a set of experiments was conducted using 5 mM of magnesium. The concentration of U(VI) in the synthetic solution mixture was 2 ppm.

Past observations showed that the concentration of Al released during the dissolution from soil by 1 mol L^{-1} NaOH is relatively small, resulting in 5.1 mM of Al in the soil solution (Qafoku et al. 2003). Because of increasing soil pH, the concentration of Si in pore water was observed to be as high as 10 g L^{-1} (Szecsody 2010b). For these reasons, the tests were carried out with varied Si concentrations such as 5 mM, 50 mM, 100 mM, 150 mM, 200 mM, and 250 mM to study different Si:Al molar ratios. The experiments were conducted by limiting Si concentration to a maximum of 250 mM (7.0 g L^{-1}) since the increase in Si concentration up to 10g L^{-1} doesn't show a difference on the results of U(VI) removal. The Al concentration was kept constant at 5 mM. This report provides the complete range of data for U(VI) removal in the presence of 5 mM of Al across all Si and HCO_3 concentrations tested in addition to Ca and Mg that area commonly present in the pore water composition. To evaluate the effect of divalent ions on the U(VI) removal, two sets of experiments were conducted: one that included 5 mM of Ca ions and 5 mM of Mg in the water composition and one that included only 5 mM or 10mM of Ca ions.

Sample Preparation Procedures

Sample preparation procedures at different molar ratios of Si:Al included mixing calculated volumes of the silicate and aluminum stock solutions. This mixture was combined with a measured volume of the appropriate bicarbonate stock solution (unless no bicarbonate was used). The pH of the resulting solution was adjusted to 8.0 by titration with concentrated nitric acid; deionized water (DIW) was then added to each test solution; so, each test solution had a total final volume of 50 mL. The pH value of 8.0 was observed in the natural conditions of the pore water at the Hanford Site 200 Area vadose zone (Szecsody et al. 2012). NH_3 gas (5% NH_3 in 95% N_2) was injected into each solution through 20 µm pores of a metal gas sparger (Mott Corporation) until the pH of the solution reached a value of approximately 11 (Figure 2).

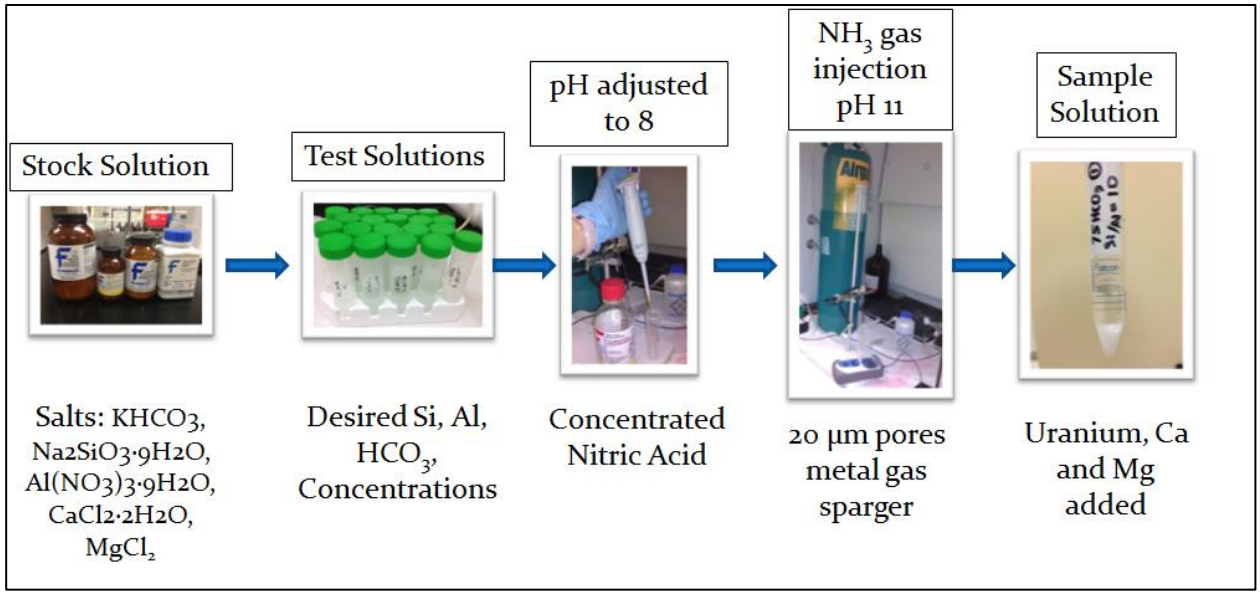

Figure 2. Experimental procedure for sample preparations to evaluate the removal of elements from the solution mixture.

Duplicate samples of 5 mL were extracted from NH_3 augmented aluminum-silicate-carbonate test solutions to 15-mL individual polyethylene tubes. The addition of Ca and Mg was achieved by rapid mixing of the test solution in the 15-mL tube with 20 µL of $CaCl_2$ and $MgCl_2$ stock solutions (Table 2). The resulting mixture was then spiked with uranium to yield an overall concentration within a solution matrix of 2 ppm. Control samples were prepared in DIW amended with U(VI) at a concentration of 2 ppm U(VI) to test for U(VI) losses from the solutions due to sorption to the tube walls and caps. All control and experimental tubes were vortexed and then kept in an incubator/shaker at 100 rpm and at a temperature of 25°C. After two days, the solutions were centrifuged for 15 minutes at 4000 rpm and supernatant was extracted and analyzed for U(VI), Si, Al, Ca, Mg, and inorganic carbon (IC). Preliminary experiments showed that the removal efficiency of U(VI) reached a plateau after two days of agitation on the shaker.

For this year, all sets were amended with 5 mM of Al and were prepared with U (VI) concentrations of 2 ppm; the new varying parameters were the concentration of Ca and Mg. There were six sets with 5 mM of Ca only and six sets for with 5 mM of Ca and 5 mM of Mg in the solution mixture. There were also six sets with 10 mM of Ca only (Table 1). Each set had six different test solutions prepared in duplicate with a different Si:Al molar ratio, for a total of 216 sample solutions, excluding control samples. Table 1 presents a description of the experimental matrix based on the Si/Al molar ratios for the solution mixtures amended with 5 mM of Al and Si concentrations of 5 mM, 50 mM, 100 mM, 150 mM, 200 mM, and 250 mM. Si/Al molar ratios for 5 mM of Al used for all tests and the same Si concentrations match to 1, 10, 20, 30, 40, and 50 respectively.

Table 1. Experimental Matrix

Batch number	HCO_3, mM	Initial Si concentrations in the solution mixture, mM					
1	0	5	50	100	150	200	250
2	2.9	5	50	100	150	200	250
3	25	5	50	100	150	200	250
4	50	5	50	100	150	200	250
5	75	5	50	100	150	200	250
6	100	5	50	100	150	200	250
Batch number	**HCO_3, mM**	**Si:Al molar ratio (Ca=5mM, Ca=5mM and Mg=5mM, Ca=10mM)**					
1	0	1	10	20	30	40	50
2	2.9	1	10	20	30	40	50
3	25	1	10	20	30	40	50
4	50	1	10	20	30	40	50
5	75	1	10	20	30	40	50
6	100	1	10	20	30	40	50

Stock solutions of Al (50 mM), Si (422 mM), and HCO_3^- (400 mM) were first prepared in deionized water (DIW) from the salts $Al(NO_3)_3 \cdot 9H_2O$, $Na_2SiO_3 \cdot 9H_20$, and $KHCO_3$, respectively (Table 2); the final volume of these solutions was 50 mL in order to reach the desired concentrations. The 100-ppm stock solution of uranyl nitrate dissolved in DIW was prepared from uranyl nitrate hexahydrate 1000-ppm stock (Fisher Scientific).

Table 2. Stock Solutions Used to Prepare Various Si/Al Molar Ratios

Stock Solution	Salt Used	Molecular Weight of Salt (g/mol)	Stock Solution Concentration (mM)	Amount to prepare 50 mL (g)
Bicarbonate	$KHCO_3$	100.114	400.00	2.002
Metasilicate	$Na_2SiO_3 \cdot 9H_2O$	284.196	422.24	5.998
Aluminum	$Al(NO_3)_3 \cdot 9H_2O$	375.129	50.00	0.938
Calcium	$CaCl_2 \cdot 2H_2O$	147.01	1250.0	9.188
Magnesium	$H_{12}O_6MgCl_2$	203.3	1250.0	12.706

Analytical Procedures

Samples of the supernatant from each vial were analyzed to determine the remaining U(VI) concentration using a Kinetic Phosphorescence Analyzer KPA-11 (Chemcheck Instruments, Richland, WA) instrument, and the concentrations of Al, Si, and Ca were analyzed in each solution, using inductively coupled plasma-optical emission spectroscopy (ICP-OES) (PerkinElmer). In addition, the accuracy of the initial Al, Si, and Ca stock solutions, prepared by weight, were tested with ICP-OES. For better precision, the concentration of elements was analyzed using different dilutions factors.

For analysis with the KPA, an aliquot was extracted from the supernatant of each test sample and diluted with 1% nitric acid between 5 to 100 times. For analysis with the ICP-OES, an

aliquot extracted from the supernatant of each test sample was diluted in conical polypropylene tubes between 100 to 200 times with DIW. The total organic carbon (TOC) of the supernatant solutions was analyzed using a Shimadzu TOC analyzer with an autosampler (TOC-V CSH). Each analysis was repeated until the standard deviation was less than 3%.

Speciation Modeling

Geochemical equilibrium modeling was performed by means of Visual MINTEQ (v. 3.0, maintained by J.Gustafsson at KTH, Sweden, available at http://www.lwr.kth.se/English/OurSoftware/vminteq/) updated with the Nuclear Energy Agency's thermodynamic database for uranium (Guillaumont et al. 2003) and calcium-uranyl-carbonate complexes from Dong and Brooks (2006) to identify the predominant uranium species. The software was used to calculate uranium speciation in the presence of Si, Al, HCO_3, Ca and Mg ions and 2 ppm of U and predict phases that might precipitate. The example on Table 3 presents elemental concentration data for utilized silica, bicarbonate, 5 mM Al and 10 mM Ca/ 5 mM Ca and 5 mM Mg ion concentrations with the addition of 2 ppm of U(VI). All concentrations were entered for the model calculations to give the most important species with respect to uranium complexation. The temperature was set to 25^{o}C and the CO_2 pressure was fixed to atmospheric pressure (3.9 x10^{-4} bar) as the samples were in contact with air during the experiment.

Table 4 presents elemental concentration data considered for speciation. The resulting charge difference in the anion and cation balance was no more than 10-16%.

Table 3. Stock Solutions used for Speciation Modeling of 2 ppm U

Stock Solution	Concentration (mM)					
	HCO_3 + *Si + 5 Al + 10 Ca + 2ppm U					
$KHCO_3$	0	2.9	25	50	75	100
$Al(NO_3)_3$	5	5	5	5	5	5
$Na_2SiO_3 \cdot 9H_2O$	*5-250	*5-250	*5-250	*5-250	*5-250	*5-250
$CaCl_2 \cdot H_2O$	10 (**5)	10(**5)	10(**5)	10(**5)	10(**5)	10(**5)
$H_{12}O_6MgCl_2$	**5	**5	**5	**5	**5	**5
$UO_2(NO_3)_2 \cdot 6H_2O$	0.0084	0.0084	0.0084	0.0084	0.0084	0.0084
HNO_3	Calculated from difference between anions and cations					
5% NH_3+ 95% N_2 GAS	Adjusted in each case to reach pH~11					

*Si concentrations: 5, 50, 100, 150, 200, and 250 mM
**Stock solution concentrations for the set using a mixture of 5 mM of Ca and 5 mM of Mg

Table 4. Input Components for Speciation Modeling with 5 mM of Ca and 5 mM of Mg Ions

Minteq components input	Concentration (mM)								
	H^{+1}	*Si (H_4SiO_4)	Al^{+3}	CO_3^{-2}	K^{+1}	Cl^{-1}	Ca^{+2}/Mg^{+2}	**Na^{+1}	U(VI) (UO_3)
* Si + 0mMHCO_3 + 5mM Al + 5 mM Ca + 5mMMg+2ppm U	0	*5-250	5	0	0	20	5/5	*10-500	0.084
*Si + 3 mM HCO_3 + 5mM Al + 5 mM Ca +5 mM Mg+ 2ppm U	3	*5-250	5	3	3	20	5/5	*10-500	0.084
*Si +25 mM HCO_3 + 5 mM Al + 5 mM Ca +5 mM Mg + 2ppm U	25	*5-250	5	25	25	20	5/5	*10-500	0.084
*Si +50 mM HCO_3 + 5 mM Al + 5 mM Ca +5 mM Mg + 2ppm U	50	*5-250	5	50	50	20	5/5	*10-500	0.084
*Si +75 mM HCO_3 + 5 mM Al + 5 mM Ca +5 mM Mg + 2ppm U	75	*5-250	5	75	75	20	5/5	*10-500	0.084
*Si+100 mM HCO_3 + 5 mM Al + 5 mM Ca +5 mM Mg + 2ppm U	100	*5-250	5	100	100	20	5/5	*10-500	0.084
NH_3 GAS	Adjusted in each case to reach pH~ 11								

*Si concentrations: 5, 50, 100, 150, 200, and 250 mM **Na^{+1}: 10,100, 200, 300, 400, and 500 mM

Methods for Mineralogical and Morphological Characterization of U(VI)-bearing Precipitates

In the experiments done in parallel to the supernatant analysis, the dried uranium-bearing precipitates were characterized using a collection of analytical techniques. Precipitates that contain metal silicate are difficult to characterize because they are not homogeneous in composition. Due to the complex heterogeneous nature of the samples produced, no one technique will provide enough information to characterize the product. The morphology and the development of crystalline structures were monitored by means of SEM/EDS and Raman spectroscopy methods. The analytical results in conjunction with following thermodynamic speciation modeling of the experimental systems and XRD analysis would allow for identification of the U(VI) solid phases present, and the morphological features of the amorphous precipitates. The sample preparation process for these precipitate characterization studies closely mirror those of the uranium removal experiments; the difference being that the latter concerns the liquid supernatant while the former deals with the dried solid precipitate. In each of the three (3) batches prepared, four similar sets of samples were prepared in a combination with calcium and high and low concentrations of bicarbonate. The stock solutions were prepared and mixed at the appropriate concentrations. Nitric acid was used to lower the pH to 8. Ammonia gas (NH_3) was sparged to increase pH to 11 to complete the sample preparation. Lastly, the uranium addition completed the sample solutions formulations. The samples were left in solution for a span of time ranging from 2 days to 4 months to assess the effect of time in solution. The concentrations of the elements used in preparation of the solutions are presented in Table 5.

Table 5 Stock Solutions for SEM/EDS Analysis of 200 ppm U

Stock Solution	Stock Solution Concentration (mM)	Concentration (mM)			
		100 mM Si + 3 mM HCO_3 + 5 mM Al + 200 ppm U	3 mM HCO_3 +100 mM Si + 5 mM Al + 200 ppm U	100 mM Si + 50 mM HCO_3 + 5 mM Al + 200 ppm U	50 mM HCO_3 +100 mM Si + 5 mM Al + 200 ppm U
$KHCO_3$	400	3	3	50	50
$Al(NO_3)_3$	422.24	5	5	5	5
Na_2SiO_3 - $9H_2O$	50	100	100	100	100
$UO_2(NO_3)_2$ - $6H_2O$	4.2	0.84	0.84	0.84	0.84
$CaCl_2 \cdot 2H_2O$	147.01	5	0	5	0
HNO_3	-	Used to adjust pH of the mixture solution to 8			
5%NH_3 + 95%N_2 GAS	-	adjusted in each case to reach pH 11			

Three batches were prepared for these experiments. The first batch (batch 1) consisted of identical multiples of each sample prepared for analysis over a range of times in a sacrificial mode. It differed from other batches in that no samples were prepared with calcium and all solutions were centrifuged to separate the phases. The first sample was taken for precipitate drying after 2 days (set #1) of being prepared and kept in the "mother solution" on the shaker. The next samples were taken after being kept in the "mother solution" for 2 weeks (set #2), 1 month (set #3), 1.5 months (set #4), 2 months (set #5), 3 months (set #6) and 4 months (set #7). All the samples were placed on the shaker at 100 rpm and kept at a constant temperature of 25^{o}C for future analysis. At the assigned time intervals, the sample precipitate from each set was extracted by centrifugation followed by decantation of the supernatant. Solid products were dried over time at 25°C in anticipation of impending analysis. A total of 14 sample test tubes of 5 mL were prepared. Supernatant solutions were kept for U(VI) analysis via kinetic phosphorescence analyzer (KPA).

The second batch (batch 2) of samples for the study characterization of uranium-containing precipitates over time was prepared with and without calcium in the solution composition. Samples for these sets were not centrifuged prior to drying. This batch used the 4 sample set described in Table 5. The 4 solutions were sub-divided into 5 individual sample solutions which would be used for time studies. The samples were left in the "mother solution" for 2 days (#1), 2 weeks (#2), 1 month (#3), 2 months (#4), and 3 months (#5) before analysis. A total of 20 samples were prepared and placed in the incubator/shaker at 25^{o}C and 100 rpm. At their assigned time, samples were decanted, and the precipitate set aside for drying in preparation for SEM/EDS analysis. Supernatant solutions were again kept for U(VI) analysis via KPA

The third batch (batch 3) differed from its predecessors in that from each of the primary solutions, 5 sample solutions were prepared by withdrawing an aliquot of solution after 2 days (#1), 2 weeks (#2), 1 month (#3), 2 months (#4), and 3 months (#5). Two smaller samples of 15

mL and 5 mL were taken each time from the primary solution and transferred into the separate 15-mL polystyrene tubes. The tubes with 5 mL of sample were centrifuged for 2 min at 2000 rpm, decanted, and the precipitates were then set to dry. The 15-mL tubes were carefully decanted once the sample had settled and the precipitates were then set to dry without preliminary centrifugation. In order to ensure that each extraction was homogeneous, tubes with primary solutions were vortexed before each extraction. The uranium concentration in batch 3 was slighter higher, 238 ppm, in an attempt to increase the uranium atomic percentage present in the sample composition.

Scanning Electron Microscope-Energy Dispersive Spectroscopy

The samples' surface composition was analyzed after precipitate solidification via scanning electron microscopy and energy-dispersive-spectrometry (SEM-EDS). Two instruments were employed for this analysis. The uranium-containing dry precipitate samples were mounted on aluminum stubs with double-sided carbon tape and then coated for 60 seconds with a thin layer of gold to increase conductivity.

For batch 1, the surface composition of gold-coated samples (Pelco SC-7, Auto sputter coater) was analyzed using a JOEL, JSM-6330F SEM SEM-Energy-Dispersive-Spectrometry (SEM-EDS) Noran System Six Model 200 at 15 kV at magnifications of 2000-5000. For batches 2 and 3, electron microscopy was performed using a JEOL-5910-LV with accelerative potentials between 10 kV and 20 kV. For conduction purposes, all samples were gold coated using an SPI-Module Control and Sputter unit. EDS analysis was accomplished using an EDAX Sapphire detector with UTW Window paired with Genesis software. Micrographs were prepared in both secondary electron and backscatter modes with the objective lens aperture 2 at 30 µm diameter and the spot sizes (condenser lens) ranging from 35-40".

Powder X-Ray Diffraction

X-ray diffraction analyses were performed on the dried precipitates at 35 kV and 40 mA via Bruker 5000D XRD instrument. Diffraction patterns were obtained using a copper Cu Kα radiation source (λ=0.154056 nm) with a tungsten filter. The XRD was programmed to run over a 2-theta (2θ) range from 5° to 70° with a 0.02° step size and 3 second counting per step. Selected precipitate samples were carefully ground into a fine powder using a mortar and pestle in anticipation of the analysis. The pulverized sample was packed into the small recess of a plastic sample holder that was designed specifically for the small amount available. Two method blanks, prepared identically to the experimental sample with the exception of the analyte of interest (uranium), were also ground and analyzed.

Micro-Raman Spectroscopy

The RamanMicro 300 microscope (*Perkin-Elmer*) was used to perform Raman spectroscopic analysis. The instrument is equipped with the Olympus Bx51 microscope frame and a 100W halogen lamp and high definition camera. A 785nm laser (250mW output) functions at the excitation source. The system has a minimum spot size of 10µm using the 100x objective lens. The preliminary analysis was done with the 20x objective. The software used for post-analysis

investigation of the resulting spectra was *KnowItAll® Academic Edition*, a free spectroscopic analysis suite by Bio-Rad Laboratories.

TASK 1.1 RESULTS AND DISCUSSIONS

The Effect of Ca and Mg Ions on the Removal of U(VI)

As outlined in the experimental matrix in Table 1, experiments initiated last year to study uranium removal at concentration of 2 ppm from the solution mixture were continued using six Si/Al ratios of 1, 5, 10, 20, 30, 40, and 50 that corresponded to Si concentrations of 5 mM, 50 mM, 100 mM, 150 mM, 200 mM, and 250 mM, respectively. Each experiment was conducted at six bicarbonate concentrations of 0 mM, 2.9 mM, 25 mM, 50 mM, 75 mM, and 100 mM. Two calcium concentrations were used in the experiments: 5 mM and 10 mM. In addition, the U(VI) removal was evaluated for the mixture of 5 mM Ca and 5 mM Mg. Experimental results were assessed based on the percent removal of the elements of interest: U(VI), Si, Al, Ca, Mg and inorganic carbon (IC). **Error! Reference source not found.** - Figure 17 depict the percent removal of these elements in solutions where pH was increased up to 11 as a result of NH_3 gas injection.

The removal of U(VI) involves a phenomenon of Si precipitation following trapping of U by the co-precipitation process (Allard et al. 1999). It is known that dissolved silica polymerizes in Si-rich alkaline solutions (Iler 1979). This process involves nucleation reactions and the formation of amorphous silica particles by polymerization of $Si(OH)_4$. Si sols also precipitate by coagulation of alkali earth carbonates when precipitate is formed by aggregation of colloidal particles. In the absence of a coagulant, silica does not precipitate from the solution at any pH. The additions of divalent ions such as calcium or magnesium are commonly used for coagulation of colloidal silica from water. They flocculate colloidal silica along with other suspended or precipitated matter (Iler 1979).

Figure 3 shows the removal of U(VI) in the solution prepared with 5 mM and 10 mM of Ca. The results indicated that the percentage of U(VI) removal was largely controlled by the Si/Al ratios and calcium concentrations. Together, the percent of U(VI) removal increased as Si/Al ratios and bicarbonate concentrations were increased. The uranium removal varied between 87% - 100% starting at Si/Al ratio 10 for all bicarbonate concentrations tested. The higher Ca concentration correlated with higher U(VI) removal at low Si/Al ratios ranging between 96%-99%. Possible mechanisms responsible for the U(VI) removal include the cumulative effect of nucleation reactions forming calcium carbonate clusters upon mixing $CaCl_2$ and Na_2CO_3 and then uptake of uranyl by precipitating calcium carbonate (Reeder et al. 2000, Reeder et al. 2001). The following deposition of hydrated amorphous silica layers on the precipitated calcium carbonate grains creates silica layers coating the aggregates (Klein and Lynn 1995, Voinescu et al. 2007, Kellermeier et al. 2010). Previous studies on U(VI) trapping in natural Si/Al-rich gels were consistent with a co-precipitation process of U, Si and Al and discussed encapsulation of U(VI) within a silicate polymer (Allard et al. 1999).

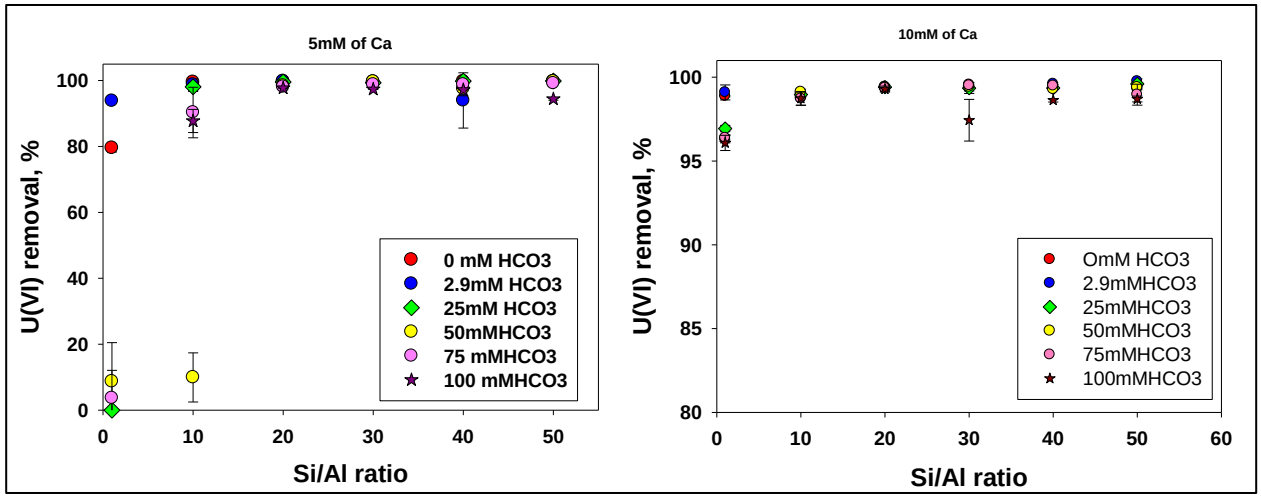

Figure 3. Removal of U(VI) in the solution mixture prepared with 5 mM and 10 mM of Ca.

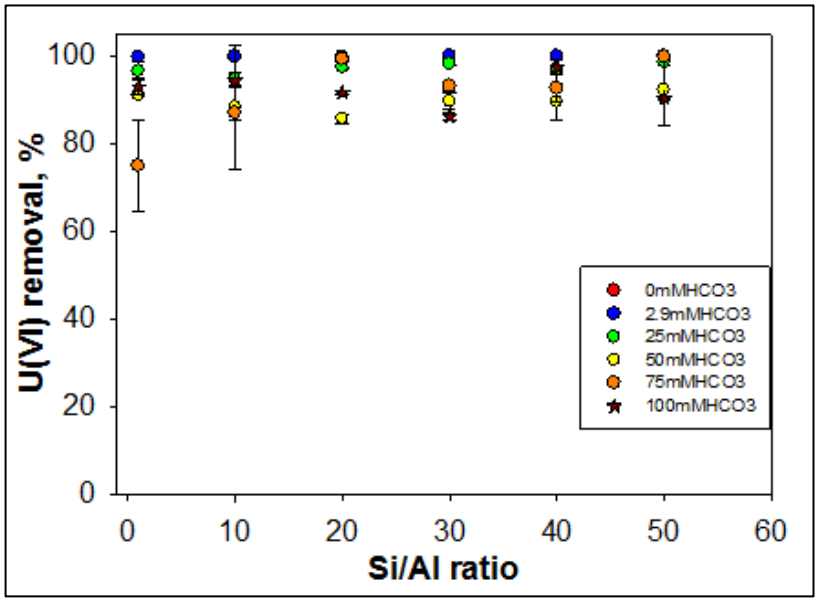

Figure 4. Removal of U(VI) in the solution mixture prepared with 5 mM of Ca and 5 mM of Mg.

Figure 4 shows the removal of U(VI) in the synthetic solution mixtures amended with 5mM of Ca and 5mM of Mg. The results indicate that U(VI) removal is greater as Si/Al ratios increased and remained between 75% and 99% at all Si/Al ratios and bicarbonate concentrations tested.

The low solubility magnesium and calcium carbonates may form from the synthetic solutions amended with bicarbonate, magnesium, calcium and silica at high pH values between 10 and 11. According to Kellermeier et al. (2010), at alkaline pH, precipitation of the amorphous calcium carbonate in Si-rich solutions induces dissociation of bicarbonate and the release of protons, which decreases the pH near the growing carbonate phases:

$$HCO_3^- \leftrightarrow CO_3^{2-} + H^+ \xrightarrow{Ca^{2+}} CaCO_3 \downarrow \quad [5]$$

The release of hydrogen ions reduces the solubility of Si at alkaline pH leading to Si polymerization reactions according to (Iler 1979, Kellermeier et al. 2010):

$$Si-O^- + H^+ \leftrightarrow -SiOH + HO-Si \xrightarrow{-H_2O} Si-O-Si \rightarrow SiO_2 \downarrow \quad [6]$$

Therefore, the decrease in pH caused by the precipitation of carbonate increases the local supersaturation of silicic acid in the surrounding environment of the growing carbonate phases, thus, provoking precipitation of silica (García-Ruiz, et al. 2009).

When a soluble silicate is mixed with solutions containing metals other than the alkali metal group, insoluble amorphous metal silicates along with other elements are precipitated out of solution (Iler 1979). Iler (1975) proposed mechanisms of silica coagulation by calcium ions leading to precipitation of those elements from solution. The adsorption of a calcium ion on the negatively charged silica surface liberates by ion exchange only one hydrogen ion, thus creating one additional negative site on the Si surface (Iler, 1975). This negative site is neutralized by one adsorbed calcium ion that retains a single positive charge.

$$Ca^{2+} + Si <^{OH}_{OH} \rightarrow H^+ + Si <^{OH}_{O-Ca^{2+}} \quad [7]$$

Iler (1975) assumed that a possible mechanism of Si coagulation is through interparticle bonding that involves bridging by positively charged calcium ions and attraction between surfaces bearing a mosaic of positive and negative sites. However, equilibrium modeling indicated that at alkaline conditions solid-phase precipitation of calcium silicate species was not likely. The equilibrium distribution of dissolved aqueous and solid phase species is discussed later in this report.

The removal of silica concentrations in the tested solutions is shown in Figure 5-Figure 7. In bicarbonate-free and 2.9 mM HCO_3 solution mixtures amended with 5 mM of Ca, the percentage of silica removal at Si/Al ratios of 1 and 10 remained between 13% and 40%. At higher Si/Al ratios greater than 10, the percentage of Si removal was found between 89% and 99% for all bicarbonate solution concentrations tested. It is clear that the increase in Ca concentration correlated with higher removal of Si from the solution mixture.

When the Ca concentration was increased up to 10 mM, the percentage of silica removal at Si/Al ratio 1, the lowest ratio investigated in this study, was increased to 93-99%. The precipitates formed after combining all stock solutions are usually not homogeneous in composition. This depends on the degree of Si polymerization and precipitation reactions that occur in the solution mixture. This causes some discrepancies in the results between replicate samples, especially those prepared for low Si/Al ratios.

Figure 7 shows the removal of Si in the presence of 5 mM of Ca and 5 mM of Mg in the tested solutions; it indicates a consistent Si removal between 92% and 100% at all Si/Al ratios and bicarbonate concentrations tested. The percentage of Si removal was noted to decrease at higher concentrations of bicarbonate solutions of 75 mM and 100 mM. This finding is the opposite of the results obtained in the previous tests without Ca when higher bicarbonate concentrations correlated with higher yields in Si and U removals.

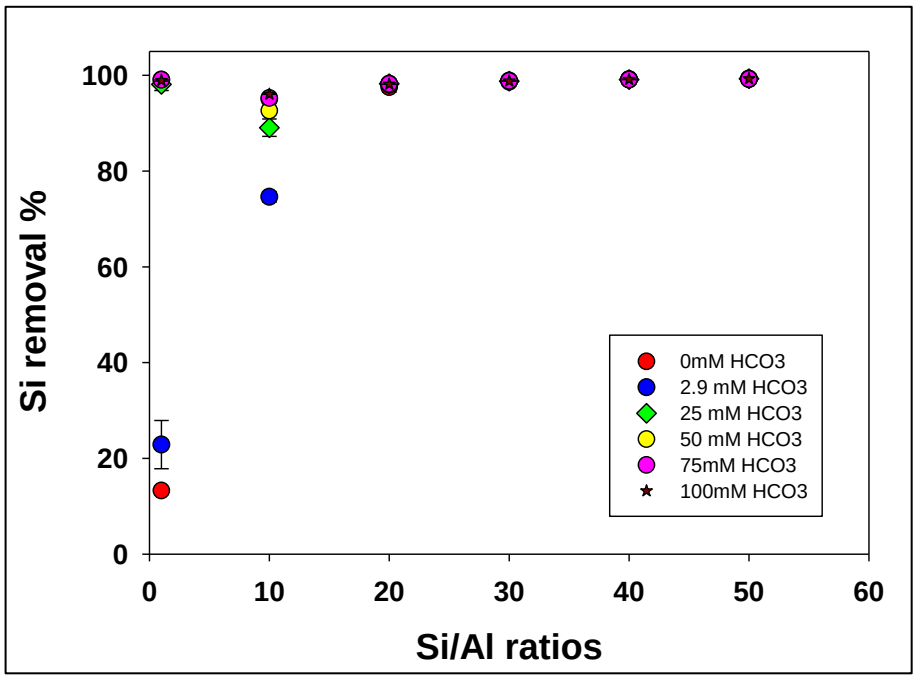

Figure 5. Removal of Si in the solution mixture prepared with 5 mM of Ca.

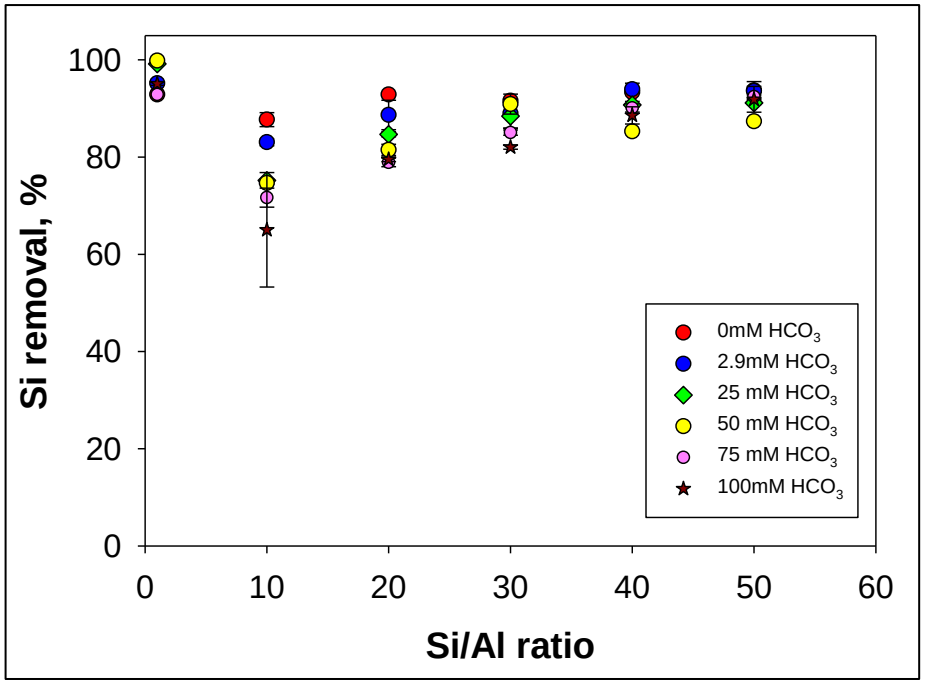

Figure 6. Removal of Si in the solution mixture prepared with 10 mM of Ca.

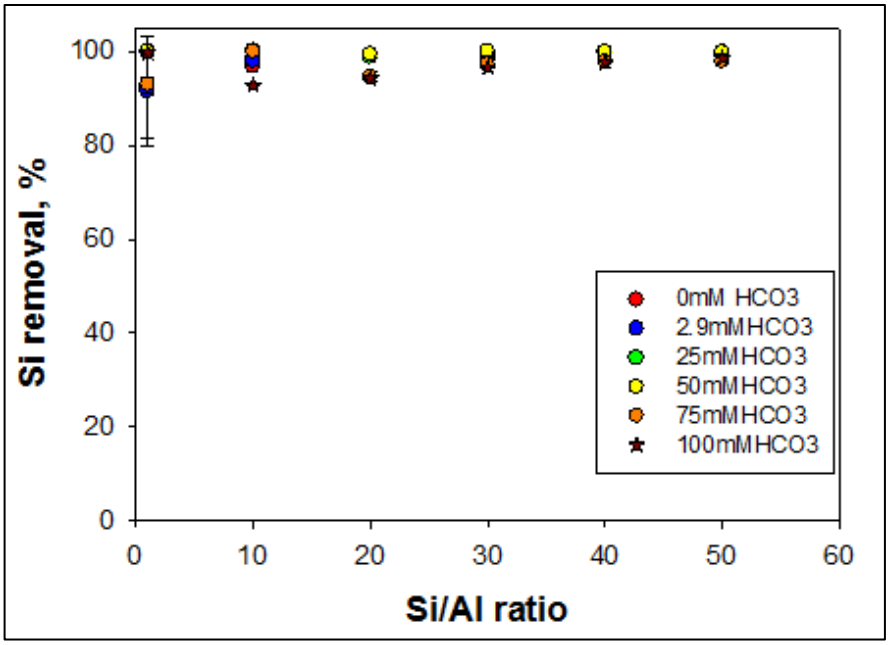

Figure 7. Removal of Si in the solution mixture prepared with 5 mM of Ca and 5 mM of Mg,

In all of the experiments, the removal of Si correlated with the removal of U(VI) from solutions. If the supernatant solutions showed a small decline in Si concentrations, the removal in U(VI) was diminutive or not observed.

Figure 8-Figure 10 shows the removal concentration of aluminum in the tested solutions. As discussed in previous reports, there is an affinity between aluminum and silicon. Monomeric silica reacts with Al^{3+} ions following its precipitation due to a reaction between $Si(OH)_4$ and crystalline $Al(OH)_3$. When the silica concentration is below the solubility of amorphous silica in water, no polymerization occurs except when alumina is added. Iler (1979) proposed that SiO_2 surfaces exposed to solutions containing aluminum formed aluminosilicate surface complexes by reaction with the hypothetical stoichiometry:

$$> SiOH + Al(OH)_3^+ \leftrightarrow \quad > SiOAl(OH)_2 + H^+ \qquad [8]$$

Iler (1979) also showed that low aluminum concentrations gave a significant reduction in solubility of silica gel. The presence of the aluminum results in an entire armored surface coating, which is extensive enough to reverse the net negative Si surface charge to positive (Iler 1973, Dove and Rimstidt 1994).

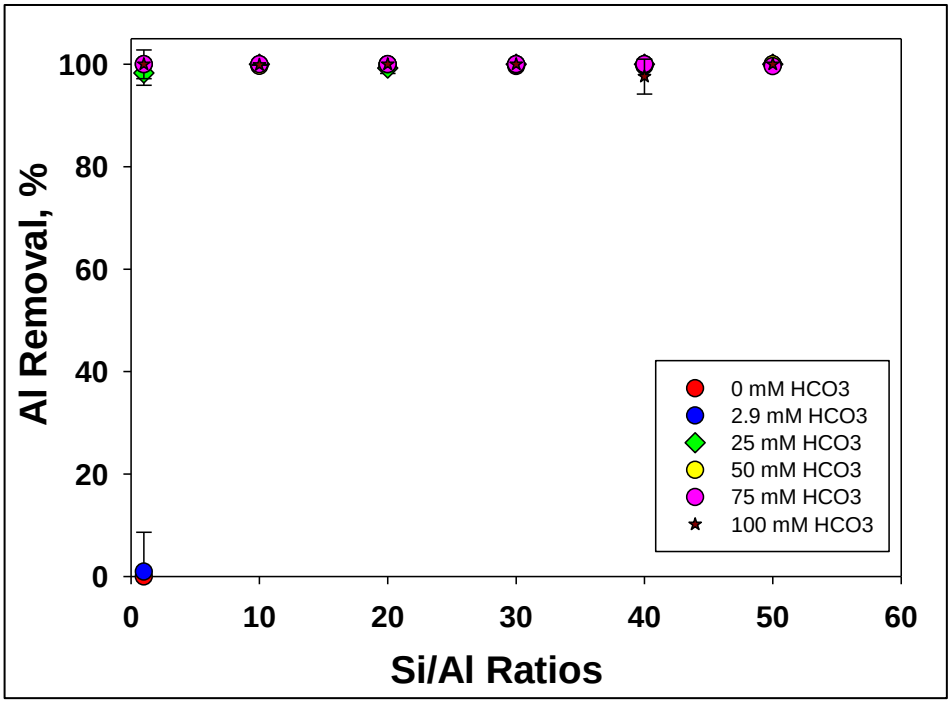

Figure 8. Removal of Al in the solution mixture prepared with 5 mM of Ca.

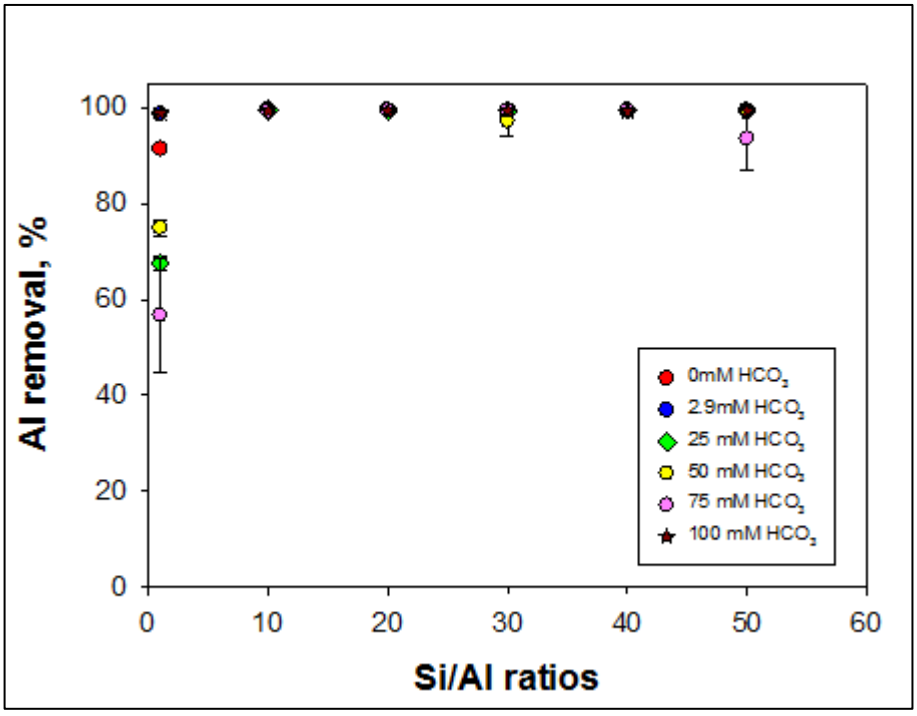

Figure 9. Removal of Al in the solution prepared with 10 mM of Ca.

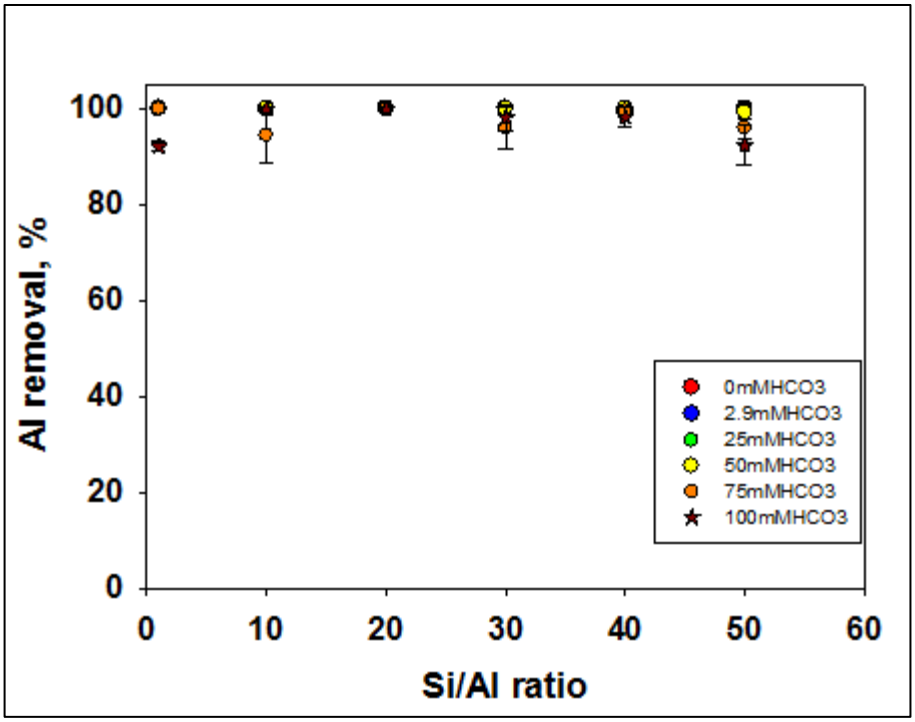

Figure 10. Removal of Al in the solution mixture prepared with 5 mM of Ca and 5 mM of Mg.

Similar to speciation predictions for 5 mM of Ca, the dominant Ca species at initial Ca concentration in the solution of 10 mM at alkaline pH 10-11 are free Ca^{2+} ions, $CaHCO_3^+$, $CaCO_3$ with minor formation of $CaNH_3^{+2}$, $Ca(NH_3)_2^{+2}$ and Ca-U-CO_3. The speciation modeling hasn't predicted the formation of calcium silicate at this elevated pH condition. The removal of Ca^{2+} ion from the solution apparently is due to the precipitation of calcium carbonate. In alkaline conditions (pH 8.5-11), the dissociation of bicarbonate ions results in a local decrease in pH. Silicate species respond to these local pH changes by polymerization reactions resulting in particle aggregation and flocculation (Kellermeier 2011). Higher concentrations of soluble silicates lead to a higher degree of polymerized silica species. The addition of $CaCl_2$ solution to the mixture of Si and $NaCO_3$ also influences silica polymerization reactions and the formation of Si-Al-$CaCO_3$ precipitates, which could retain co-precipitated uranium (as U hydroxide or/and carbonate) within its amorphous structure.

Another possible mechanism of Ca removal is the adsorption of Ca ions on the silica sols surface (Figure 11-Figure 13). The adsorption of a divalent cation on the surface of amorphous silica may increase the development of positive charge sites making a bridge by reacting with two particles at their point of contact. The adsorption of metal ions on the silica surface may also affect the surface properties and, in addition, displace H^+ in the solution (Iler 1975, Dove and Rimstidt 1994):

$$SiOH + Ca^{2+} \rightarrow SiOCa^{+} + H^{+} \quad [9]$$

Kellermeier et al., (2011, 2012) examined the formation of cluster-like species grown when alkaline-earth carbonates and silica are co-precipitated at elevated pH. In their experiments,

silica sols was coagulated by the addition of $CaCl_2$. Analyses of the flocculated material showed that it essentially consisted of amorphous silica (no calcium silicate), with minor amounts of calcium entrapped between the coagulated particles. They ruled out precipitation of calcium-rich silica particles in the samples and expected that the major fraction of the Ca^{2+} ions to be free and available for interaction with carbonate under the experimental conditions. Their conclusions correlate with speciation modeling results conducted for this study. The equilibrium speciation modeling results are discussed later. Results for Mg^{2+} follows a similar pattern as for Ca^{2+} with the total of 80-99% removal for the range of conditions studied.

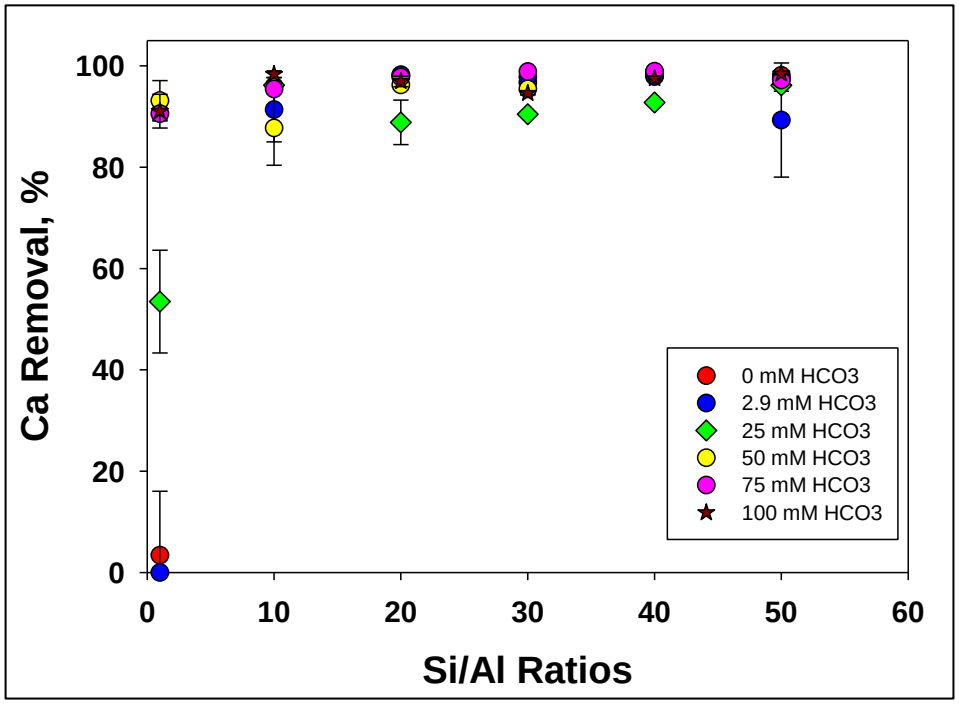

Figure 11. Removal of Ca in the solution mixture prepared with 5 mM of Ca.

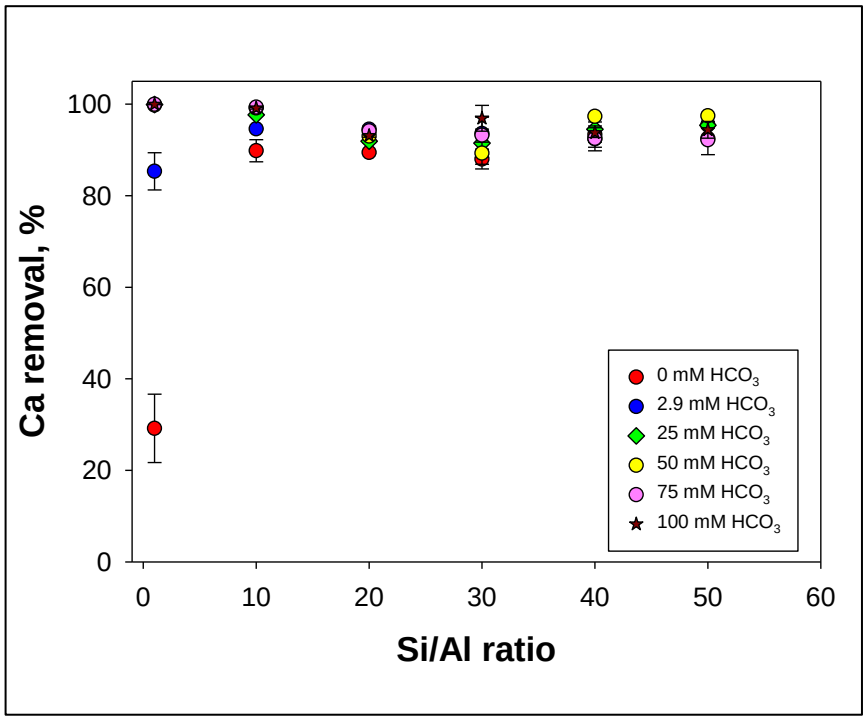

Figure 12. Removal of Ca in the solution mixture prepared with 10 mM of Ca.

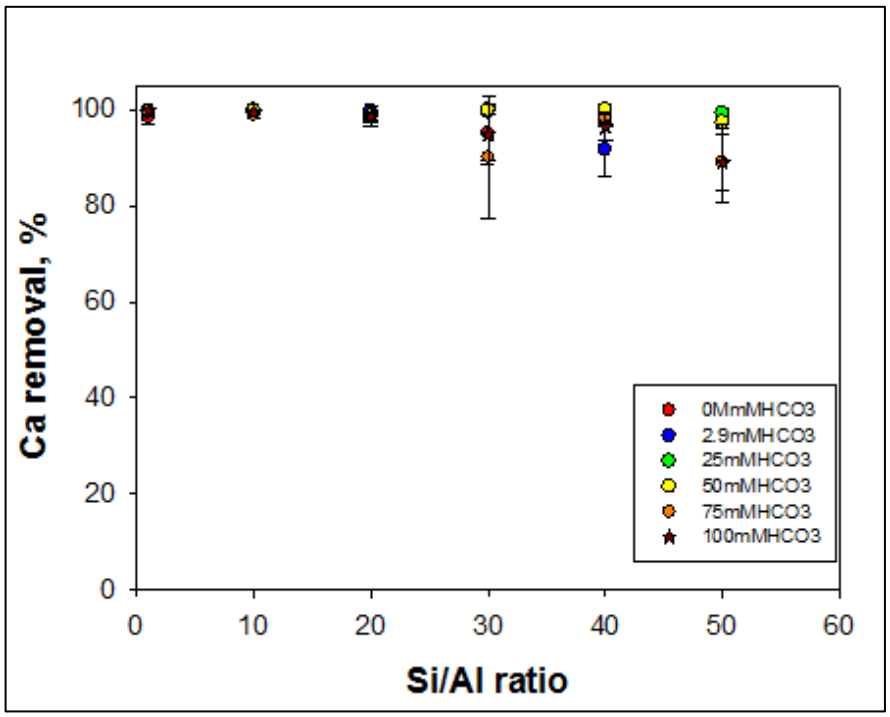

Figure 13. Removal of Ca in the solution mixture prepared with 5 mM of Ca and 5 mM of Mg.

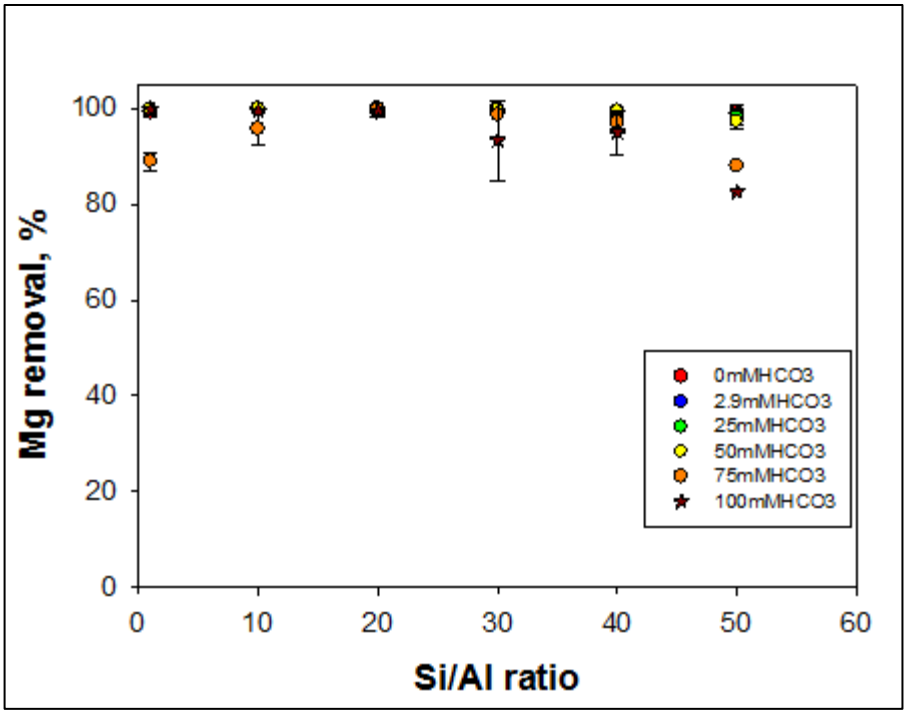

Figure 14. Removal of Mg in the solution mixture prepared with 5 mM of Ca and 5 mM of Mg.

According to the speciation modeling predictions, carbonate at pH 10-11 are mainly distributed between CO_3^{2-}, HCO_3^-, $CaCO_3$, $CaHCO_3^+$ and $NaCO_3^-$ species. From those species, only the precipitation of calcium carbonate can control the removal of inorganic carbon from the aqueous solution. Speciation modeling suggested that the percent of total calcium carbonate species accounts for 19.1-68.1%, 14.1-20.5%, and 8.0-19.0% of the total concentration of bicarbonate present initially in the solution as 3 mM, 25 mM and 50-100 mM range, respectively. However, experimental results showed that the removal of inorganic carbon was much higher and in some instances increased up to 80% for 2.9 mM of HCO_3 (Figure 15-Figure 17). In addition, the removal of inorganic carbon at Si/Al ratios ranging from 30 to 50 was found to be 3-5 times higher than the MINTEQ-predicted percentage for the $CaCO_3$ formation. We hypothesized that the discrepancies between MINTEQ- predicted CO_3^{2-} precipitation as a calcium carbonate and the percent of IC removal obtained in the experiments are due to silica sols coagulation and encapsulation within the silicate polymer that retained the carbonate solids with a coagulated layer of silica gel. It is especially noticeable at higher Si and HCO_3^- concentrations in solution. In previous studies, silica uptake onto calcium carbonate was shown to increase in higher-ionic-strength solutions and higher silica aqueous concentration (Kitano et al. 1979). The reaction continues with carbonate solid phases, most likely via hydroxyl groups, a mechanism that provokes silica flocculation (Garcia-Ruiz 1998). Iler (1979) made an example of this case and reported that lime, Mg-salts and Mg-carbonates adsorbed silica from industrial waste-water streams at low temperatures. So, the precipitation of $CaCO_3$ and its encapsulation within Si sols causes changes in the carbonate system due to the decrease in the calcium carbonate saturation state. Coating by silica may force a shift in the equilibrium with the free ions towards ion-bound states and generation of $CaCO_3$, which precipitates out of solution.

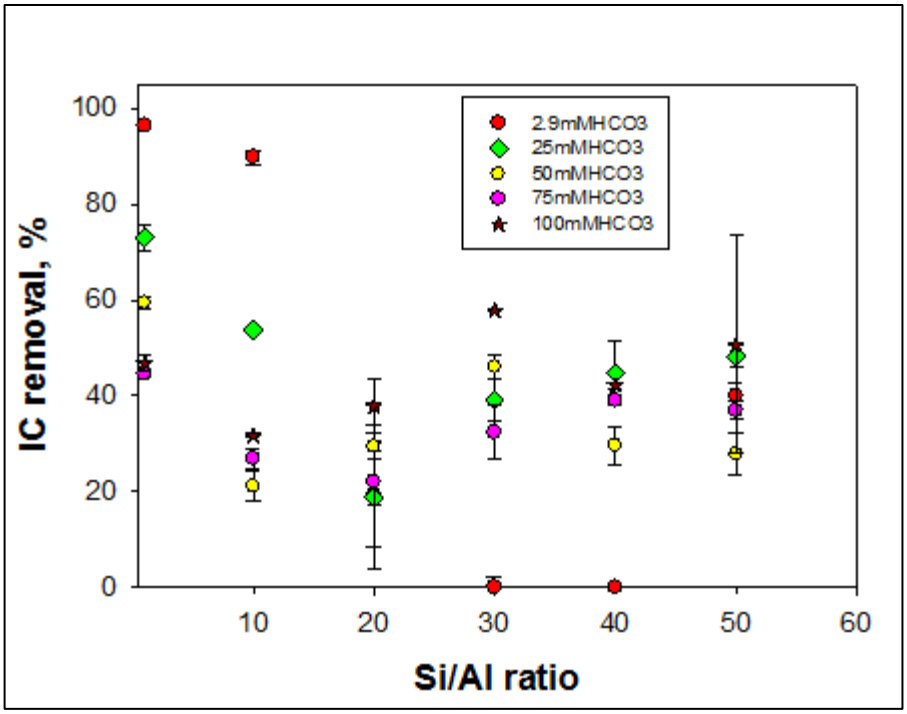

Figure 15. Removal of inorganic carbon from the solution mixture prepared with 5 mM of Ca.

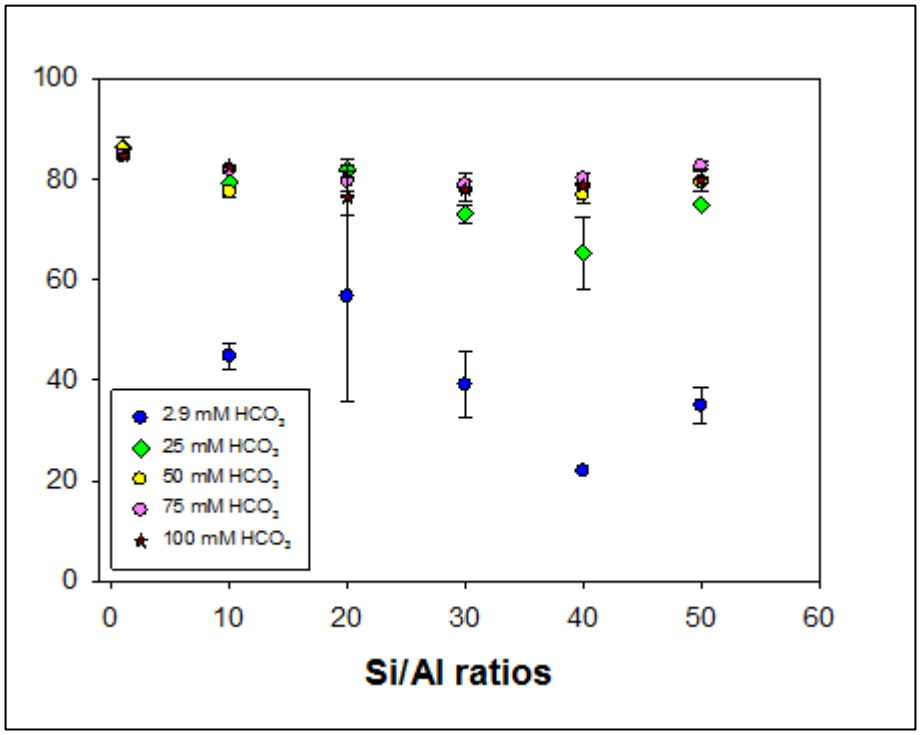

Figure 16. Removal of inorganic carbon from the solution mixture prepared with 10 mM of Ca.

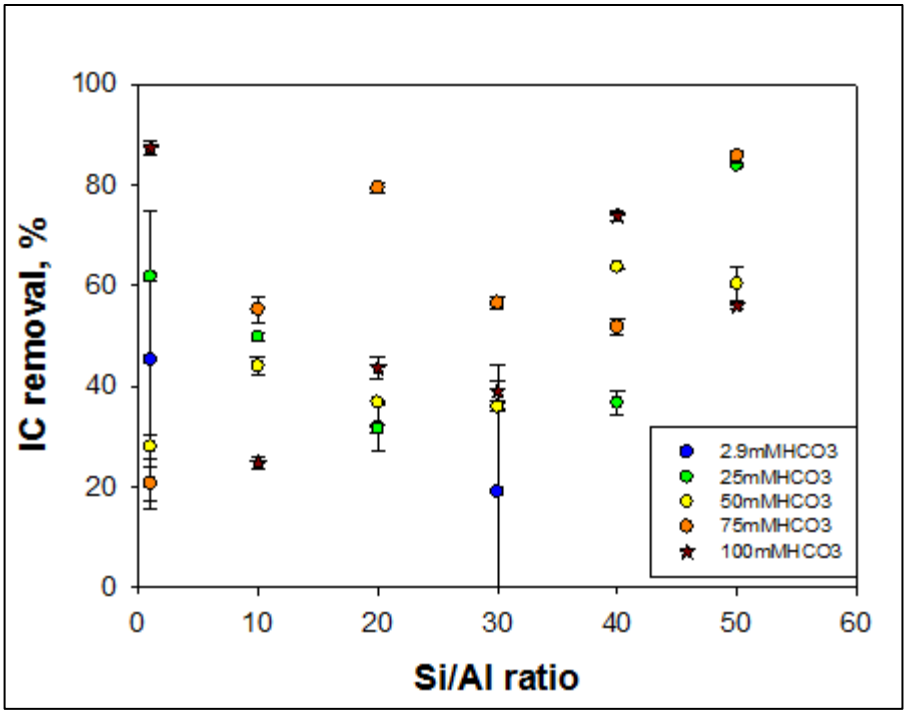

Figure 17. Removal of inorganic carbon from the solution mixture prepared with 5 mM of Ca and 5 mM of Mg.

According to the speciation modeling predictions, at 0 mM HCO_3, U(VI) is present in the solution dominantly as $UO_2(OH)_3^-$. In the solutions amended with bicarbonate, $Ca_2UO_2(CO_3)_3$ and $CaUO_2(CO_3)_3^{-2}$ are the predominant species accounting for 30%- 84% of the total uranium species (Table 6, Table 7).

Saturation indexes showed that potential U-bearing secondary phases as becquereline, gummite, rutherfordine, and schoepite are undersaturated at all conditions tested (Table 8, Table 9). However, speciation modeling predicted the formation of aragonite and calcite in addition to various aluminosilicate and aluminum hydroxide solid phases created out of elements present in the solution. These solid phases can serve as potential nuclei that trigger Si polymerization reactions. This leads to the co-precipitation of U solids (as U hydroxide and/or Ca-U-CO_3) within the amorphous structure of Si-Al-$CaCO_3$ precipitates.

In the presence of magnesium, speciation modeling predicted the formation of magnesium hydroxide, magnesium carbonate, and hydrated magnesium silicate solid phases (sepiolite) along with aragonite and calcite in addition to various aluminosilicate and aluminum hydroxide solid phases (Table 8). Magnesium cations at alkaline pH conditions are available for adsorption on the surface of silica gel leading to coagulation and silica removal from the solution mixture. The formation of solid phases can serve as potential nuclei that prompt Si polymerization reactions. In addition, under alkaline conditions, the presence of Mg^{2+} ions can accelerate silica precipitation due to the formation of magnesium hydroxide and magnesium silicate complexes. The precipitation of silica gel leads to the co-precipitation of U phases (as U hydroxide or Ca-U-CO_3) with amorphous Si-Al-$CaCO_3$–Mg_2SiO_4 precipitates.

Table 6. MINTEQ-Predicted Distribution of U(VI) Species in the Presence of 10 mM of Ca^{2+}

Si (mM)	HCO_3^- (mM)	$UO2^{+2}$ species in the presence of various bicarbonate and silica concentrations,%						
		$UO_2(OH)_3^-$	$UO_2(OH)_4^{-2}$	$UO_2(OH)_2$	$(UO_2)_3(OH)_7^{--}$	$UO_2(CO_3)_3^{-4}$	$Ca_2UO_2(CO_3)_3(aq)$	$CaUO_2(CO_3)_3^{-2}$
5	0	88.971	10.9	0.092	0.037			
	2.9	0.223	0.027			0.193	83.814	15.743
	25					1.666	65.106	33.228
	50					5.005	50.052	44.943
	75					8.711	40.832	50.456
	100					12.271	34.583	53.145
50	0	83.533	13.356	0.082	0.029			
	2.9	0.514	0.079			0.886	74.597	23.923
	25					4.79	51.195	44.014
	50					0.818	52.843	46.338
	75					1.749	58.647	39.604
	100					1.785	66.357	30.76
100	0	85.121	14.778	0.075	0.025			
	2.9	1.044	0.182			1.996	67.546	29.23
	25					6.374	49.665	43.958
	50					4.471	56.32	39.209
	75					8.223	44.931	46.846
	100					9.932	39.163	51.905
150	0	93.222	6.6	0.117	0.061			
	2.9	0.568	0.04			0.568	94.28	5.107
	25					0.044	84.22	15.734
	50					0.056	82.437	17.507
	75					0.231	67.654	32.116
	100					0.154	72.663	27.183
200	0	84.529	15.375	0.071	0.024			
	3	2.815	0.512			3.234	59.718	33.717
	25					6.479	49.704	43.809
	50					10.577	39.184	50.238
	75					0.392	64.245	35.363
	100					0.67	56.121	43.209
250	0	84.612	15.293	0.07	0.024			
	3	3.944	0.707			3.067	58.755	33.522
	25					5.656	51.308	43.025
	50					8.745	42.047	49.206
	75					11.898	35	53.101
	100					0.511	60.363	39.126

Table 7. Predicted Distribution of U(VI) Species in the Presence of 5mM of $Ca^{2+}$and 5mM of Mg^{2+}

Si (mM)	HCO_3^- (mM)	$UO2^{+2}$ species in the presence of various bicarbonate and silica concentrations,%						
		$UO2(OH)_3^-$	$UO2(OH)_4^{-2}$	$UO_2(OH)_2$	$(UO_2)_3(OH)_7^{--}$	$UO_2(CO_3)_3^{-4}$	$Ca_2UO_2(CO_3)_3(aq)$	$CaUO_2(CO_3)_3^{-2}$
5	0	88.46	11.42	0.09	0.035			
	2.9	0.559	0.073			2.91	53.41	43.05
	25					7.12	24.9	67.99
	50					12.50	15.77	71.73
	75					13.96	12.07	73.96
	100					15.98	9.45	74.57
50	0	86.28	13.61	0.08	0.03			
	2.9	1.48	0.23			5.77	47.20	45.32
	25					7.47	35.25	57.27
	50					14.6	22.06	63.34
	75					21.72	14.86	63.41
	100					28.322	10.58	61.1
100	0	85.10	14.8	0.075	0.025			
	2.9	3.99	0.7			15.51	29.14	50.65
	25					26.69	19.69	53.61
	50					33.65	12.57	53.78
	75					35.09	10.45	54.48
	100					40.73	7.98	51.29
150	0	84.64	15.26	0.07	0.02			
	2.9	7.04	1.27			18.18	24.72	48.78
	25	0.01				27.76	19.2	53.02
	50					23.94	19.52	56.53
	75					24.42	15.48	60.10
	100					31.4	11.04	57.56
200	0	84.58	15.32	0.07	0.02			
	2.9	10.91	1.98			18.18	22.32	46.18
	25	0.02				26.84	19.64	53.49
	50					22.09	21.25	56.65
	75					29.29	13.29	56.76
	100					31.72	11.55	56.72
250	0	84.65	15.26	0.07	0.02			
	2.9	15.52	2.77	0.01		16.38	21.04	44.28
	25	0.03				24.61	20.77	54.58
	50					20.8	22.56	56.64
	75					28.34	14.33	57.33
	100					29.66	12.74	57.6

Table 8. Mineral Saturation Indices Based on Solution Compositions from 2 ppm U at 10 mM of Ca and Several Bicarbonate and Silica Concentrations

Mineral	Saturation indices for 50 mM Si			Saturation indices for 100 mM Si		
	0mM HCO_3^-	2.9mM HCO_3^-	50 mM HCO_3^-	0mM HCO_3^-	2.9mM HCO_3^-	50 mM HCO_3^-
Kaolinite	6.534	6.539	6.917	7.069	7.068	13.532
Halloysite	4.394	4.399	4.777	4.93	4.929	11.392
Imogolite	3.571	3.574	3.859	3.821	3.821	9.027
Diaspore	2.713	2.714	2.81	2.696	2.696	4.671
Gibbsite (C)	1.846	1.847	1.943	1.829	1.829	3.804
Quartz	1.399	1.4	1.493	1.683	1.683	2.94
Al(OH)3 (Soil)	1.296	1.297	1.393	1.279	1.279	3.254
Boehmite	1.008	1.009	1.105	0.991	0.991	2.966
Chalcedony	0.949	0.95	1.043	1.233	1.233	2.49
Cristobalite	0.749	0.75	0.843	1.033	1.033	2.29
SiO2 (am,ppt)	0.139	0.14	0.233	0.423	0.423	1.68
SiO2 (am,gel)	0.109	0.11	0.203	0.393	0.393	1.65
Becquerelite	2.98			2.783		
CaCO3xH2O(s)		1.067	1.899		0.945	1.448
Calcite		2.402	3.234		2.28	2.783
Aragonite		2.259	3.09		2.136	2.64
Vaterite		1.836	2.668		1.714	2.217
Al2O3(s)						3.435
Al(OH)3 (am)	1.296	1.297	1.393		1.279	0.744

Table 9. Mineral Saturation Indices Based on Solution Compositions from 2 ppm U at 5 mM Ca^{2+} and 5 mM Mg^{2+}, 50 and 100 mM of Silica Concentrations, and 0, 2.9 and 50 mM of Bicarbonate Concentrations

Mineral	Saturation indices for 50 mM Si			Saturation indices for 100 mM Si		
	0mM HCO3-	2.9mM HCO3-	50 mM HCO3-	0mM HCO3-	2.9mM HCO3-	50 mM HCO3-
Al(OH)3(soil)	1.39	1.34	1.42	1.37	1.37	1.38
Aragonite		1.87	2.71		1.61	2.5
Artinite		3.02	3.52		2.68	3.22
Boehmite	1.08	1.09	1.11	1.07	1.07	1.08
Brucite	1.81	1.86	1.39	1.75	1.73	1.33
CaCO3xH2O(s)		068	1.54		0.41	1.31
Calcite		2.02	2.86		1.75	2.64
Chalcedony	1.01	1.02	1.04	1.3	1.3	1.31
Chrysolite	19.57	19.72	18.37	19.98	19.91	18.73
Cristobalite	0.81	0.82	0.84	1.10	1.10	1.11
Diaspore	2.81	2.81	2.84	2.79	2.79	2.80
Dolomite(D)		3.71	5.51		3.23	5.06
Dolomite(O)		4.27	6.07		3.79	5.62
Gibbsite(C)	1.94	1.94	1.97	1.92	1.92	1.93

Mineral	Saturation indices for 50 mM Si			Saturation indices for 100 mM Si		
	0mM HCO3-	2.9mM HCO3-	50 mM HCO3-	0mM HCO3-	2.9mM HCO3-	50 mM HCO3-
Halloysite	4.69	4.7	4.81	5.24	5.23	5.28
Huntite		4.41	8.15		3.51	7.21
Hydromagnesite		2.3	5.69		1.32	4.66
Imogolite	3.81	3.82	3.9	4.07	4.07	4.10
Kaolinite	6.87	6.88	6.99	7.41	0.95	7.46
Magnesite		1.16	2.12	0.19	1.54	1.88
Mg(OH)2 (active)	0.25	0.3			0.17	
Quartz	1.47	1.47	1.5	1.75	1.75	1.76
Sepiolite	14.50	14.61	13.76	15.25	15.21	14.44
Sepiolite (A)	11.62	11.73	10.44	12.37	12.32	11.55
SiO2 (am,gel)	0.17	0.17	0.2	0.45	0.45	0.46
SiO2 (am,ppt)	0.2	0.2	0.23	0.49	0.48	0.5
Spinel	1.33	1.39	0.98	1.25	1.23	0.85
Valerite		1.45	2.28		1.18	2.07

Mineralogical and Morphological Characterization of U(VI)-Bearing Precipitates

Analysis using SEM/EDS allowed investigation of the effects of variables such as length of time in the "mother solution" and the presence of Ca in the artificial solution mixture on the morphology of the experimentally prepared uranium-bearing precipitates. The analytical techniques permitted a comparison of the qualitative and quantitative changes resultant from altering preparation methods, component concentrations, and time.

Analysis of Supernatant Solutions

Though the focus of the sub-task is the solid precipitate, the KPA analysis of the supernatant reveals a great deal of information about the samples and the sample preparation methods. For each of the precipitates prepared, the supernatant was reserved for analysis. The particularly interesting data produced related to the effects of calcium and centrifugation on the concentration of uranium (VI) in the supernatant.

To evaluate the effect of centrifugation, the supernatants of the centrifuged batch 1 samples were compared to their non-centrifuged counterparts from batch 2 using KPA analysis. The data, displayed in Figure 18, illustrates that the latter regularly had a lower concentration of U(VI) in the supernatant. After 2 months, the uranium content of the supernatant belonging to the centrifuged high bicarbonate sample was 2.4 times that of the corresponding non-centrifuged sample. It is hypothesized that the high separation forces of the centrifuge is responsible for driving the dissolved uranium from the amorphous precipitate and into the supernatant, resulting in the low amounts of uranium present in the associated precipitates.

A similar assessment was performed gauging the effect of the presence of calcium on the concentration of uranium in the supernatant. The data, imaged in Figure 19, suggest that the presence of Ca in the sample mixture caused a reduction of uranium in the supernatant solution.

In the case of the low bicarbonate (3 mM) samples, the figure shows a significant 3-fold decrease compared to their calcium-withheld equivalents. This reduction is especially evident by the drastic variation for the high bicarbonate set (Figure 19).

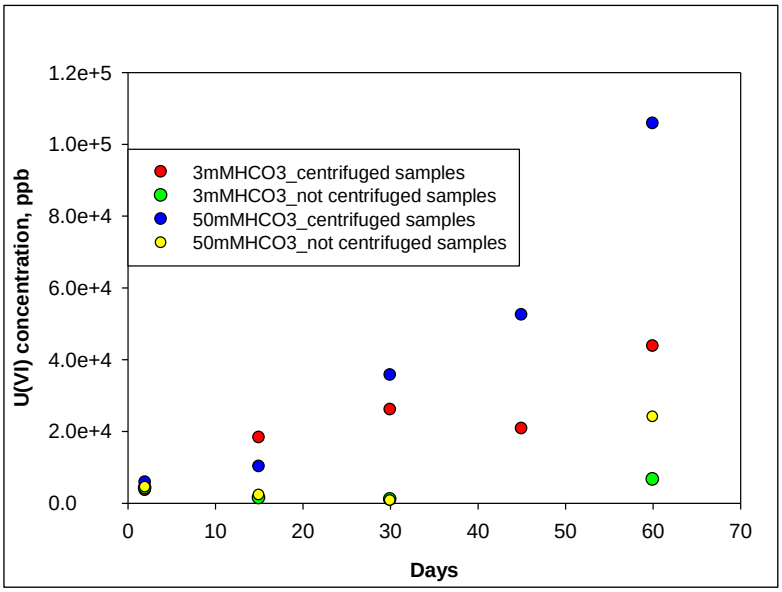

Figure 18. Effect of sample centrifugation on the concentration of U(VI) in the supernatant solution.

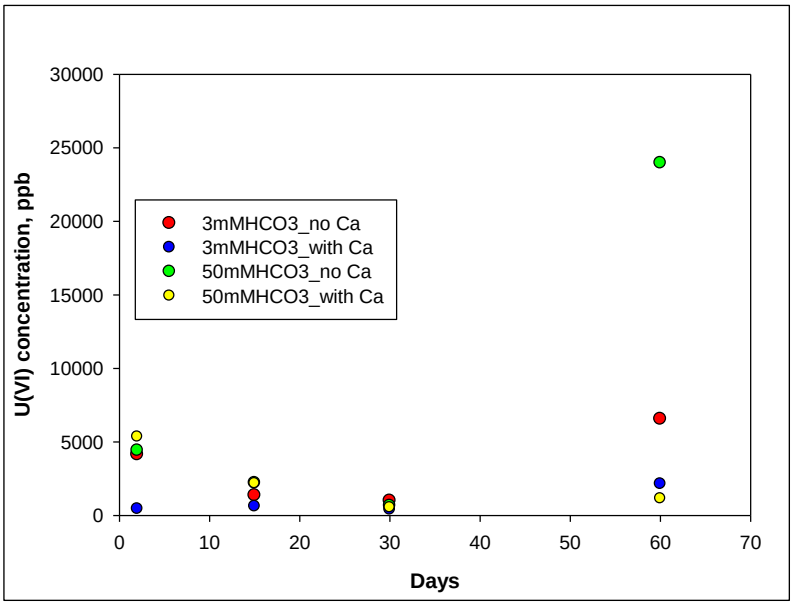

Figure 19. Effect of 5 mM Ca on the concentration of U(VI) in the supernatant solution.

SEM-EDS

Analysis using SEM/EDS allowed investigation of the effects of variables such as length of time in the "mother solution" and the presence of Ca in the artificial solution mixture on the

morphology of the experimentally prepared uranium-bearing precipitates. The analytical techniques permitted a comparison of the qualitative and quantitative changes resultant from altering preparation methods, component concentrations, and time.

Analysis of Batch 1 Samples

Figure 20 through Figure 26 present data on the sets of sample precipitates prepared out of the solution mixture composed of 100 mM Si, 5 mM Al, 3 mM $HCO3^{-}$, and 200 ppm U(VI). All samples were centrifuged and then decanted before placing the precipitates to dry. The SEM images pertaining to these samples show that precipitates are typically amorphous silica globules. This is consistent with Iler's (1979) observations who reported that most synthetic silicates are amorphous when precipitated from aqueous solution. After 2 weeks of being kept in the "mother solution," the sample surface morphology of set # 2 (Figure 21) showed evidence of elongated forms grown on the surface of alkaline silica gel. This is contrasted to the more spherical silica colloidal particles found at high pH in set #1 (Figure 19). Quantitative measurements of the composition in these elongations revealed little to no uranium and a considerably higher atomic percentage of sodium, oxygen and silica (Figure 20). EDS indicated that samples were not homogeneous and featured a non-uniform distribution of uranium throughout the sample. The highest atomic percentage of U, ranging between 0.8% and 1.1%, was found in set #1 (after 2 days) and set #4 (1 month); the atomic percentage of U in the following samples were much less, in the range of 0.02 to 0.56%. No crystalline structures were found in these sets. The decline in U was attributed to the sample preparation procedures, particularly centrifugation when samples were prepared for drying (Figure 18).

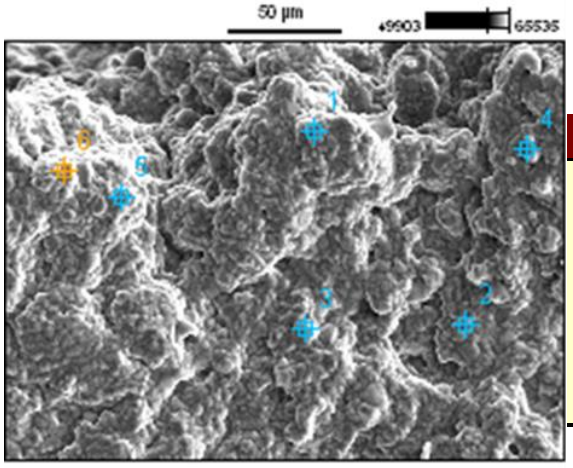

	O-K	NA-K	AL-K	SI-K	K-K	U-M
PT1	51.69	21.21	2.54	24.05	0.28	0.23
PT2	47.97	34.41	0.33	16.78	0.31	0.21
PT3	43.19	24.98	2.25	29.10	0.32	0.16
PT4	47.22	45.75	0.80	5.78	0.18	0.27
PT5	48.46	33.03	0.60	16.60	0.49	0.81
PT6	41.39	53.37	0.02	5.16	0.02	0.04

Figure 20. Set # 1 (after 2 days) SEM image (left) and EDS data (right) for centrifuged samples amended with 3 mM HCO_3.

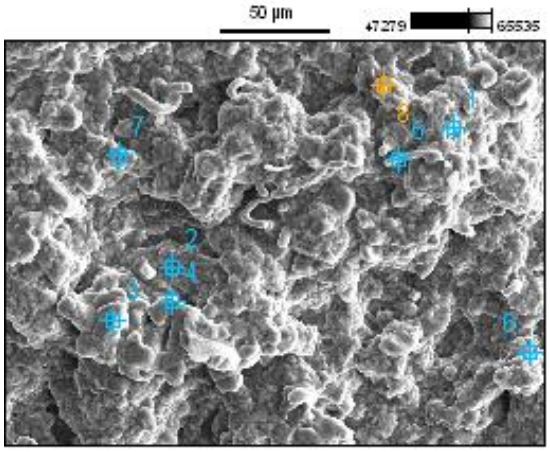

	O-K	Na-K	Al-K	Si-K	K-K	U-M
PT1	57.25	30.84	0.88	10.75	0.19	0.09
PT2	54.67	27.14	1.81	16.06	0.24	0.08
PT3	51.37	48.36	0.00	0.23	0.05	0.00
PT4	52.21	42.21	0.80	4.64	0.09	0.03
PT5	52.54	43.95	0.08	3.39	0.00	0.04
PT6	60.01	25.32	1.58	12.89	0.12	0.07
PT7	53.97	27.37	1.75	16.46	0.31	0.14
PT8	52.96	35.48	0.95	10.49	0.08	0.05

Figure 21. Set # 2 (after 2 weeks) SEM image (left) and EDS data (right) for centrifuged samples amended with 3 mM HCO_3.

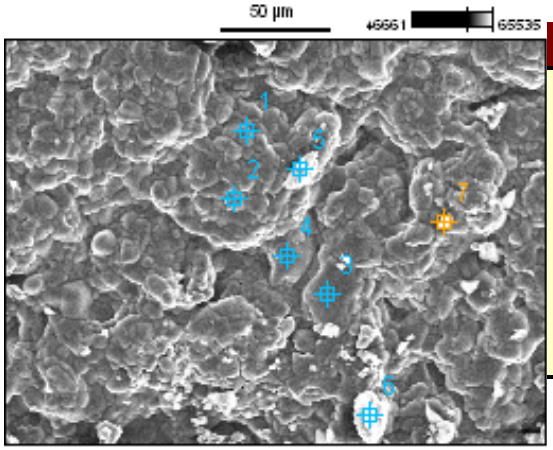

	O-K	Na-K	Al-K	Si-K	K-K	U-M
PT1	54.14	41.05	0.21	4.43	0.08	0.04
PT2	45.27	51.95	0.35	2.26	0.01	0.16
PT3	51.02	48.50	0.00	0.19	0.09	0.20
PT4	50.06	49.67	0.00	0.21	0.06	0.00
PT5	45.20	22.51	0.97	28.87	1.34	1.11
PT6	64.35	8.25	2.74	24.15	0.31	0.19
PT7	57.81	22.82	0.43	18.45	0.23	0.26

Figure 22. Set # 3 (after 1 month) SEM image (left) and EDS data (right) for centrifuged samples amended with 3 mM HCO_3.

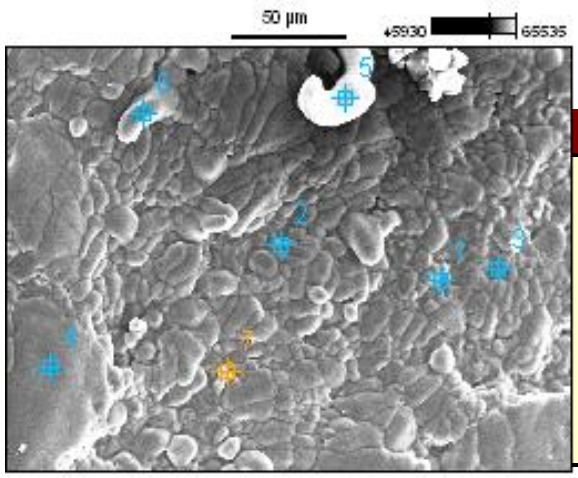

	O-K	Na-K	Al-K	Si-K	K-K	U-M
pt1	39.85	34.71	1.17	17.53	0.70	0.22
pt2	55.82	42.73	0.08	1.29	0.02	0.06
pt3	53.66	46.24	0.00	0.10	0.00	0.00
pt4	50.96	48.55	0.00	0.28	0.15	0.07
pt5	47.09	52.87	0.00	0.00	0.00	0.03
pt6	50.19	49.34	0.00	0.30	0.18	0.00
pt7	57.00	41.21	0.11	1.60	0.04	0.03

Figure 23. Set # 4 (after 1.5 month) SEM image (left) and EDS data (right) for centrifuged samples amended with 3 mM HCO3.

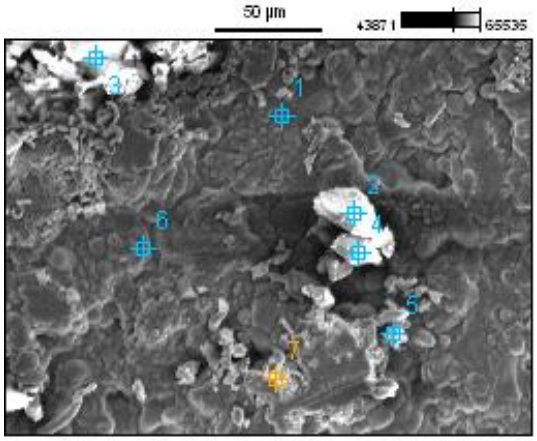

	C-K	O-K	Na-K	Al-K	Si-K	K-K	U-M
pt1	0.00	51.78	47.98	0.00	0.21	0.00	0.02
pt2	6.71	42.57	10.00	1.30	37.87	0.98	0.56
pt3	7.19	50.32	26.44	0.55	15.02	0.32	0.16
pt4	0.00	49.27	46.13	0.00	4.32	0.29	0.00
pt5	0.00	56.96	37.23	0.24	5.48	0.07	0.02
pt6	0.00	56.18	43.71	0.00	0.11	0.00	0.00
pt7	9.36	54.31	33.57	0.15	2.52	0.08	0.02

Figure 24. Set # 5 (after 2 month) SEM image (left) and EDS data (right) for centrifuged samples amended with 3 mM HCO_3.

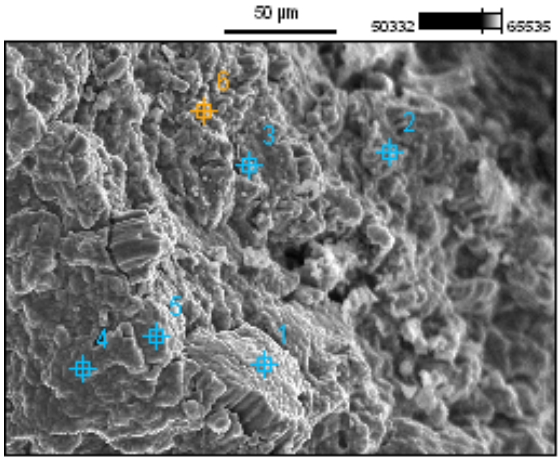

	C-K	O-K	Na-K	Al-K	Si-K	K-K	U-M
pt1	12.29	52.10	35.19	0.06	0.34	0.02	0.00
pt2	10.38	54.90	34.24	0.00	0.43	0.00	0.04
pt3	7.74	55.48	34.35	0.11	2.26	0.01	0.04
pt4	49.25	27.05	21.79	0.93	0.41	0.00	0.56
pt5	0.00	48.60	51.25	0.00	0.11	0.00	0.03

Figure 25. Set # 6 (after 3 month) SEM image (left) and EDS data (right) for centrifuged samples amended with 3 mM HCO3.

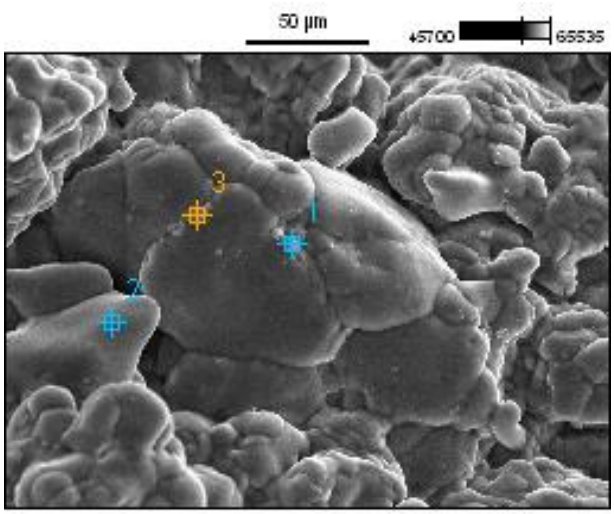

	C-K	N-K	O-K	Na-K	Al-K	Si-K	K-K	U-M
pt1	12.52	12.10	51.54	19.68	0.56	3.47	0.05	0.04
pt2	2.85	16.39	50.52	30.08	0.00	0.04	0.00	0.04
pt3	7.49	10.88	51.80	22.67	0.34	6.64	0.01	0.07

Figure 26. Set # 7 (after 4 month) SEM image (left) and EDS data (right) for centrifuged samples amended with 3 mM HCO3

The most interesting results in these experiments were observed in the samples that combined 100 mM Si, 5 mM Al, 50 mM HCO_3^-, and 200 ppm U (Figure 27-Figure 33). The development of crystalline structures was observed after keeping the precipitates for 1.5 months in the "mother solution" (Figure 30). Several EDS points taken on the crystals and around the sample surface showed that the distribution of uranium was not uniform, with the atomic percentage ranging between 0.01-2.57%. The higher U atomic percentage correlated with higher C atomic percentages; however, we were not able to confirm this correlation with other samples.

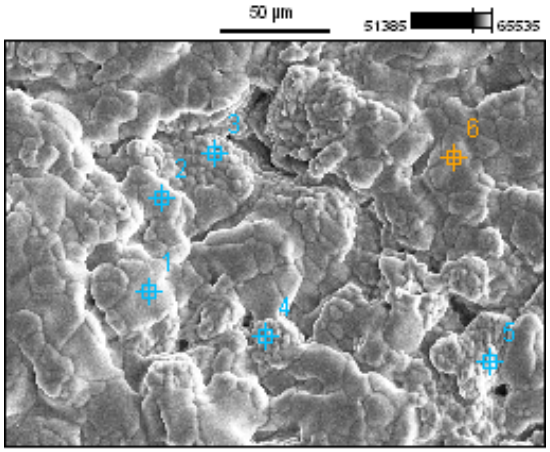

	O-K	Na-K	Al-K	Si-K	K-K	U-M
pt1	45.35	24.53	0.99	22.34	6.45	0.33
pt2	47.71	31.68	0.44	15.76	4.19	0.21
pt3	54.17	24.70	1.10	18.35	1.59	0.09
pt4	49.18	31.12	0.83	16.95	1.79	0.14
pt5	58.38	27.08	0.80	12.80	0.86	0.09
pt6	45.60	32.97	0.11	16.13	4.82	0.37

Figure 27. Set # 1 SEM image (after 2 days) and EDS data (right) for centrifuged samples amended with 50 mM HCO3.

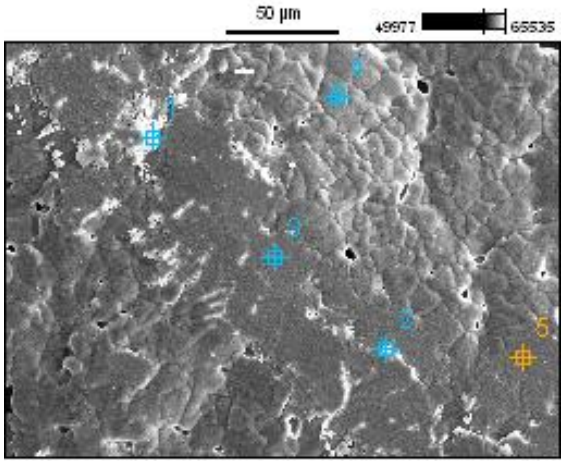

	O-K	Na-K	Al-K	Si-K	K-K	U-M
pt1	52.31	47.16	0.12	0.00	0.28	0.14
pt2	53.10	46.62	0.00	0.10	0.17	0.01
pt3	49.28	45.92	0.10	0.00	4.68	0.01
pt4	49.79	48.79	0.18	0.28	0.95	0.00
pt5	50.05	46.00	0.09	0.00	3.85	0.00

Figure 28. Set # 2 SEM image (after 2 weeks) and EDS data (right) for centrifuged samples amended with 50 mM HCO_3.

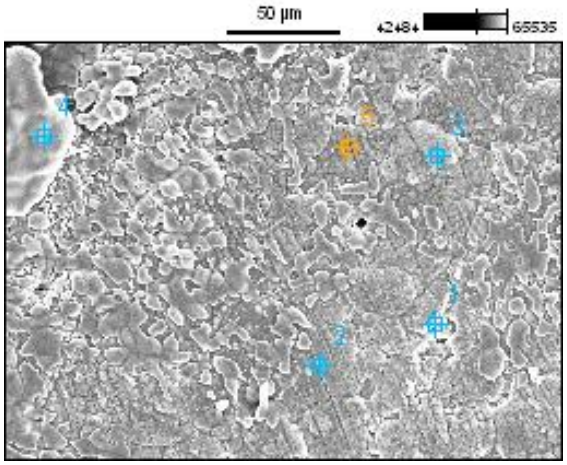

	O-K	Na-K	Al-K	Si-K	K-K	U-M
pt1	57.70	18.46	1.09	19.76	2.84	0.16
pt2	53.83	19.56	1.34	21.47	3.57	0.23
pt3	49.65	24.27	1.02	18.78	6.02	0.26
pt4	52.42	47.06	0.00	0.26	0.24	0.02
pt5	58.31	16.31	1.07	20.82	3.43	0.06

Figure 29. Set # 3 SEM image (after 1 month) and EDS data (right) for centrifuged samples amended with 50 mM HCO_3.

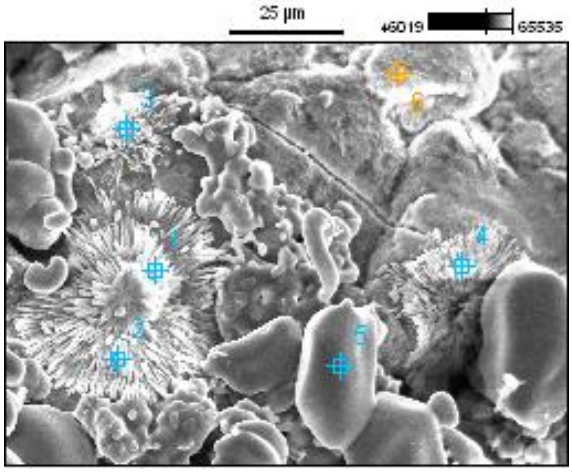

	C-K	O-K	Na-K	Al-K	Si-K	K-K	U-M
pt1	46.37	38.46	5.83	0.00	1.16	5.97	2.22
pt2	42.15	36.91	6.22	0.23	4.92	7.31	2.26
pt3	31.35	45.59	19.61	0.04	2.22	1.01	0.18
pt4	44.98	37.63	6.38	0.11	1.80	6.81	2.31
pt5	26.01	50.49	0.26	0.00	0.00	23.24	0.00
pt6	13.45	54.42	10.79	0.80	15.28	5.16	0.10

Figure 30. Set # 4 SEM image (after 1.5 month) and EDS data (right) for centrifuged samples amended with 50 mM HCO_3.

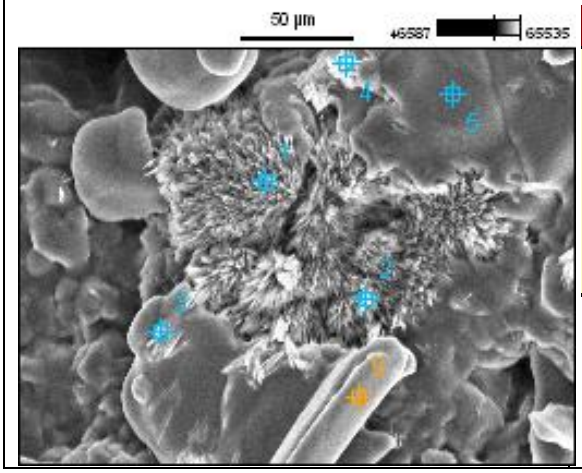

	C-K	O-K	Na-K	Al-K	Si-K	K-K	U-M
pt1	34.37	44.55	20.24	0.00	0.64	0.18	0.03
pt2	32.15	46.83	20.90	0.00	0.00	0.12	0.00
pt3	24.34	48.73	22.55	0.01	0.12	4.25	0.00
pt4	33.30	45.73	20.16	0.00	0.43	0.35	0.04
pt5	17.63	38.08	43.88	0.00	0.27	0.14	0.00
pt6	24.51	52.31	0.60	0.00	0.03	22.54	0.02

Figure 31. Set # 5 SEM image (after 2 month) and EDS data (right) for centrifuged samples amended with 50 mM HCO3.

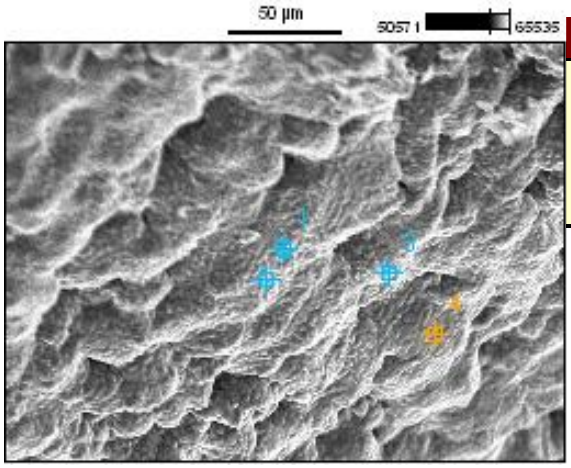

	C-K	O-K	Na-K	Al-K	Si-K	K-K	U-M
pt1	50.20	30.72	10.53	0.14	6.02	1.25	1.14
pt2	42.40	36.17	11.77	0.19	7.29	1.21	0.97
pt3	63.31	19.97	6.28	0.19	7.83	1.39	1.03
pt4	21.38	50.42	12.26	0.76	13.32	1.40	0.46

Figure 32. Set # 6 SEM image (after 3 month) and EDS data (right) for centrifuged samples amended with 50 mM HCO_3.

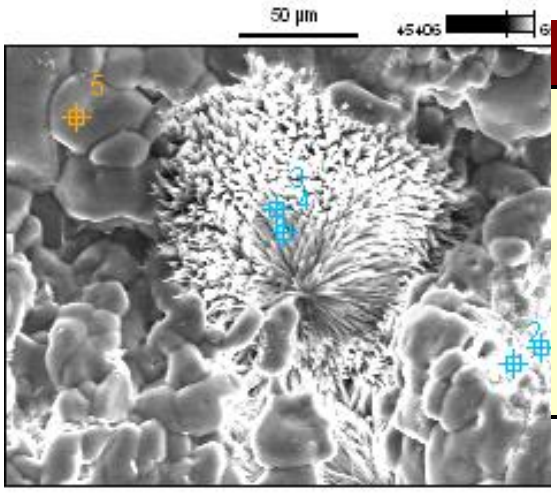

	C-K	N-K	O-K	Na-K	Al-K	Si-K	K-K	U-M
pt 1	9.25	8.61	48.77	14.53	0.29	13.02	4.44	1.09
pt 2	25.46	7.88	46.31	15.53	0.08	2.08	1.66	1.00
pt 3	32.20	0.00	44.40	21.37	0.00	0.41	1.63	0.00
pt 4	22.57	0.00	47.14	25.42	0.00	1.46	3.17	0.25
pt 5	3.24	15.88	50.61	27.84	0.00	0.17	2.18	0.07

Figure 33. Set # 7 SEM image (after 4 month) and EDS data (right) for centrifuged samples amended with 50 mM HCO_3.

Observations of Batches 2 and 3

The effect of bicarbonate (HCO_3) concentrations and addition of calcium (Ca)

During the SEM-EDS analysis, samples prepared using high (50 mM) and low (3 mM) concentrations of bicarbonate were used to evaluate the effect on precipitate morphology with varying times. Backscatter electron capture (BEC) detection mode allows for the areas of higher average atomic number to show up as "hot spots" which appear brighter than their surrounding areas. This attribute allowed potentially uranium-rich areas to be identified before being confirmed with semi-quantitative EDS analysis. The uranium–rich areas often showed crystal-like structures (Figure 34A) that were consistent with what was expected based on SEM analysis of prior samples. The amorphous uranium-bearing areas were often highly incorporated into the sample, unlike the needle-shaped uranium crystals, which appeared to be growing on, within, and/or through the rest of the precipitate (Figure 34B). In uranium-rich areas, EDS indicated significant oxygen, silica and uranium content and minor calcium concentrations. The geochemical modeling predicted that uranium is mostly distributed between $Ca_2UO_2(CO_3)_3$ (aq), $CaUO_2(CO_3)_3^{-2}$ and $UO_2(CO3)_3^{-4}$ with the latter being the minor species. However, EDS analysis indicated only a small presence of Ca in the uranium "hot" spots. Uranyl carbonate minerals have the common building unit of the structures such as tri-carbonate cluster with U : C = 1 : 3. Based on the ratio of elements, identifying the uranyl phase as uranyl carbonates with U : C = 1 : 3 phase resulted in an excess of Si, oxygen and sodium. This indicates the phase is a mixed uranyl-carbonate- silica, possibly sodium/calcium uranyl carbonate mixed with SiO_2. Kellermeier et al. (2012) investigated the formation of precipitated aggregates consisting of amorphous calcium carbonate and hydrated amorphous silica with minor amounts of calcium entrapped between the coagulated particles. The aforementioned precipitation process resulted in a coating of calcium carbonate with a siliceous shell all over the particles. By comparison, if a similar precipitation of calcium-rich silica particles in the experimental samples occurred, the calcium content determined via EDS analysis would have exceeded that which was observed. The ruling out of calcium-silica

products leaves the possibility for the formation of calcium-carbonate phases in the system. These results are in agreement with the speciation modeling.

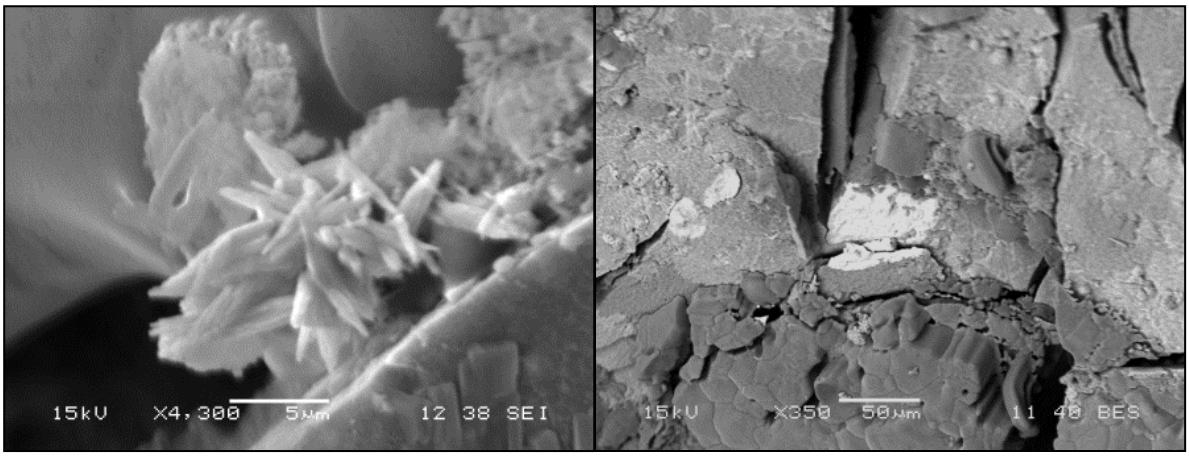

Figure 34. (Batch 2) Uranium-rich regions of the A) 50 mM HCO3 - 2 day sample and B) 50 mM HCO3- + 5 mM Ca - 3 month sample.

The samples prepared with high bicarbonate concentrations (50 mM) showed the uranium-dense regions as crystal-like structures or as an amorphous collection. While either or both forms could be present, the majority of 50 mM HCO_3^- samples that exhibited hot spots showed them in this crystal-like form. EDS analysis of these areas resulted in uranium atomic percentages that regularly exceeded 1% and often reached up to 10% (Figure 35). Studies on uranium-heavy regions on prior samples (Year-End Technical Report for Project 2, May 2012) rarely reached 1%. The change can most likely be attributed to the increase in uranium to 200 ppm added in more recent precipitate preparation methods.

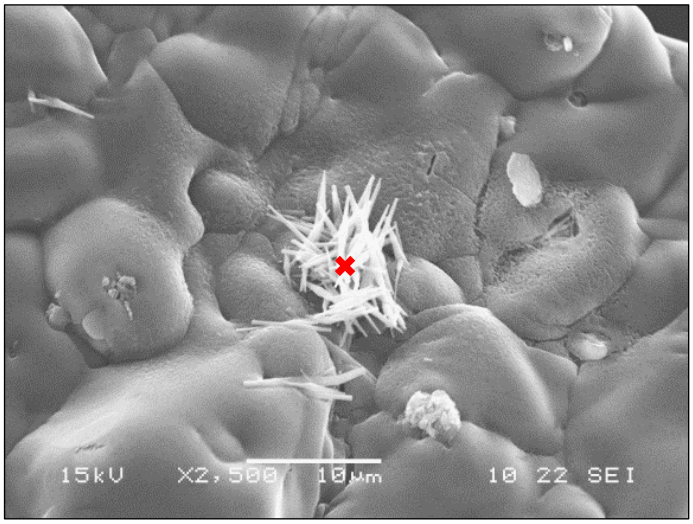

Element	Wt%	At%
CK	12.11	20.26
NK	08.25	11.83
OK	39.22	49.27
NaK	18.18	15.89
AlK	00.16	00.12
SiK	00.46	00.33
SK	00.14	00.09
ClK	00.17	00.10
UM	20.60	01.74
KK	00.61	00.31
CaK	00.11	00.05
Matrix	Correction	ZAF

Figure 35. SEM image of (Batch 2) 50 mM HCO_3^- + 5 mM Ca - 2 month sample.

While the high bicarbonate (50 mM) samples repeatedly showed uranium-bearing crystal-like formations, the low bicarbonate version showed none. The only significant uranium-rich areas that were identified and confirmed by EDS were amorphous uranium-dense areas with U

atomic percentages that did not exceed 1%. These findings were consistent with previously reported conclusions (2011 YER). The report concluded that there was in increase in uranium removal from the supernatant solution when bicarbonate concentration increase from 3 mM to 50 mM.

Despite the apparent increase in uranium removal from the solution with the addition of calcium, the qualitative and semi-quantitative SEM/EDS analyses showed no appreciable difference between samples prepared with and without calcium. The spectra produced by EDS showed no correlation between the presence of calcium and the percentage of uranium in the sample. Spectroscopic analysis of the "hot spots" that were observed by BEC micrographs of the low bicarbonate, calcium-containing sample precipitates were revealed to be rich in calcium, carbon, and oxygen as opposed to uranium.

The effect of sample centrifugation

Batch 3 allowed for a comparison of centrifuged and non-centrifuged samples which enabled the impact of centrifugation on precipitate morphology to be evaluated. In order to match up the two batches, the assessment was limited to the 2 day, 1 month, and 3 month, calcium-containing samples. The lack of uranium-rich sites on the 3 mM bicarbonate samples demanded that the studies be limited to the samples with higher concentrations.

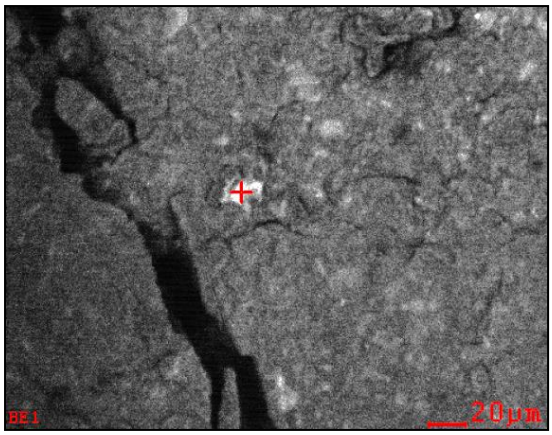

Element	Wt%	At%
CK	07.17	13.77
NK	03.16	05.21
OK	38.13	55.03
NaK	03.36	03.37
AlK	01.57	01.35
SiK	19.64	16.14
ClK	00.42	00.27
UM	21.89	02.12
KK	03.49	02.06
CaK	01.17	00.67
Matrix	Correction	ZAF

Figure 36. (Batch 3) BEC image and EDS data for 50 mM HCO3-+5 mM Ca - 3 month sample (centrifuged) sample.

The light and dark patches that spanned the BEC images of the centrifuged samples show that the areas vary in average atomic number, though EDS showed no significantly high percentage of uranium at any of them. The pattern was fairly consistent across the time study. With one exception, EDS revealed no "hot spots" signaling areas of concentrated uranium (Figure 36). The tandem of backscatter electron capture imaging and EDS analysis revealed at least one area of increased uranium content, relative to the rest of the sample, in the 3 month version. The uranium-bearing area in this sample showed no discernible systematic structure. Increased magnification did not reveal any of the crystal-like structures observed in samples analyzed previously.

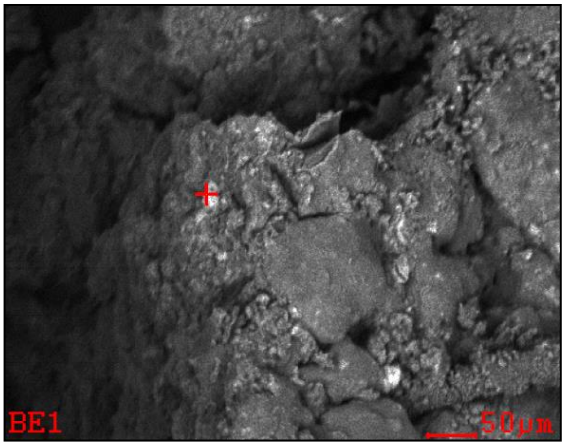

Element	Wt%	At%
CK	07.13	13.93
NK	02.26	03.79
OK	33.90	49.72
NaK	03.45	03.52
AlK	00.81	00.70
SiK	24.54	20.50
ClK	00.56	00.37
UM	17.70	01.75
KK	04.35	02.61
CaK	05.30	03.10
Matrix	Correction	ZAF

The non-centrifuged samples produced images revealing a rough, uneven textured surface. On the two shorter duration samples, backscatter detection revealed some light and dark areas but none with a significant uranium increase. Similar to centrifuged samples, only the 3 month, non-centrifuged precipitate showed "hot spots" with localized uranium atoms (Figure 37). Further magnification of these uranium-rich sites showed no sign of crystal formation.

All samples featured enhanced silica condensation and EDS analysis provided evidence that the vast majority of cluster species observed in the solutions are composed of $CaCO_3$ (Figure 38).

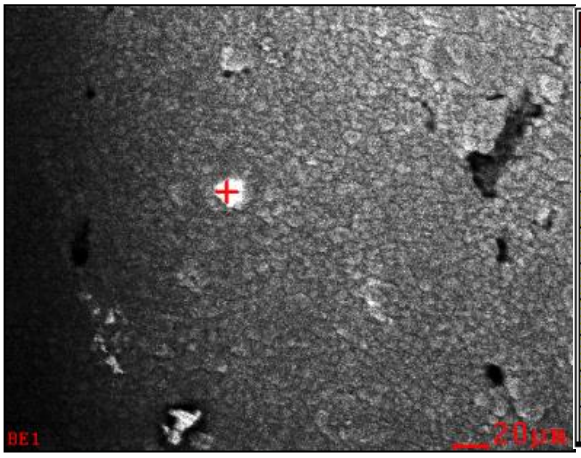

Element	Wt%	At%
CK	13.70	22.68
NK	01.89	02.69
OK	44.29	55.07
NaK	00.53	00.46
AlK	00.00	00.00
SiK	00.87	00.62
ClK	00.12	00.07
UM	01.82	00.15
KK	00.34	00.17
CaK	36.44	18.09
Matrix	Correction	ZAF

Figure 38. (Batch 3) 50 mM HCO_3+5 mM Ca - 1 month (non-centrifuged) sample BEC image and EDS data.

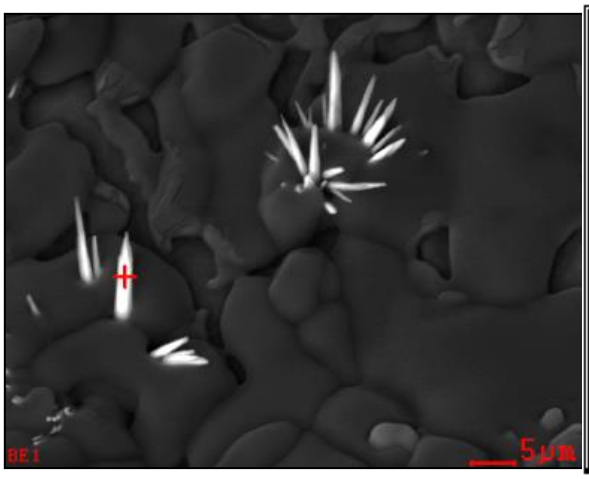

Element	Wt%	At%
CK	04.32	07.49
NK	11.75	17.47
OK	39.67	51.62
NaK	22.75	20.60
AlK	00.28	00.21
SiK	00.21	00.16
ClK	00.28	00.17
UM	19.71	01.72
KK	00.84	00.45
CaK	00.19	00.10
Matrix	Correction	ZAF

Figure 39. (Batch 2) 5 0mM HCO_3+5 mM Ca - 1 month sample BEC image and EDS data.

The consequences of changing the preparation method for batch 3 were evaluated by comparison to their batch 2 equivalents. Qualitatively, the two batches showed stark differences on their surfaces. The smooth Si-rich areas present in batch 2 are not seen in the batch 3 samples (Figure 38). The frequent vortexing that the batch 3 procedure requires to ensure a homogenous sample are thought to be the reason for the difference. The most blatant difference between the two classes is the presence, or lack of, crystal-like and/or amorphous uranium-rich areas. Compared to batch 2 (Figure 39), which often showed an abundance of these areas, batch 3 was barren.

Morphological changes with time

The evolution of sample morphology with increased time in solution for the high bicarbonate precipitates is similar for samples prepared with and without calcium. Early on in the experiment, the uranium-rich, needle-like forms appear to grow on, in, and through the precipitate (Figure 40 A-D & Figure 41 A-C). As the amount of time in solution increases, it appears as though the smooth Si-rich component that coats the precipitate increasingly overtakes the uranium-bearing solids. In the case of the sample of the precipitate prepared without calcium, after 3 months, rather than the crystal-like structures found previously, uranium-rich areas appear as amorphous areas with no discernible structure (Figure 41D). The backscatter imaging of Figure 42 shows the high level of incorporation into the precipitate after 3 months in solution. Based on the crack in the material, it is clear that the uranium-dense region of this sample extends into the sample.

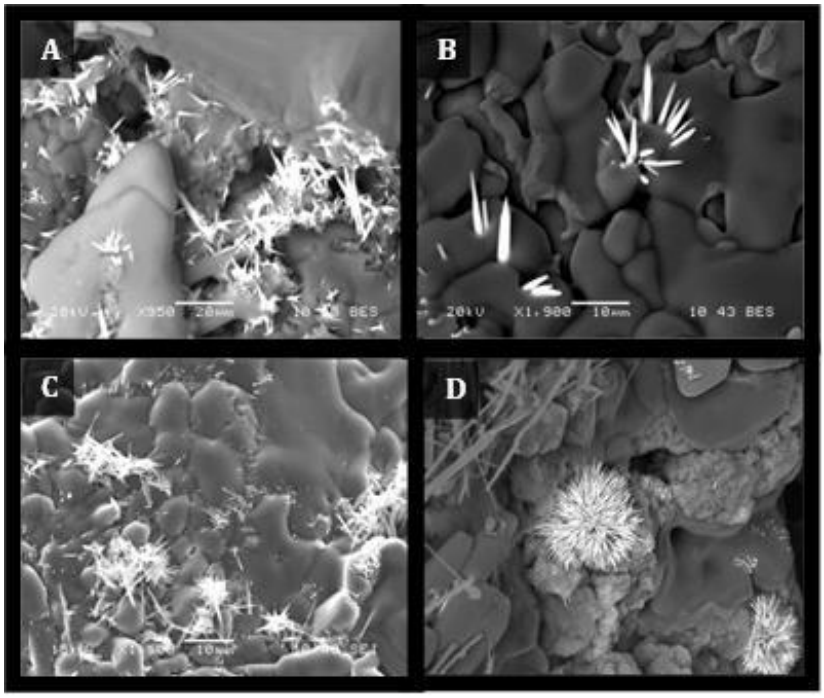

Figure 40. Precipitates formed from batch 2 solutions containing calcium (5 mM) and high bicarbonate (50 mM) concentration after 2 weeks (A), 1 month (B), 2 months (C), and 3 months (D).

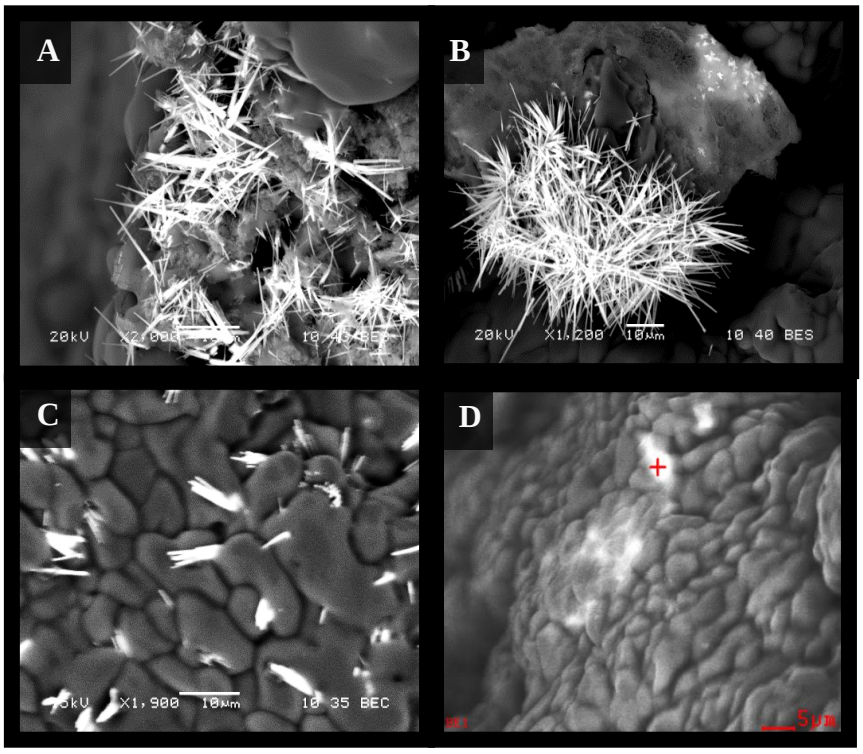

Figure 41. Precipitates formed from batch 2 solutions containing high bicarbonate (50 mM) concentration (no calcium) after 2 weeks (A), 1 month (B), 2 months (C), and 3 months (D).

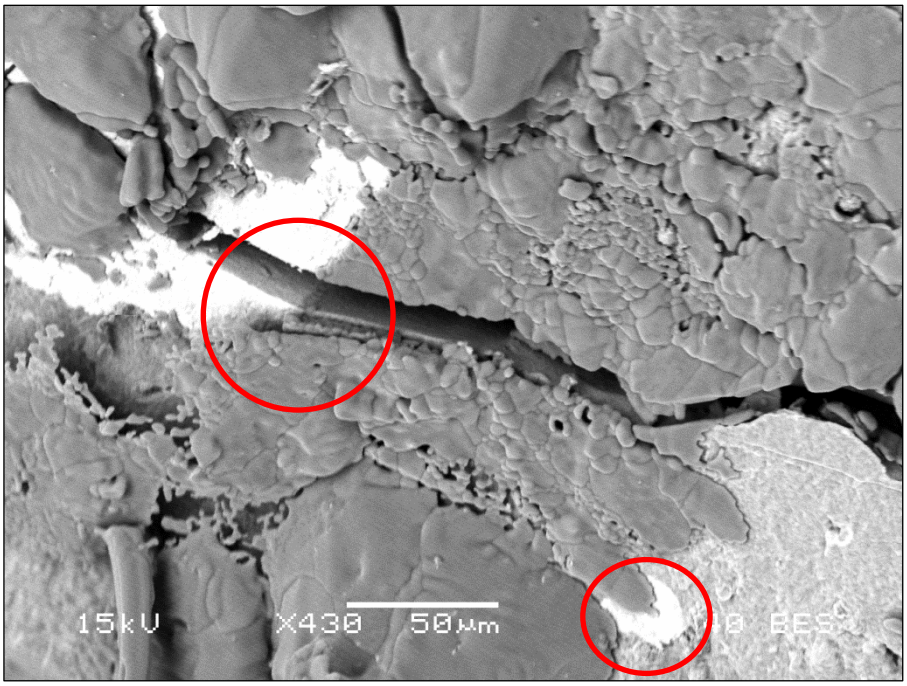

Figure 42. BEC image of a uranium-rich region of a 50 mM HCO3 + 5 mM Ca - 3 month sample.

Micro-Raman Spectroscopy

MRS analysis was limited to the high bicarbonate 2 weeks samples, with and without calcium. These precipitates were selected due to the abundant amount of the crystal-like uranium-rich forms observed during SEM/EDS analysis. Based on the *KnowItAll*® software, weak bands present in the 1025-1100 (Figure 44 & Figure 45) could be representative of a silica polymer (SiO_2). This result could be anticipated because of the dominance of silica in the samples. Under the microscope, the sample looked like a mass of glass, making it impossible to distinguish the areas of interest as was done with BEC imaging (Figure 42).

The bands for uranyl-minerals should be predictably located but factors like overlap affect the spectroscopic frequencies. Ideally, reference samples would be available for comparison. Alternatively, this early investigation compared spectra to published results. The Raman bands present on the spectra recorded showed promise when compared to the values/ranges in peer-reviewed reports. The symmetric stretches potentially belonging to $(UO_2)^{2+}$ and anionic component [$(CO_3)^{2-}$ in this case] are present in their anticipated 700-900 cm^{-1} and 900-1100 cm^{-1} ranges, respectively (Figure 44 & Figure 45) (Stefaniak 2009).

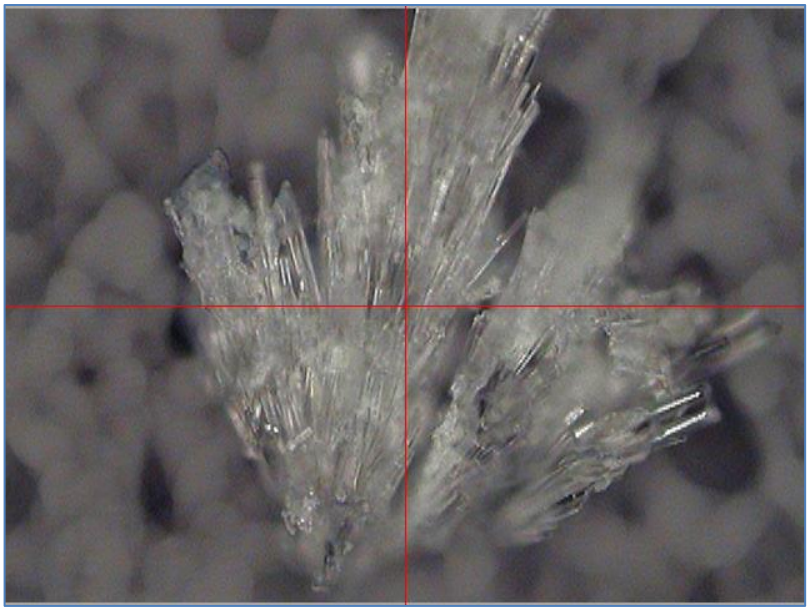

Figure 43. Raman Microscope image of the high (50 mM) bicarbonate + 5 mM Ca- 2 week sample.

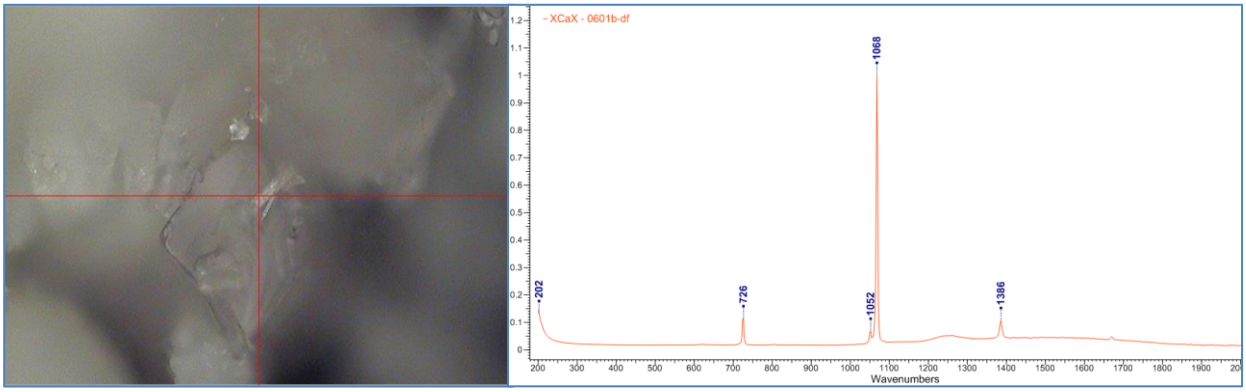

Figure 44. MRS image and spectra of the high (50mM) bicarbonate - 2 week sample.

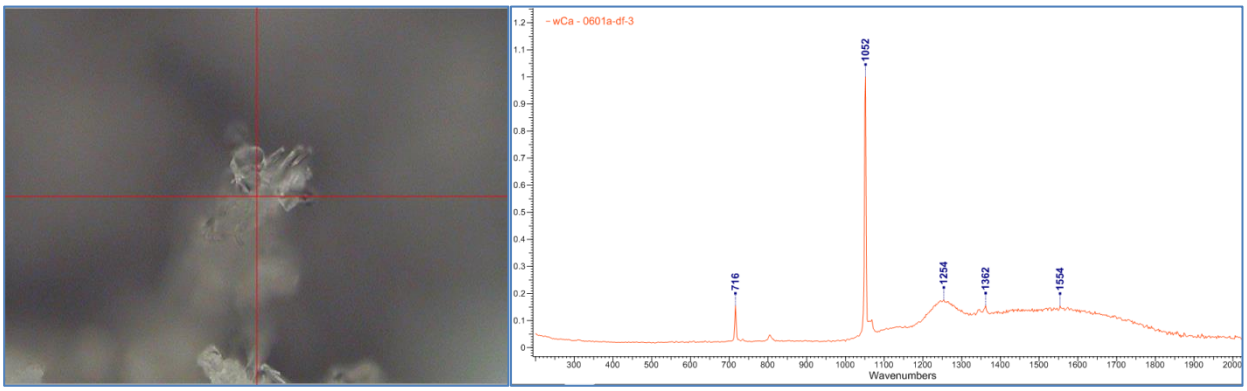

Figure 45. MRS image and spectra of the high (50mM) bicarbonate + 5mM Ca - 2 week sample.

XRD

Each pure substance produces a unique the X-Ray Diffraction (XRD) pattern, which like a fingerprint for phase identification. The technique is used to discern the atomic structure of

crystalline substances by relying on the regularly repeating pattern of the crystal structure. The periodic arrangement of atoms in a crystalline solid will scatter x-rays in particular directions, contrasted with the random directions of scatter seen with amorphous materials. While the random scattering of amorphous samples lead to broad undefined single peak, the constructive interference of scattering from a crystalline sample form well defined peaks of a somewhat consistent pattern.

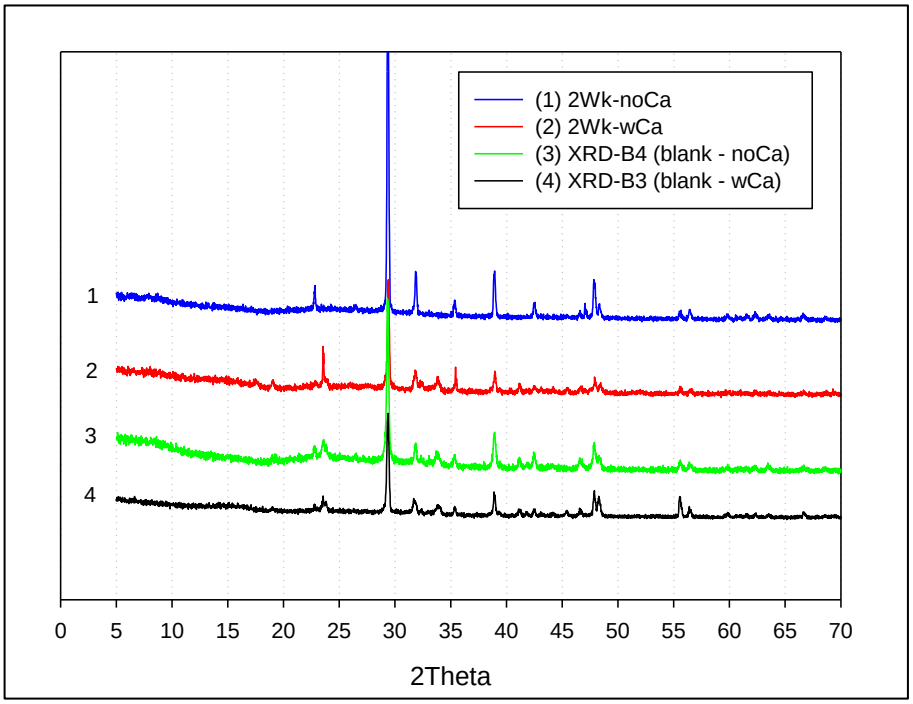

Figure 46. Comparison of the diffraction patterns of sample precipitates prepared with and without calcium and their corresponding U-free blanks (*intensities presented at different scales)

The powder XRD analysis of the select samples resulting in patterns of well-defines peaks for all four samples (Figure 46), confirming the presence of a crystalline material. The majority of the peaks of significant intensity have at least a semblance of a match at the corresponding 2Θ of the other diffraction patterns, despite differences in uranium and/or calcium content. The regularities in these strikingly similar patterns suggest the presence of a crystalline solid phase that is consistently present, regardless of the other varying factors. Between the two uranium-containing sample diffraction patterns, it is worth noting that several of the matching peaks are of higher intensity in the calcium-free sample. It is believed that this difference in signal vs. background noise could explain the difficulty identifying any smaller peaks in the calcium-free sample.

XRD data evaluation, using *Match!* ® software, endorsed nitratine ($NaNO_3$) as the most probable major constituent of the precipitate. High concentrations of sodium silicate and concentrated nitric acid used at different stages of sample preparation can justify the formation of this solid phase. The comparison of both the calcium-containing and calcium-free samples with the diffraction pattern for nitratine show that the majority of the pattern's peaks align with a peak on the sample patterns (Figure 47 & Figure 48). The principal difference between the

two is the intensity of the most prominent peak in both patterns, $2\Theta \approx 29$, which peak near 3500 and 1200 in the calcium-free and calcium-containing samples, respectively. In the calcium-free sample, the clear disparities occur at peaks present in the sample at $2\Theta \approx 26.5$ & 47, though the relatively high background early in the pattern is believed to obscure other potentially significant peaks. Similarly, the calcium-containing sample shows peaks, some of which are of considerable intensity, which do not have a complement on the nitratine diffraction pattern, i.e., $2\Theta \approx 23.5$, 32.5, 34, & 41. If the nitratine identification is accurate, these unpaired peaks could substantiate the presence of a second crystalline phase. More specifically, they may represent the uranium-containing phase observed in prior SEM/EDS evaluation.

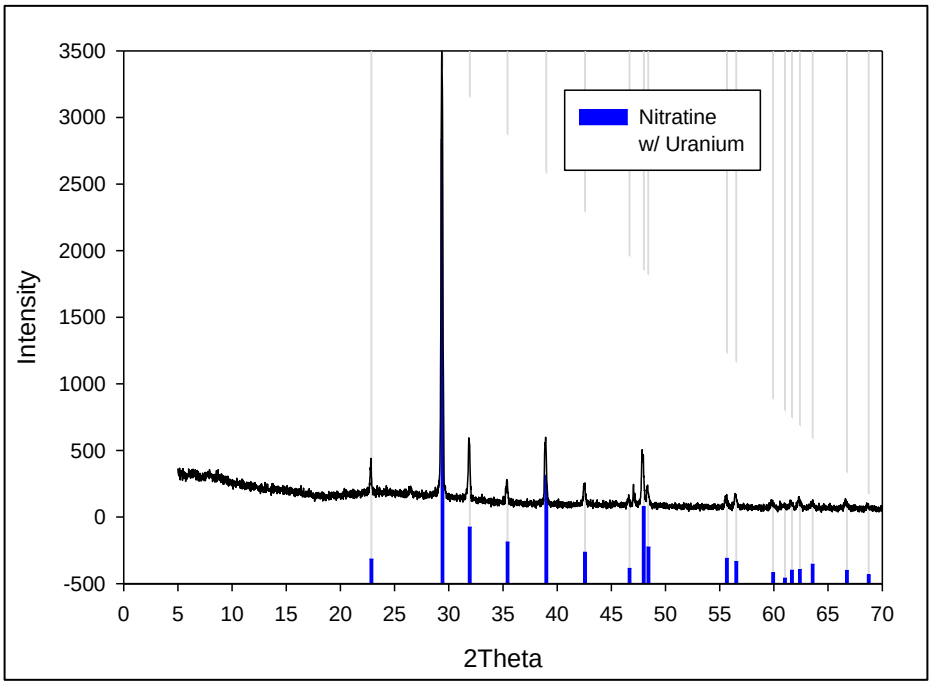

Figure 47. Comparison of the diffraction patterns of the uranium-containing (calcium-free) sample precipitate with the pattern for nitratine ($NaNO_3$)

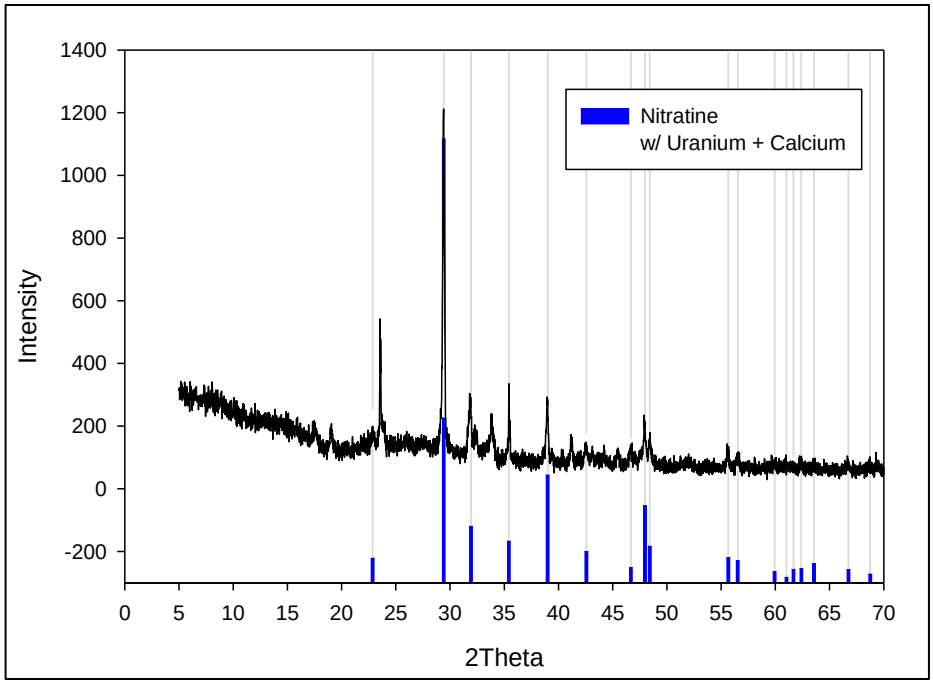

Figure 48. Comparison of the diffraction patterns of the uranium and calcium-containing sample with the pattern for nitratine ($NaNO_3$)

The visual MINTEQ speciation modeling predicted the formation of three modifications of calcium carbonate ($CaCO_3$) such as vaterite, aragonite, and calcite. The comparison of the experimental x-ray diffraction patterns with that of calcite showed that the samples' highest peak ($2\Theta \approx 29$) was aligned well with the most intense of the calcite peaks (Figure 49 & Figure 50). The additional peaks showed that some nearly aligned with those of the calcium carbonate pattern, though the ratios of their intensities did not match those of the reference. The calcite prediction is further complicated by the fact that the differences in the 2Θ values are in both directions. A uniform increase or decrease in all of the relevant diffraction angles would substantiate a systematic error that caused the shift, which could be corrected for, theoretically. This does not appear to be the case for these samples, though further analysis is ongoing. Characteristic peak data for aragonite and vaterite did not show any match with the samples' X-ray diffraction patterns (data not shown).

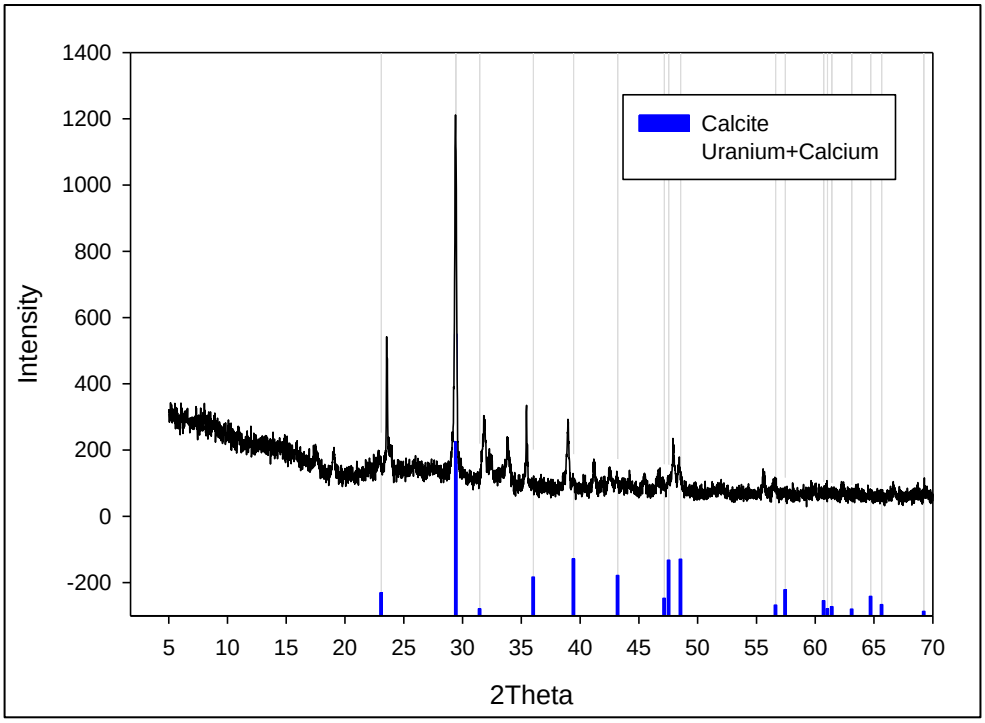

Figure 49. Comparison of the diffraction patterns of the uranium and calcium-containing sample with the pattern for calcite ($CaCO_3$)

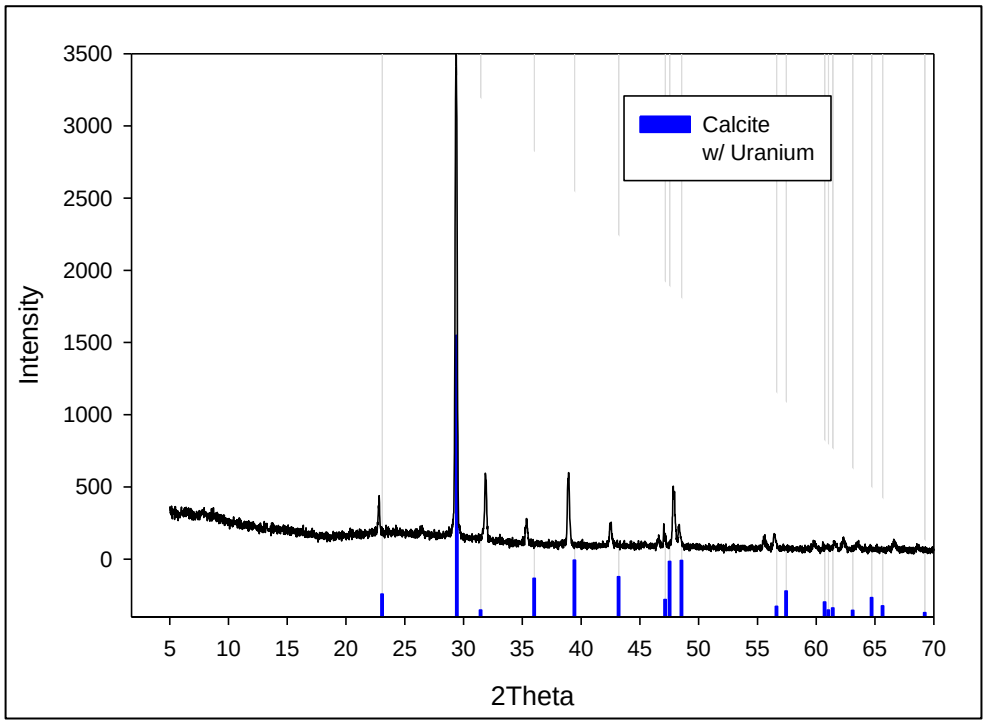

Figure 50. Comparison of the diffraction patterns of the uranium-containing (no calcium) sample with the pattern for calcite (CaCO3)

Though it had not been predicted by geochemical modeling software, cejkaite ($Na_4(UO_2)(CO_3)_3$) has emerged as a potential identity of the uranium-bearing phase that was visualized in the scanning electron micrographs. The comparison of the diffraction patterns revealed that two of the three most prominent peaks ($2\Theta \approx 17.5$ & 19) appear to have a corresponding match in the experimental diffractogram for the calcium-containing sample (Figure 51). A match for the third largest peak ($2\Theta \approx 11$) could not be conclusively identified though it is believed to have been concealed by the noisy background. The comparison to the calcium-free sample to the cejkaite XRD pattern show no apparent peaks at the same 2Θ values (Figure 52). If it is concluded that cejkaite is not formed in this sample, the higher peak intensities, compared to the calcium-containing sample could signify an indirect relationship between inclusion of calcium and the formation of cejkaite.

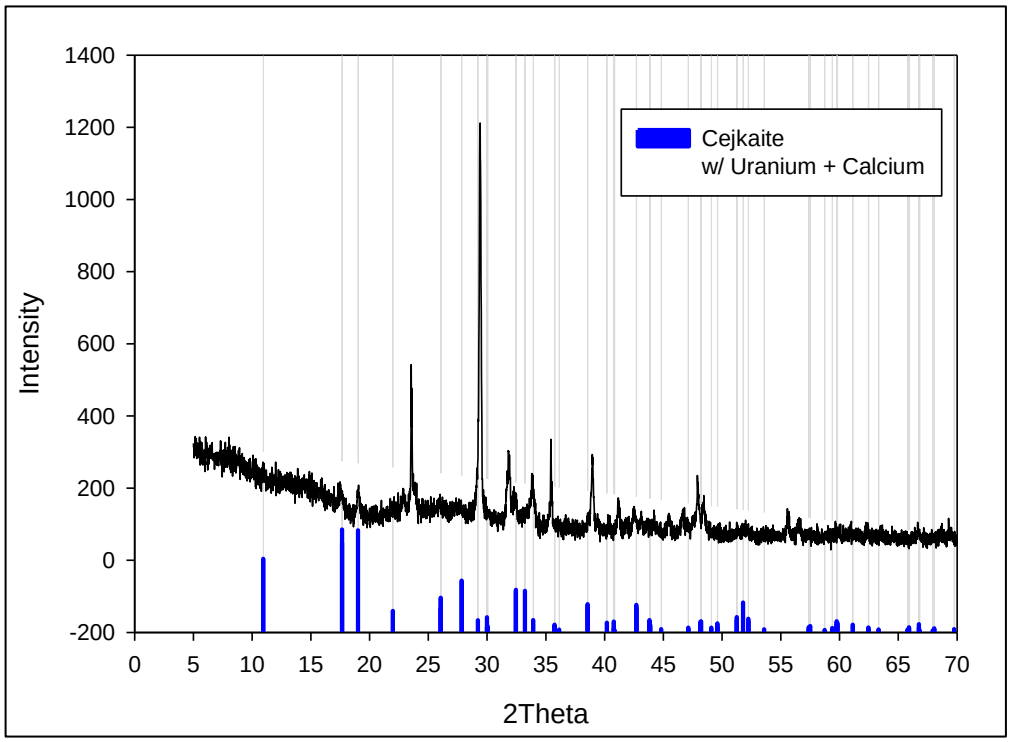

Figure 51. Comparison of the diffraction patterns of the uranium and calcium-containing sample with the pattern for Cejkaite ($Na_4(UO_2)(CO_3)_3$)

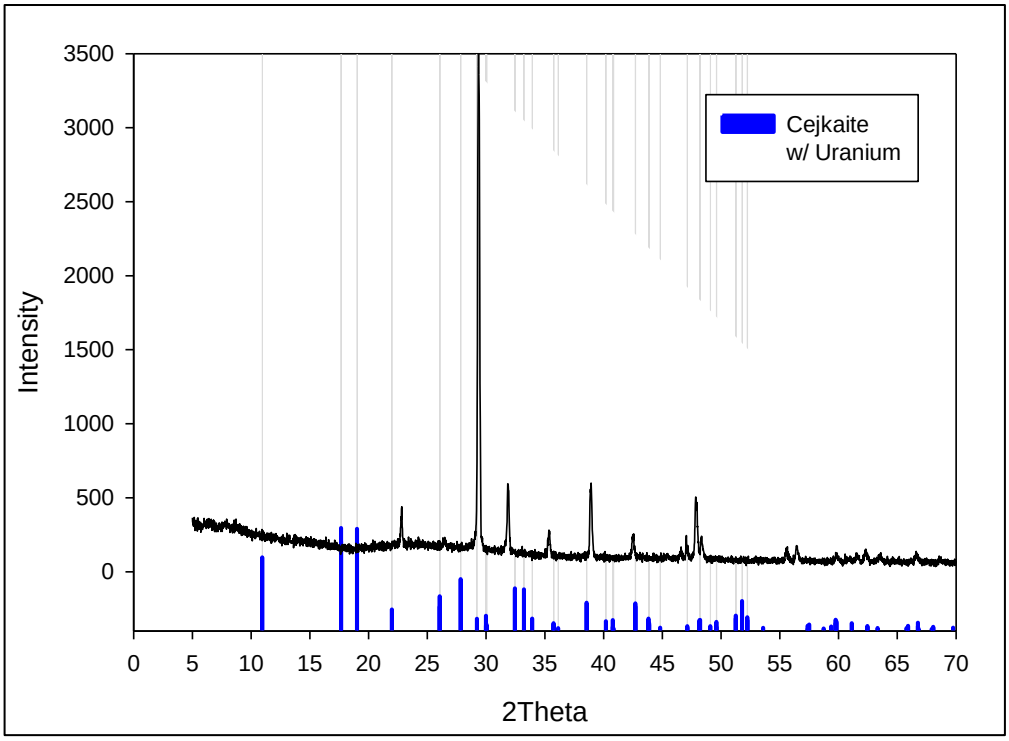

Figure 52. Comparison of the diffraction patterns of the uranium-containing sample with the pattern for Cejkaite ($Na_4(UO_2)(CO_3)_3$)

TASK 1.1 CONCLUSIONS

Uranium-bearing precipitates prepared with and without Ca and with "high"(50 mM) and "low" (3 mM) concentrations of bicarbonate were evaluated by means of SEM/EDS analysis. The experiments were also designed to test the effect of the centrifugation step during sample preparation procedures on the morphology of the precipitates. A comparison of the 50 mM and 3 mM bicarbonate samples definitively showed that the expected uranium-rich crystal forms were exclusive to samples prepared with a high bicarbonate concentration. Similarly, the amorphous uranium-dense areas were far more prevalent in the high bicarbonate samples. Uranium solids were found on the surface of amorphous precipitates and were trapped within internal structures and cavities of amorphous phases.

Though the EDS comparison of the centrifuged and non-centrifuged samples provided little insight into the differences between the two, the evaluation of the supernatant solutions of the two samples showed a distinct increase in uranium content with centrifugation, signifying a decrease of uranium in the precipitate. The loss of uranium from the precipitate not being ideal, it was concluded that the centrifugation step was not suitable for use in future experimentation. The comparison of the individual solution method analyzed in a sacrificial mode applied for batch 2 sample preparation, and the single primary "mother solution" method, used for batch 3, showed a stark contrast. The most noticeable difference included the scarcity of crystalline-like areas with high uranium content in samples prepared by the latter. This unambiguous difference allowed it to be decided that the batch 2 sample preparation procedure was the best process for

future use. Together, these experimental results allow for optimization of a sample preparation methodology that can be used as the project continues forward.

Although Raman Microscopy did not allow for a distinction between the fine uranium-bearing particulates and the rest of the sample for more precise analysis, general scans of the sample revealed peaks consistent with what would be expected of a uranyl carbonate. The experimental findings published in 2009 by Stefaniak et al. showed relatively consistent bands for the major components of a variety of uranium minerals when analyzed by Raman Microscopy, which support our conclusions. Further Raman analyses to corroborate these inferences are ongoing.

Based on the analysis of X-ray diffraction data by *Match!* software, the majority of the more intense peaks, including the intense band featured around the 2Θ value of 29 in all analyzed samples, best corresponded to the diffraction pattern of nitratine ($NaNO_3$). Though the accuracy of this identification is still being investigated, it is plausible based on the abundance of sodium and nitrate ions provided to the system through the addition of sodium silicate (Na_2SiO_3) and the adjustment of pH by concentrated nitric acid. If the nitratine prediction is further validated, an alternative sample preparation method that limits its formation will be investigated.

The theorized identity of the uranium-bearing solid phase observed in the calcium-containing samples is Cejkaite, a sodium-uranium-carbonate mineral of the formula $Na_4UO_2(CO_3)_3$. Due to the limited library, this phase was not predicted or considered by the geochemical modeling software employed. Complimentary experimentation and analysis to corroborate this prediction are ongoing.

TASK 1.2 INVESTIGATION ON MICROBIAL-META-AUTUNITE INTERACTIONS: THE EFFECTS OF BICARBONATE AND CALCIUM IONS

TASK 1.2 BACKGROUND

Aqueous carbonate present in the soil and ground water is a primary species increasing uranium mobility by affecting the dissolution of actinide and promoting the uranium desorption reaction from soil (Langmuir 1978). In a calcium-rich environment, the large formation constants of soluble and stable calcium uranyl carbonate complexes [$Ca_2UO_2(CO_3)_3^0$(aq); $CaUO_2(CO_3)_3^{2-}$] influence the speciation of uranium (Langmuir 1978, Bernhard et al. 2001). Previously, the significance of bacteria-uranium interactions has been illustrated by focusing on three bacterial strains of *Arthrobacter* sp, isolated from Hanford Site soil (Katsenovich et al. 2012b). The *Arthrobacter* bacteria are one of the most common groups in soils and are found in large numbers in Hanford soil as well as other subsurface environments contaminated with radionuclides (Boylen 1973, Balkwill et al. 1997, Van Waasbergen et al. 2000, Crocker et al. 2000). Balkwill et al. (1997) reported the predominance of the genus *Arthrobacter* among the culturable aerobic heterotrophic bacteria from the Hanford Site sediments with this group accounting for roughly up to 25% of the subsurface isolates. In addition, *Arthrobacter*-like bacteria were the most prevalent in the highly radioactive sediment samples collected underneath the leaking high-level waste storage tanks and accounted for about one-third of the total soil isolatable bacterial population (Fredrickson et al. 2004). Furthermore, a previous study conducted using the *Arthrobacter oxydans* G975 strain illustrated a bio-enhanced release of U (VI) from natural Ca-autunite in the presence of various concentrations of bicarbonate. G975 was found to be the fastest growing and the most uranium-tolerant strain among the studied microorganisms obtained from the Subsurface Microbial Culture Collection (SMCC) (Katsenovich et al. 2012b). This bacterial strain is ubiquitous in subsurface microbial communities and can play a significant role in the dissolution of minerals and the formation of secondary minerals (Katsenovich et al. 2012b). This research was extended to investigate the stability of autunite mineral in oxidized conditions pertaining to the Hanford Site and to study the effect of *Arthrobacter* oxydans SMCC G968 strain on the U (VI) release from autunite. This strain was found to be less resistant to the U (VI) toxicity. The alteration in surface morphology for G968 was noted at 0.5 ppm of U (VI); in comparison, G975 shows signs of cell inhibition at the much higher concentration of 19 ppm of U (VI). Additionally, the G975 strain accumulated up to 92% of uranium in the studied U (VI) concentration range up to 27 ppm, which is almost triple the value compared to the G968. The results on cell density for G968 determined via hemocytometer showed slightly lower values for the same period compared to G975 (Katsenovich et al. 2012a).

TASK 1.2 OBJECTIVES

The main objective of this investigation was to analyze the bacterial interactions of a less U (VI)-tolerant bacteria strain under oxidizing conditions with uranium and to study the potential role of bicarbonate, which is an integral complexing ligand for U (VI) and a major ion in groundwater compositions. More specifically, the objectives of this task were to: (1) Investigate

the effect of bicarbonate on the microbial dissolution of the autunite mineral and U (VI) adsorption by Arthrobacter G968; (2) Make a comparison between G975 and G968 strains; (3) Inspect bacterial surface in the presence of bicarbonate and uranium in the solution using atomic-force microscopy (AFM); (4) Determine the difference between microbial dissolution of synthetic autunite versus natural autunite.

TASK 1.2 MATERIALS AND METHODS

Arthrobacter Strains and Growth Culture Conditions

The strains were cultured in 5% PYTG liquid culture media and agar plates consisting of 5 g/L peptone, 5 g/L tryptone, 10 g/L yeast extract, 10 g/L glucose, 0.6 g/L $MgSO_4.7H_2O$, and 0.07 g/L $CaCl_2.2H_2O$. Media was prepared in deionized water (DIW) (Barnstead NANOpure Diamond Life Science (UV/UF), Thermo Scientific), autoclaved at 121^oC and 15 psi for 15 minutes, then allowed to cool before being used.

To account for viable bacteria, a well-mixed homogeneous aliquot (0.01 mL - 0.1 mL) of the suspension from each test vial was uniformly spread on sterile Petri dishes containing a 5% PTYG growth media mixed with 15 g/L of agar. Inoculated plates were kept inverted in an incubator at 29^oC. Viable microorganisms were calculated from the number of colony-forming units (CFU) found on a specific dilution. In addition, the agar plating was used to provide a quick visual check for contamination and to maintain colonies from each stage of the enrichment for the duration of the experiment. The cell density (cells/mL) was calculated with the help of a glass hemocytometer (Fisher Scientific, Pittsburg, PA). Cell counts in the samples containing uranium employed INCYTO C-Chip disposable hemocytometers. The hemocytometer is a microscope slide with a rectangular indentation, creating a chamber that is engraved with a grid of perpendicular lines. Having known the area bounded by the lines as well as the depth of the chamber, the cell density in a specific volume of fluid and in a bacterial broth solution was calculated from a sample, homogenously distributed inside the chamber. Once the average cell count was obtained, it was multiplied by the dilution factor and the volume factor, 10^4, in order to calculate the final concentration of cells per mL.

Dissolution of U(VI) from Autunite

Two different kinds of bioreactors were used in the bioleaching experiments: (1) Sterile 100 mL glass mixed reactors served as the major bioreactor for initial experimentation. These autunite-containing bioreactors were injected with bacterial cells after the autunite equilibrated with the media solution. (2) Sterile culture ware with inserts where bacteria and autunite were kept separated.

Bicarbonate Media Solution Preparation

The media solution to conduct the autunite dissolution experiments was prepared using 0.25 g/L peptone, 0.25 g/L tryptone, 0.5 g/L glucose, 0.6 g/L $MgSO_4$, and 0.07 g/L $CaCl_2{\cdot}2H_2O$. Due to the high phosphorus content, yeast extract was not included in the media. Media was prepared in deionized water (DIW) (Barnstead NANOpure Diamond Life Science (UV/UF), Thermo Scientific), autoclaved at 121^oC, 15 psi for 15 minutes, and cooled to about 30^oC. After sterilization, the media was equally distributed between four 200-mL bottles and separately

adjusted to contain 0 mM, 3 mM, 5 mM, and 10 mM of $KHCO_3$. The media was adjusted to pH 7.5 with 0.1 mol/L HCl or NaOH and buffered with 0.02 M 2-(2-hydroxyethyl)-1-piperazine ethanesulfonic acid sodium salt hydrate (HEPES-Na) buffer. Each of the individual four bicarbonate media solutions were filtered-sterilized (0.2 µm) and kept refrigerated until time of use.

Autunite bioleaching in mixed reactors

Natural Ca meta-autunite, $Ca[(UO_2)(PO_4)]_2 \cdot 3H_2O$, obtained from Excalibur Mineral Corporation (Peekskill, New York), was previously characterized using ICP-OES, ICP-MS analyses, X-ray diffraction and SEM/EDS to confirm the mineral composition, structure, and morphology as 98-99% pure autunite (Wellman et al. 2006). The autunite sample was powdered to have a size fraction of 75 to 150 µm or -100 to +200 mesh with a surface area of 0.88 m^2/g determined by Kr-adsorption BET analysis (Wellman et al. 2006). Autunite microbial bioleaching experiments were conducted with 100-mL foam-stoppered glass serum bottles containing 50 mL of sterile media buffered with 20 mM HEPES-Na and 91 mg of meta-autunite to provide an U(VI) concentration of 4.4 mmol/L. The suspensions were slightly agitated at 60-rpm in incubator/shaker at 25 ^oC. G968 *Arthrobacter* cells in the amount of 10^6 cells/mL were injected into the reactors after 27 days, giving time for the autunite to reach steady state. During the inoculation, reactors kept their sterile foam stoppers to sustain aerobic conditions within the reactors. Abiotic non-carbonate controls were kept without bacterial inoculation to provide a control for the biotic samples.

Autunite bioleaching in culture ware with inserts

Synthesis of Na-autunite, $Na\ [(UO_2)\ (PO_4)] \bullet 3H_2O$, was followed by a modified direct precipitation method described by Wellman et al. (2005). Uranyl nitrate and sodium phosphate dibasic solutions were mixed in a volumetric ratio of 1:7.5 at 70^oC while stirring; heat was terminated after a yellowish green precipitate was formed. X-ray diffraction analysis was performed on the synthesized autunite mineral at 40 kV and 40 mA using a Bruker 5000D XRD instrument. Diffraction patterns were obtained using a copper radiation source with a tungsten filter. The sample was analyzed in the range of 2 to 35^o for the 2-theta (2Θ) with a 0.04^o step increment and a two-second count time at each step. The XRD diffraction patterns were consistent with PDF# 049-0432 for Na-meta-autunite I (mAut I), $Na\ [(UO_2)\ (PO_4)] \bullet 3H_2O$, obtained from PNNL for comparison. The synthesized autunite solids were characterized by a JSM-5900-LV low vacuum scanning electron microscope (SEM) at 15kV for identification of the particle sizes. The elemental composition and purity of the solids were determined via a Noran System Six Model 200SEM Energy Dispersive X-Ray Spectroscopy (EDS). The Na: O: P: U atomic ratios of 1.08:5.69:1.00:1.04, determined by means of EDS analysis, corresponded to an ideal empirical formula of $Na\ [UO_2PO_4]$ as 1:6:1:1. Pre-experimental surface area analysis was conducted following the N_2-adsorbtion BET method (Brunauer et al. 1938) by using a Micromeritics ASAP 2020 surface and porosity analyzer at PNNL. Sterile 6- well cell culture plates with inserts were used in the non-contact bioleaching experiments with natural Ca meta-autunite and bacteria cells were kept separately. A 3.2 ml aliquot of sterile media was dispensed in the appropriate well and 2.5 ml inside the insert receptacle. The total volume inside each well added up to 5.7 ml. The culture ware inserts have 0.4 µm cylindrical pores that transverse the membrane and only allow the diffusion of soluble

uranium. Ten mg (10 mg) of sterilized autunite powder was added to the bottom of the wells to reach a concentration of 4.4 mmol/L. Abiotic controls were prepared to make a comparison with the bacteria bearing wells. Uranium leaching from autunite was established by taking a 20µL sample from the inserts and processing it on the KPA instrument, described in greater detail in the next section.

Analytical Procedures

Every few days, a 0.3 mL sample of the solution was aseptically withdrawn from each bottle, filtered (0.2 µm), and then analyzed for dissolved U(VI) by means of kinetic phosphorescence analyzer KPA-11 (Chemcheck Instruments, Richland, WA). The dilution factors for sample analysis were 100 for low concentrations of bicarbonate and 200 for high concentrations of bicarbonate. Prior to this analysis, sample aliquots were ashed on a hot plate with the addition of concentrated plasma-grade nitric acid and hydrogen peroxide solutions. Wet digestion was continued until a dry white precipitate formed, and then dry ashing was performed in the furnace at 450^{o}C for 15 min. Samples were allowed to cool at room temperature followed by the dissolution of the precipitate by the addition of 1 M nitric acid (HNO_3). Aqueous concentrations of calcium and phosphorus were determined from the digested samples by means of Optima 7300 ICP-OES (Perkin Elmer). Uranium calibration standards (SPEX certiPrep), blanks and check standards (95-105% recovery) were analyzed for quality control.

Statistical Analysis

The bioleaching experiment was conducted in triplicate to obtain descriptive statistical analyses such as mean, standard deviation and confidence interval of the mean. Uranium calibration standards (SPEX certiPrep), blanks, and check standards (95-105% recovery) were analyzed for quality control before each experiment utilizing the KPA to check the variability of the machine.

SEM/EDS microscopy analysis

Growth Conditions

The Arthrobacter strains were aerobically grown to reach confluency in 15-mL polypropylene sterile foam-stoppered centrifuge tubes amended with 4 mL of Na- HEPES buffer media at 25˚C. The cell stock suspension was counted using an INCYTO C-chip disposable hemocytometer to establish the number of cells in the media needed to obtain the desired concentration. The tubes were inoculated with approximately log 7.5 bacterial cells/mL. Uranium was injected in the form of uranyl nitrate stock solution to produce the desired concentration of 5 ppm and 10 ppm. The samples were prepared at 24 hours to: obtain cell count, prepare samples for microscopy analysis via AFM, scanning electron microscope (SEM) and energy dispersive x-ray spectroscopy (EDS).

Cell Surface Composition Analysis

The purpose of SEM/EDS was to show surface morphology and cell surface composition in the presence of bicarbonate. Sample preparation for this analysis included centrifugation of the G968 bacterial cells at 4000 rpm for 5 min from PTYG media amended with certain concentrations of U (VI) and washed twice with deionized water. The pH of the HEPES media

was adjusted to 7.2 with concentrated Fisher Scientific nitric acid (HNO_3). The cells were fixed in the 5 ml of 2% glutaraldehyde in 0.1M HEPES buffer at pH 7.2 for 2h at 4^{o}C. The material was removed by centrifugation and washed with 50 mM HEPES buffer three times for 10 min. The rinsed cells were then dehydrated in ethanol/ water solutions of 35% (v/v), 70% (v/v), and 90% (v/v) each for 10 min, and two times in 100% (v/v) for 10 min. Dehydrated samples were immersed for 10 min each in 50% and 100% pure hexamethyldisilazane (HMDS) (Pierce Biothechnology, Inc, obtained from Fisher Scientific) followed by 10 min of air-drying to allow the liquid to evaporate from the sample. The dehydrated specimens were then kept in the desiccators until the time of SEM/EDS assay. The dehydrated specimens were mounted on the SEM mounting plates with double-sided sticky carbon tape and then coated for one minute with a thin layer of gold to increase conductivity. The cell surface composition of gold-coated samples (PAC-1 PELCO Advanced coater 9500) was analyzed using a SEM-Energy-Dispersive-Spectrometry (SEM-EDS) JEOL System Model 5900LV.

AFM microscopy analysis on bacteria uranium interactions

Sample Preparation for AFM Imaging

The bacterial cells were grown in a synthetic groundwater (SGW) media that contained 5.22 mg/L of KCl, and 520.58 mg/L of HEPES. The lack of organic nutrition in the media is to prevent an interface with the imaging in case the uranium interacts with the organics to produce a precipitate. The media was prepared in deionized water, autoclaved at 121^{o}C, 15 psi for 15 minutes, and allowed to cool to about 30^{o}C. Then it was equally distributed between three 250-mL bottles and separately amended to contain 0 mM, 3 mM and 5 mM $KHCO_3$. The samples that were analyzed included: 0 mM HCO3 with 5 ppm U, 0 mM HCO3 with 10 ppm U, and 5 mM HCO3 with 5 ppm U. The bacterial samples were washed three times with deionized water from U (VI) and media residuals and were then immobilized onto the 3-aminopropyltrimethoxysilane coated silicon wafer substrates. A concentrated sample of about 7 µl was dropped onto a silanized silicon wafer. Samples were air dried until excess moisture was evaporated. The substrates were then fixed onto a metallic disc and transferred to an AFM stage to begin imaging. The bacterial cells must be firmly affixed onto a silicon wafer substrate so the sample remains stable during imaging.

Atomic Force Microscopy Instrumentation and Imaging

Atomic force microscopy (AFM) was conducted using a PicoScan AFM (former Molecular Imaging Inc. now Agilent Series 4500 SPM, PicoSPM) for all AFM imaging analysis. Silicon AFM probe tip (NanoAndMore, USA) with a force constant of 0.2 N/m, resonating frequency of 15 kHz was used. Due to instrumental limitations, the contact mode was used for imaging. The cantilever is 500 µm in length, 30 µm in width, and 2.7 µm thick. The tip shape is rotated and the tip radius is <10 nm. The AFM tip is 20-25 degrees along the cantilever axis; 25-30 degrees from the side and 10 degrees at the apex. In addition, information on the surface topography of cells exposed to U (VI) was obtained, while laboratory conditions were at 25ºC and 55% relative humidity. Along with topographical imaging, a quantitative analysis was conducted: roughness measurements and force spectroscopy were obtained. To avoid cells dehydration, the AFM analysis was performed within two hours of preparation.

Roughness Measurements

AFM instrument is essential for measuring and studying surface roughness at the nanoscale. The measured roughness depends on the spatial and vertical resolution of the instrument. Two main factors are capable of affecting the resolution of the surface roughness measurement: (1) the AFM instrument noise limits the vertical resolution; (2) and the tip radius limits the spatial resolution. Tip wear also affects the precision of the measurement. The roughness value was determined by taking the relative heights of individual pixels in the image over a selected area. The average roughness analysis was calculated from the average of the absolutely values of the profile height from the mean level.

Force Spectroscopy

Forces experienced by the cantilever as it approaches the sample from several microns above the surface can provide information about long-range interactions. As the tip gets closer to the surface, short-range forces, such as Van der Waals or capillary forces can be measured. Once the tip has come into contact with the sample surface, it may be pushed into the surface with some force, where viscoelastic properties can be analyzed to provide data for Young's modulus or stiffness for different strain rates or maximum applied forces. More importantly, when the cantilever is pulled away from the surface, adhesion forces can be measured. Adhesion forces are sensitive to modifications in the surface, such as physiological changes on the cellular membrane when exposed to uranium and bicarbonate. Thus, a force spectroscopy analysis was conducted to gain a full understanding of interactions at the atomic level. The force is calculated using a force distance curve which plots the retraction of the cantilever on the x-axis and the cantilever property that is being measured, such as the deflection of the cantilever on the y-axis. The average adhesion force was obtained from an average of 16 different force distance curves in a 3.2µm x 3.2µm sample surface.

TASK 1.2 RESULTS AND DISCUSSION

Bioleaching of U(VI) from Autunite

The release of aqueous U(VI) over time during the synthetic autunite dissolution experiment is presented in Figure 53. The bioreactors were injected with G968 Arthrobacter cells after 29 days, giving time for the synthetic autunite to reach steady state. The steady state maximum concentrations of U(VI) detected were 2.1, 8.8, 52.3, 88.4 fold higher than the abiotic control without the bicarbonate amendment. Furthermore, after bacteria inoculation, U(VI) concentrations measured in the reactors, increased 0.97±0.024, 0.43±0.42, 0.89±227.08, and 0.78±0.37 fold for 0 mM, 3 mM, 5 mM and 10 mM $KHCO_3$, respectively. From the figure, it can be inferred that despite the increased amount of U(VI) released in the presence of bacteria, the effect of bacteria on the synthetic autunite dissolution is reduced as the concentration of bicarbonate increases. Since the steady-state U(VI) concentration is higher for larger [HCO_3^-], the increase in soluble U(VI) concentration induced by bacteria is dwarfed. Therefore, as [HCO_3^-] increases, a diminishing trend on the effect of bacteria on autunite leaching is observed. This is very similar to previous experimentation conducted with natural autunite,

only slightly higher. Currently, the aqueous concentrations of calcium, sodium and phosphorus are being determined from the digested samples using Optima 7300 ICP-OES (Perkin Elmer).

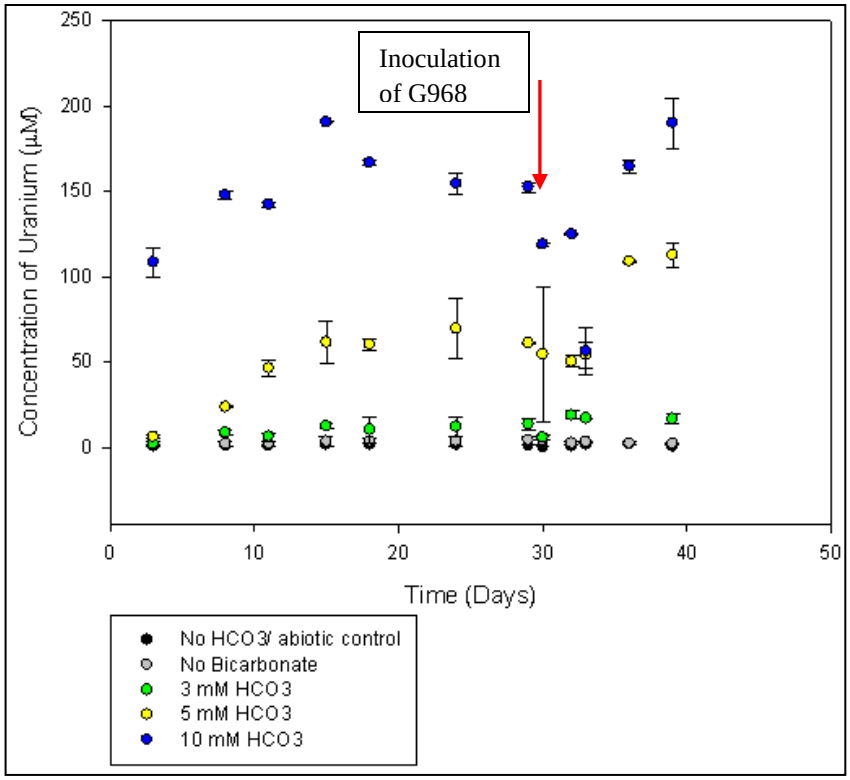

Figure 53. Changes for aqueous U (VI) as a function of time for the synthetic autunite dissolution experiments inoculated with Arthrobacter G968 strain.

In addition, an investigation with natural autunite mineral separated from bacteria was conducted using culture ware with inserts. The release of aqueous U (VI) over time during the autunite leaching in non-contact experiments is represented in Figure 54. The steady state maximum concentrations of U (VI) detected were 3.57, 1.34, 1.42, 2.27 fold higher than the abiotic control without the bicarbonate amendment. Furthermore, after bacteria inoculation, U (VI) concentrations measured in the reactors, increased 0.68 ± 1.48, 1.59 ±0.49, 1.02±0.98, 0.93 ±0.39 fold for 0 mM, 3 mM, 5 mM and 10 mM $KHCO_3$, respectively. So, there is a slight increase in the dissolution of uranium as bicarbonate increases; however, this is not as pronounced when compared to G975 or dissolution in bioreactors (when autunite, bicarbonate and bacteria have direct contact). This may be due to the preventive measures taken to reduce evaporation in the bioreactors, such as the small volume of media or low temperature. These measures were not optimum conditions for bacterial growth and proliferation.

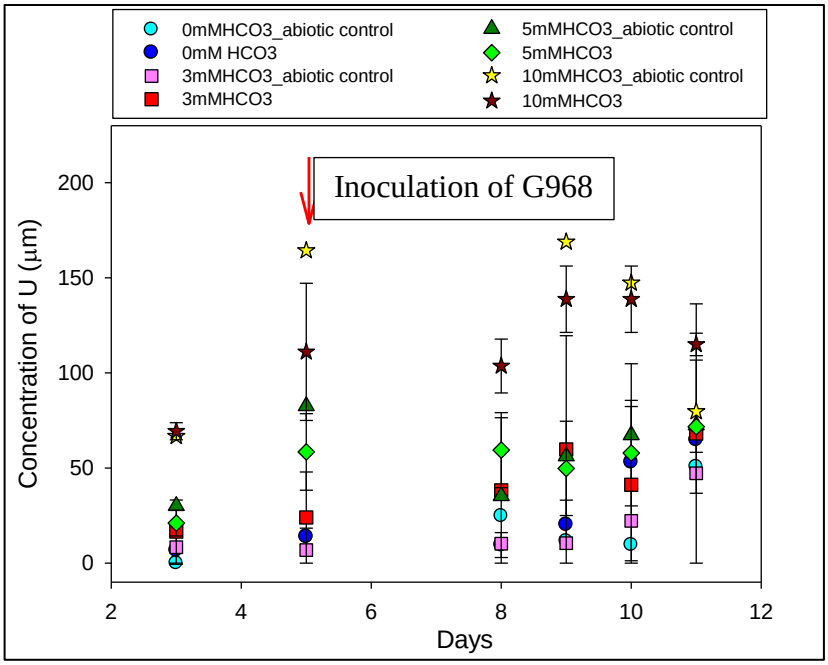

Figure 54. Changes for aqueous U (VI) as a function of time for the non-contact natural autunite dissolution insert experiments inoculated with Arthrobacter G968 strain.

SEM observations were purely qualitative analyses that showed the surface morphology of bacteria in the presence of various concentrations of uranium in bicarbonate bearing media. It also further illustrated that the bacterial cells looked healthier in the presence of bicarbonate (Figure 55 through Figure 58). Much less damaged cells were observed in the presence of bicarbonate.

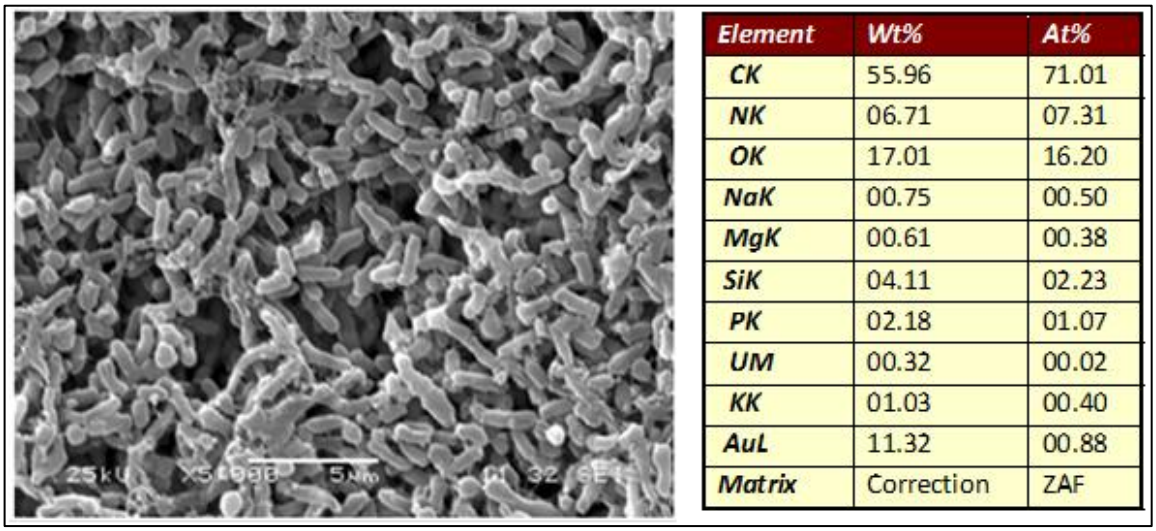

Element	Wt%	At%
CK	55.96	71.01
NK	06.71	07.31
OK	17.01	16.20
NaK	00.75	00.50
MgK	00.61	00.38
SiK	04.11	02.23
PK	02.18	01.07
UM	00.32	00.02
KK	01.03	00.40
AuL	11.32	00.88
Matrix	Correction	ZAF

Figure 55. G968 grown in the presence of 0 mM KHCO3 with 5 ppm U and EDS spectrum analysis.

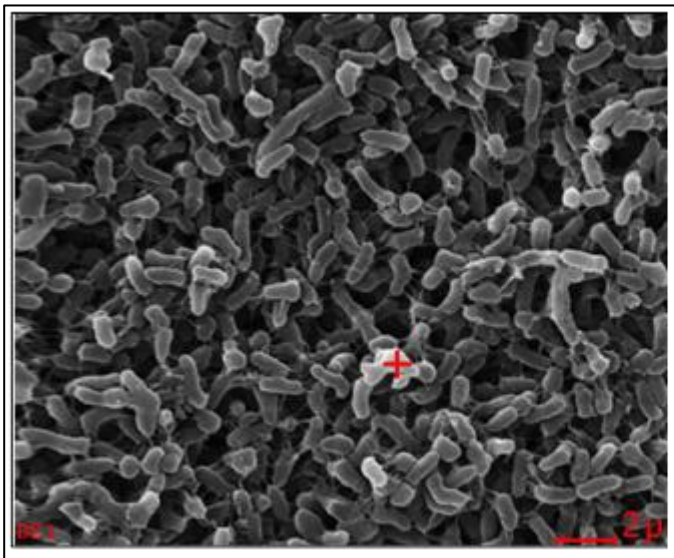

Element	Wt%	At%
CK	57.65	71.83
NK	06.06	06.47
OK	17.37	16.25
NaK	00.86	00.56
MgK	00.76	00.47
SiK	03.80	02.03
PK	02.28	01.10
SK	00.40	00.19
UM	00.25	00.02
KK	00.91	00.35
AuL	09.65	00.73
Matrix	Correction	ZAF

Figure 56. G968 grown in the presence of 0 mM KHCO3 with 10 ppm U and EDS spectrum analysis.

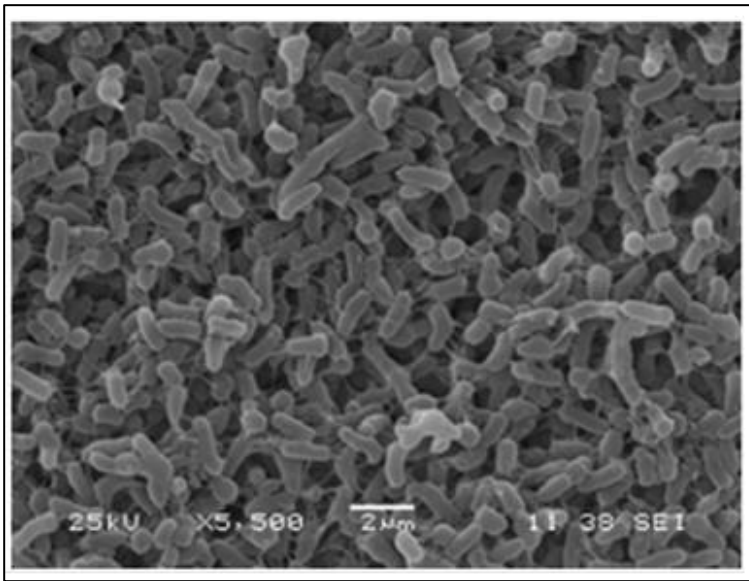

Element	Wt%	At%
CK	48.22	64.92
NK	09.08	10.48
OK	17.98	18.17
NaK	00.47	00.33
MgK	00.40	00.27
SiK	05.58	03.21
PK	01.70	00.89
UM	00.26	00.02
KK	00.92	00.38
CaK	00.20	00.08
AuL	15.18	01.25
Matrix	Correction	ZAF

Figure 57. G968 grown in the presence of 5 mM KHCO3 with 5 ppm U and EDS spectrum analysis.

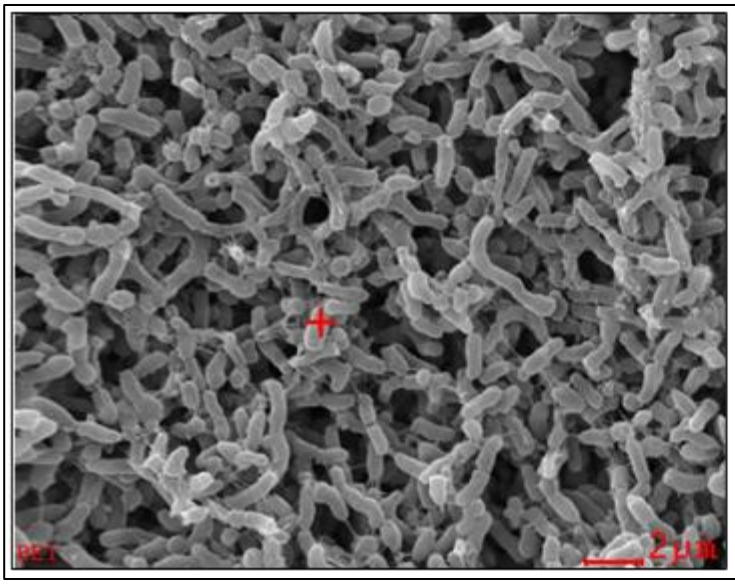

Element	Wt%	At%
CK	47.61	64.87
NK	07.24	08.46
OK	21.16	21.64
NaK	00.65	00.46
MgK	00.23	00.16
SiK	03.12	01.82
PK	01.42	00.75
UM	00.07	00.00
KK	00.56	00.23
CaK	00.34	00.14
AuL	17.60	01.46
Matrix	Correction	ZAF

Figure 58. G968 grown in the presence of 5 mM KHCO3 with 10 ppm U and EDS spectrum analysis.

The identification of the cell surface composition was achieved by EDS analysis. EDS spectrums of uranium-loaded samples have confirmed the presence of a low percentage of uranium in the cell surface composition. The EDS spectrum showed that the sample was composed of uranium, oxygen, phosphorus, carbon, silica, potassium and sodium. However, EDS analysis showed a small percent weight of uranium because the amount added to the sample solution was not sufficient to be detected by the SEM/EDS instrument. Furthermore, there was not a big different in the U atomic percentage among samples amended with bicarbonate and without bicarbonate. In addition to the qualitative images above, SEM and EDS analysis was conducted to evaluate G968 microbial growth and changes on the cell surface morphology under natural autunite exposure (a previous experiment referenced in the 2011 Year End Report) (Figure 59-Figure 62).

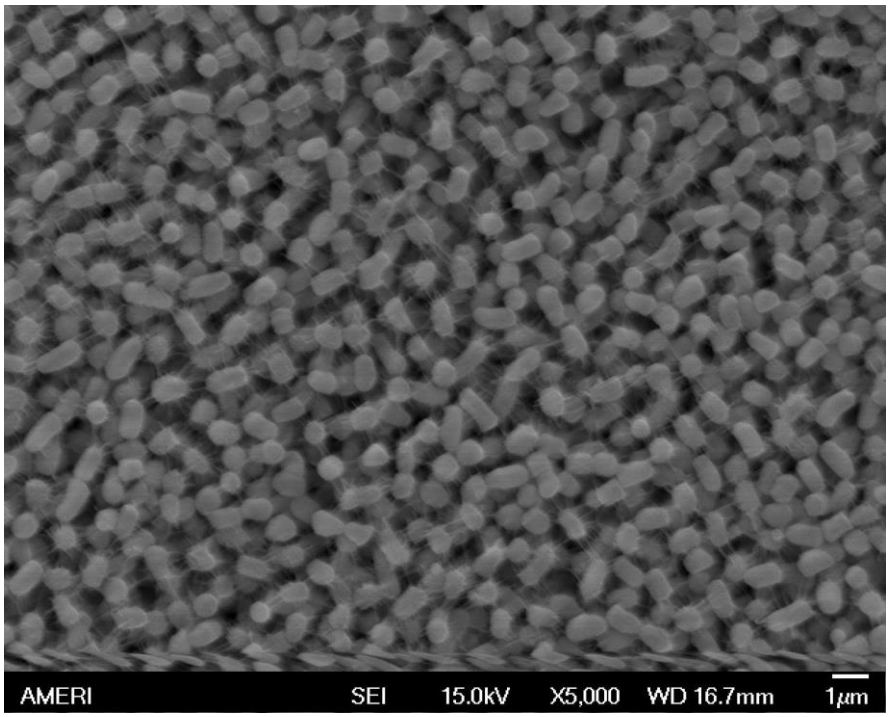

Figure 59. SEM images of G968 grown on autunite surface in the presence of 5 mM KHCO3. Bacterial cells appear to not look damaged in the presence of bicarbonate.

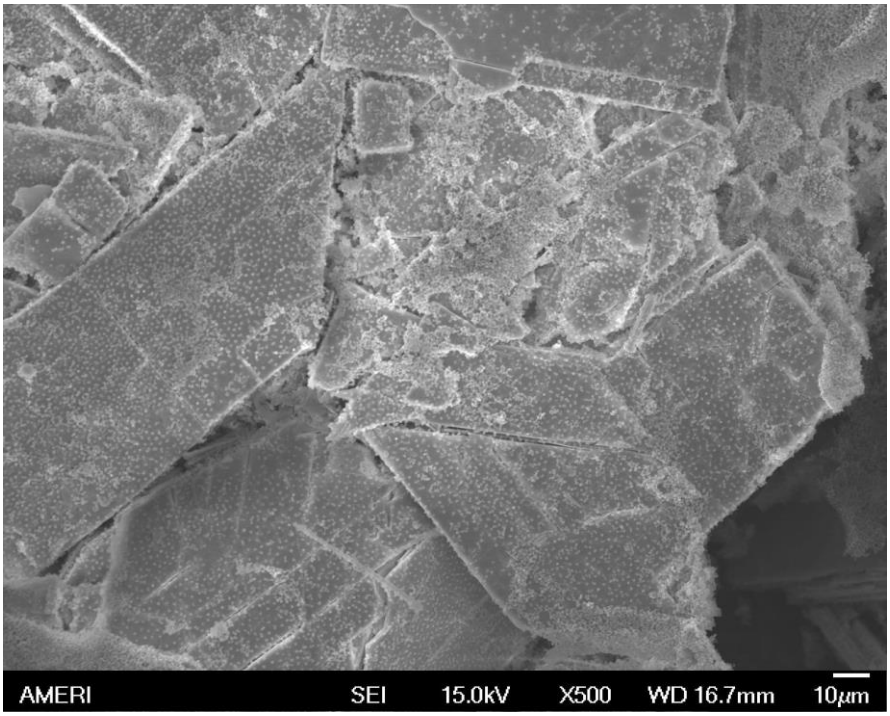

Figure 60. SEM images of post-reacted autunite mineral incubated in biotic reactors augmented with 3 mM $KHCO_3$. Illustrates the attachment of bacterial cells to autunite mineral.

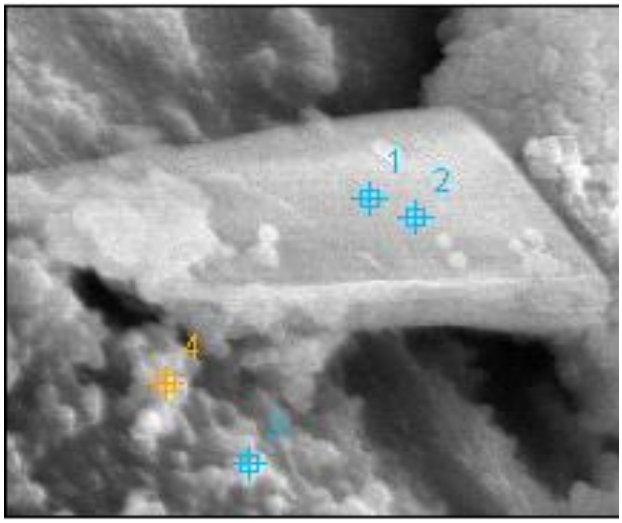

	pt1	*pt2*	*pt3*	*pt4*
C-K	24.1	25.2	70.9	67.3
N-K	3.9	2.8	9.4	12.9
O-K	29.4	29.6	17.5	18.3
Na-K	0.08	0.2	0.1	0.1
P-K	4.3	4.2	0.1	0.2
K-K	0.9	1.3	0.2	0.2
Ca-K	1.9	1.8	0.03	0.09
U-M	35.4	35	1.7	0.9

Figure 61. SEM/EDS analysis of biofilm created by G968 strain on autunite surface and compositional analysis (% weight) for each point at 5 mM HCO3. Points 1 and 2 illustrate the autunite mineral while points three and four represents bacterial cells, justifying the low % weight of uranium.

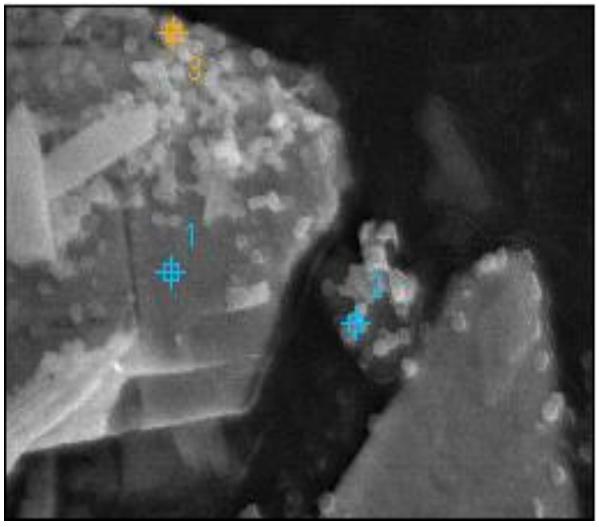

	pt1	*pt2*	*pt3*
C-K	**20.4**	**62.8**	**56.5**
N-K	**2.7**	**6.9**	**7.9**
O-K	**18**	**14.7**	**16.6**
Na-K	**0**	**0.1**	**0.1**
P-K	**5.9**	**1.3**	**1.7**
K-K	**2.5**	**1**	**0.6**
Ca-K	**0.2**	**0.02**	**0.05**
U-M	**50.2**	**13.2**	**16.6**

Figure 62. SEM/EDS analysis of biofilm created by G968 strain on autunite surface and compositional analysis (% weight) for each point at 10 mM HCO3. Point 1 illustrates the autunite mineral while points two and three represent the presence of G968 on the surface.

Effect of Uranium on Microbial Surfaces Using Atomic Force Microscopy

Atomic force microscopy (AFM) was used to monitor changes at the nanoscale level in cell surface topography, roughness and adhesion after the cells exposure to various concentrations of uranium. The aim of this task was to present high-resolution AFM results on the formation of microbial uranyl-phosphate precipitates on the bacterial surface. The results demonstrated the ability of this method to qualitatively and quantitatively analyze uranium precipitation on live bacterial cell surfaces of a less uranium tolerant Arthrobacter strain, G968.

Uranium Precipitation on the Microbial Cell Surface

Microscopic observation revealed a closer microscopic analysis on surface morphology in the presence of bicarbonate and uranium in the solution. The bright areas on the image below illustrate higher adhesion areas of the bacterial cell and uranium precipitates on the surface and can explain an increase in the surface roughness and changes in adhesion forces; while, the darker regions represents to lower adhesion areas of bacterial surface.

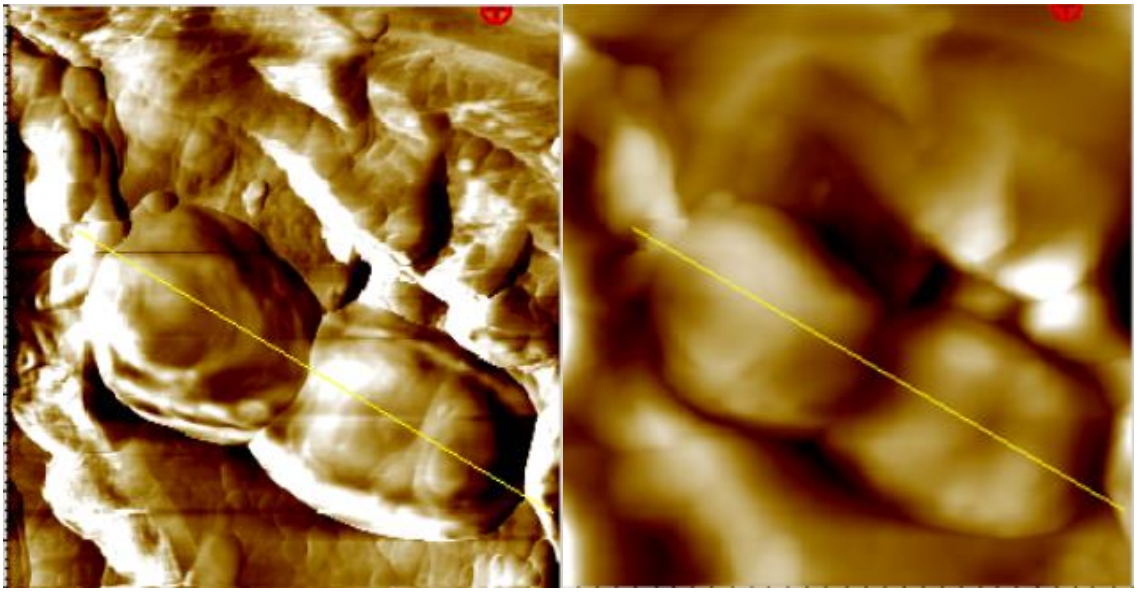

Figure 63. G968 cultured in media containing 0 mM HCO3 and 5 ppm uranium (scan size 6 x 6 µm2; z range 260 mV). Friction image on the left and topography on the right with an arbitrary cross section line (yellow) to determine the height of bacteria.

Figure 64. G968 cultured in media amended with 5 mM KHCO3 and 5 ppm uranium (scan size 5 x 5 µm2; z range 2.351 V). Deflection image on the left and topography on the right.

Roughness Analysis

Changes in the cells surface roughness in the bacterial strain when exposed to various concentration of uranium was analyzed using AFM roughness analysis. Exposure to uranium was conducted 24 hours prior to imaging. A qualitative approach shows an irregular surface, which is further complimented with a quantitative values showing that the roughness for this particular image is 1.39 E +08 nm. This number is much higher than previous experimentation and may need reevaluation. The relationship between roughness values and the various concentrations of bicarbonate and uranium are not fully understood and need further analysis.

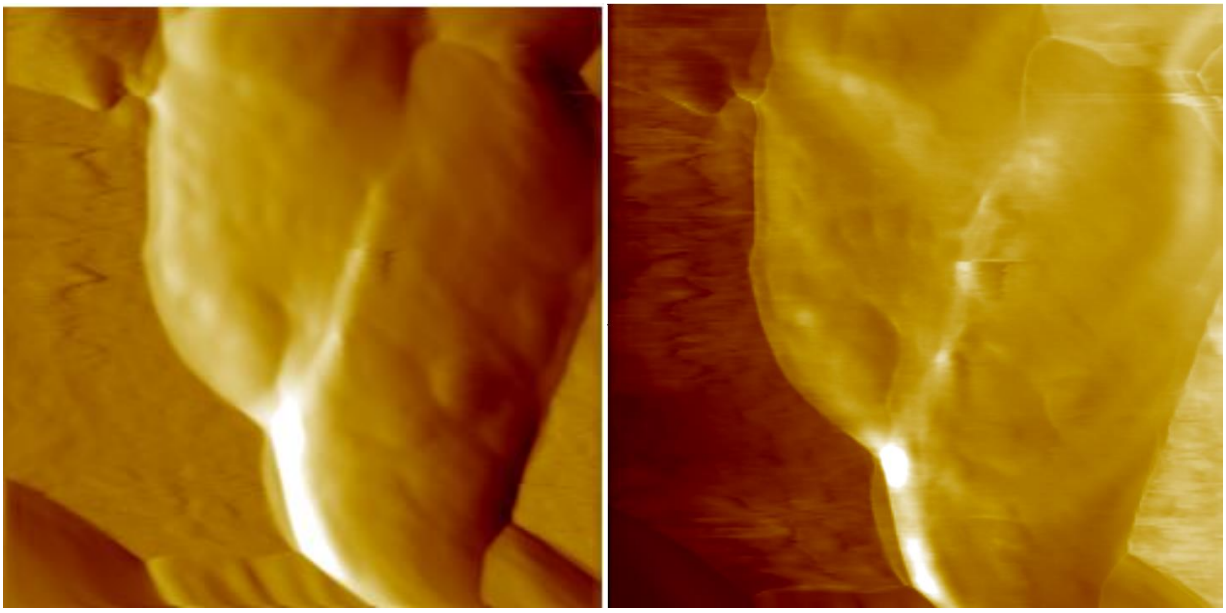

Figure 65. G968 cultured in media amended with 5 mM KHCO3 and 5 ppm uranium (scan size 3.2 x 3.2 µm2; z range 2.217 V). Deflection image on the left and friction on the right. Image illustrates two bacterial cells adhered to each other to further examine roughness.

Force Spectroscopy Analysis

It has been proposed that adhesion forces are sensitive to modifications in the surface; for example, physiological changes on the cellular membrane when exposed to uranium in bicarbonate amended media. So, it was necessary to perform a force spectroscopy analysis to gain a full comprehension of the interactions in the atomic level. The force between the tip and the sample is correlated through Hooke's Law which states that:

$$F = K * \alpha * V$$

Where k is equal to the cantilever's spring constant, V is the measured cantilever's deflections (in volts) and α is known as the deflection sensitivity which converts the units of the deflection from volts to nanometers. These variables are the main considerations when determining the force spectroscopy. The deflection is measured using a photodiode detector while the deflection sensitivity is a determined from force versus distance curve (Figure 66) by positioning the two cursors on the contract part. Both curves also ensure that the approaching and retracting of the cantilever tip is done correctly.

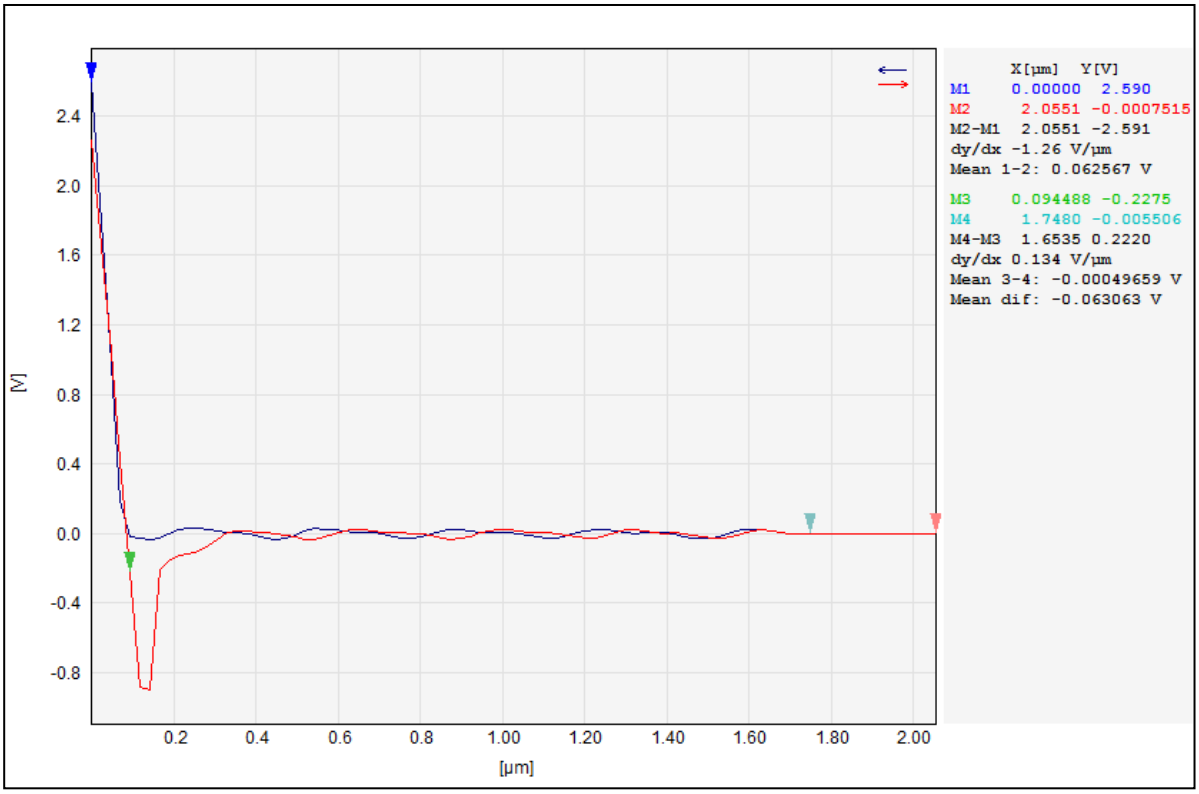

Figure 66. Force vs. distance curve of the image in Figure 65 The approach and retract portions of the force spectroscopy cycle appear in blue and red traces, respectively.

The adhesion force conducted on Figure 65, G968 cultured in media amended with 5 mM $KHCO_3$ and 5 ppm uranium**,** gave a mean adhesion force of 9.09± 4.00 nN compared to the previously observed 11.6±1.68 nN for the U-free sample. Without bicarbonate in the solution at U(VI) concentrations 5 ppm and 10 ppm, larger amounts of precipitate built up on the bacterial surface, resulting in smaller values for the adhesion forces 7.14±0.26 and 4.58±0.26, respectively (Table 10).

Table 10. Adhesion Forces for Different Concentrations of Bicarbonate and Uranium

	Adhesion (nN)	SD
Control	11.6*	1.68
0 mM HCO3, 5ppm U	7.14*	0.26
0 mM HCO3, 10ppm U	4.58*	0.26
5 mM HCO3, 5ppm U	9.09	4.0092
5 mM HCO3, 10ppm U	NA	NA

***Data was obtained from the 2010 Year End Report and recent publications (Katsenovich et al. 2012a, Katsenovich et al. 2012b)

When bicarbonate is present within the solution, the adhesion forces showed similar values to that of the control sample when no uranium is present. When bicarbonate and uranium are present in the solution, they complex, creating a negative uranyl bicarbonate species that is not adhered on the negatively charged bacterial surface. There is an inverse relationship between the adhesion forces and the concentration of uranium; as the concentration of uranium increases, the adhesion forces will decrease exponentially.

TASK 1.2 CONCLUSIONS

Two different kinds of bioreactors were used in the bioleaching experiments. Sterile 100 mL glass mixed reactors served as the major bioreactor for initial experimentation. These autunite-containing bioreactors were injected with bacterial cells after the autunite equilibrated with media solution. The second kind of bioreactors used were sterile culture ware with inserts where bacteria and autunite were kept separated. In the bioreactors containing synthetic autunite, the steady state maximum concentrations of U (VI) detected were 2.1, 8.8, 52.3, 88.4 fold higher than the abiotic control without the bicarbonate amendment. Furthermore, after bacteria inoculation, U (VI) concentrations measured in the reactors, increased 0.97± 0.02, 0.43± 0.42, 0.89± 227.08, and 0.78± 0.37 fold for 0 mM, 3 mM, 5 mM and 10 mM $KHCO_3$, respectively. It was also found that as the concentration of bicarbonate increases there is a diminishing trend on the effect of bacteria on autunite leaching; which is very similar to previous experimentation conducted with natural autunite. During the insert experimentation, the steady state maximum concentrations of U (VI) detected were 3.57, 1.34, 1.42, 2.27 fold higher than the abiotic control without the bicarbonate amendment. Furthermore, after bacteria inoculation, U (VI) concentrations measured in the reactors, increased 0.68 ± 1.48, 1.59 ±0.49, 1.02 ±0.98, 0.93 ±0.39 fold for 0 mM, 3 mM, 5 mM and 10 mM $KHCO_3$, respectively. So there is a slight increase in the dissolution of uranium as bicarbonate increases; however, this is not as pronounced when compared to the above bioleaching experiment with synthetic autunite. SEM and AFM analysis were used to investigate the qualitative and quantitative investigation on the microbial surface morphology when the cells are exposed to varying concentrations of calcium and bicarbonate. SEM imaging illustrated that precipitates among the cells were not uniform and that the cells looked healthier in bicarbonate bearing media. Furthermore, a clear relationship between the concentration of uranium and bicarbonate with roughness measurements was not found and further analysis may be needed. The force spectroscopy data demonstrated an inverse relationship between the concentration of uranium and adhesion forces; as the uranium concentration increased, the adhesion force would decrease. In addition, when bicarbonate is present within the solution, the adhesion forces showed similar values to that of the control sample when no uranium is present; which suggests a lower buildup of secondary precipitates on the bacterial surface.

ACKNOWLEDGEMENTS

Funding for this research was provided by U.S. DOE grant number DE-EM0000598. We would like to thank Dr. Patricia Sobecky and Dr. Robert J. Martinez from the Univ. of Alabama, Tuscaloosa, AL, for providing us with the *Arthrobacter* sp. strains and to acknowledge Dr. Yanqing Liu and Tom Beasley from the FIU AMERI facilities and FIU FCAEM for their assistance with the SEM/EDS analysis.

REFERENCES

Allard, T., Ildefonse, P, Beaucaire, C., Calas, G, 1999. Structural chemistry of uranium associated with Si, Al, Fe gels in a granitic uranium mine. Chemical Geology 158, 81-103.

Balkwill, D. L., Reeves, R. H., Drake, G. R., Reeves, J. Y., Crocker, F. H., Baldwin K, M., and D. R. Boone, 1997. Phylogenetic characterization of bacteria in the subsurface microbial culture collection," FEMS microbiology reviews, vol. 20, pp. 201-216.

Balkwill, D. L., Reeves, R. H., Drake, G. R., Reeves, J. Y., Crocker, F. H., Baldwin K, M., and D. R. Boone, 1997. Phylogenetic characterization of bacteria in the subsurface microbial culture collection," FEMS microbiology reviews, vol. 20, pp. 201-216.

Bernhard, G., Geipel, G., Reich, T., Brendler, V., Amayri, S., Nitsche, H., 2001. Uranyl(VI) carbonate complex formation: validation of the $Ca_2UO_2(CO_3)^3$(aq.) species. Radiochim. Acta 89, 511-518.

Bickmore, B.R., K.L. Nagy, J.S. Young, and J.W. Drexier. 2001. Nitrate-cancrinite precipitation on quartz sand in simulated Hanford tank solutions. Environ. Sci. Technol. 35(22):4481-4486. doi:10.1021/es0108234

Blum, A.E., and L.L. Stillings. 1995. Feldspar dissolution kinetics. p. 291-351. In A.F. White and S.L. Brantley (ed.) Reviews in mineralogy. Vol. 31. Chemical weathering rates of silicate minerals. Mineralogical Soc. of Am., Washington, DC.

Boylen, C.W., 1973. Survival of Arthrobacter crystallopoietes during prolonged periods of extreme desiccation. Journal of Bacteriology, vol. 113, pp. 33.

Brunauer, S., Emmett, P.H., and Teller, E. 1938. Adsorption of gases in multimolecular layers. Journal of the American Chemical Society, 60: 309-319

Busey R.H., and Mesmer R.E., 1977. Ionization equilibria of silicic acid and polysilicate formation in aqueous sodium chloride solutions to 300C. Inorg. Chem 16, 10, p.2444-2450.

Choppin, GR, Pathak, P, Punam, T, 1994. Polymerization and complexation behavior of silicic acid; a review. Main group metal chemistry, 31, 1-2, p.53-72.

Chou L and R Wollast. 1984. Study of the Weathering of Albite at Room Temperature and Pressure with a Fluidized Bed Reactor. Geochimica et Cosmochimica Acta 48, 2205-2217.

Crocker, F. H., Fredrickson, J. K., White, D. C., Ringelberg, D. B. and D. L. Balkwill, 2000. Phylogenetic and physiological diversity of Arthrobacter strains isolated from unconsolidated subsurface sediments, Microbiology, vol. 146, pp. 1295.

Dong, W. and S. C. Brooks. 2006. Determination of the formation constants of ternary complexes of uranyl and carbonate with alkaline earth metals ($Mg^{2+,}$ Ca^{2+}, Sr^{2+}, and Ba^{2+}) using anion exchange method. Environ. Sci. Technol. 40(15):4689-4695. doi: 10.1021/es0606327

Dove, PM and Nix, CJ, 1997. The influence of the alkaline earth cations, magnesium, calcium, and barium on the dissolution kinetics of quartz. Geochimica et Cosmochimica Acta, 6l, 16, pp. 3329-3340.

Felmy, AR., Cho, H., Rustad, JR.,and MJ. Mason, 2001. An aqueous thermodynamic model for polymerized silica species to high ionic strength, Journal of Solution Chemistry, 30, 6.

Fredrickson, J. K., Zachara, J. M., Balkwill, D. L., Kennedy, D., Li, S. W., Kostandarithes, H. M., Daly, M. J., Romine, M. F. and Brockman, F.J. , 2004. Geomicrobiology of high-level nuclear waste-contaminated vadose sediments at the Hanford Site, Washington State, Applied and Environmental Microbiology, vol. 70, pp. 4230.

Gallup, DL, 1997. Aluminum silicate scale formation and inhibition: scal characterization and laboratory experiments. Geothermics, 26, 4, pp.483-499.

García-Ruiz, JM., Melero-García,E., Hyde, ST., 2009. Morphogenesis of self-assembled nanocrystalline materials of barium carbonate and silica. Science, 323, p.362-365.

Gasteiger, H.A., Frederick, W.J., Streisel, R.C.,1992. Solubility of aluminosilicates in alkaline solutions and a thermodynamic equilibrium model. Ind. Eng. Chem. Res. 31, 1183-1190.

Grenthe, I., Fuger, J., Konings, R.J.M., Lemire, R.J., Muller, A.J., Nguyen-Trung, C., Wanner, H., 1992. Chemical Thermodynamics of Uranium. Elsevier, Amsterdam.

Guillaumont R., Fanghänel T., Fuger J., Grenthe I., Neck V., Palmer D.A., Rand M.H., 2003. Chemical Thermodynamics, OECD Nuclear Energy Agency vol. 5, Elsevier, 919 pp.

Hurd, DC, 1973. Interactions of biogenic opal, sediments and seawater in the central equatorial Pacific. Geochim.Cosmochim. Acta, 37, 2257-2282

Iler, R.K., 1979. The chemistry of silica: solubility, polymerization, colloid and surface properties, and biochemistry. John Wiley and Sons, p.886.

Kalmykov S.N., Choppin G. R., 2000. Mixed $Ca^{2+/}UO_2^{2+}/CO_3^{2-}$ complex formation at different ionic strengths, Radiochim. Acta, 88, 603.

Karberg, N.J., KS. Pretziger, J.S. King, A.L. Friend, and J.R. Wood, 2005, Soil carbon dioxide partial pressure and dissolved inorganic carbonate chemistry under elevated carbon dioxide and ozone, Oecologia, 142, p. 296-306.

Katsenovich, Y.P., Carvajal, D.A., Guduru, R., Lagos, L.E., 2012b. Assessment of the Resistance of Hanford Site *Arthrobacter* Isolates to Uranium (VI) Exposure. Geomicrobiology Journal. DOI:10.1080/01490451.2011.654376

Katsenovich, Y.P., Carvajal, D.A., Wellman, D.M., Lagos, L.E., 2012a. Enhanced U (VI) release from autunite mineral by aerobic *Arthrobacter* sp. In the presence of aqueous bicarbonate. Chemical Geology, V. 308-309, p. 1-9.

Kellermeier, M., Melero-Garcıa, E., Glaab, F., Klein, R., Drechsler, M., Rachel,R., Garcı´a-Ruiz, JM., Kunz, W, 2010. Stabilization of amorphous calcium carbonate in inorganic silica-rich environments. J. AM. CHEM. SOC., 132, p.17859-17866.

Kellermeier, M, 2011. Co-mineralization of alkaline-earth carbonates and silica, Ph. D. thesis.

Kellermeier, M., Gebauer, D., Melero-García, E., Klein, R., Drechsler, M., Talmon,Y., Kienle, L., Cölfen, H., Garcı´a-Ruiz, JM., Kunz, W, 2012. Colloidal Stabilization of Calcium Carbonate Prenucleation Clusters with Silica. Adv. Funct. Mater. 22, 4301–4311.

Kitano, Y., Okumura, M. and Idogaki, M., 1979. Behavior of dissolved silica in parent solution at the formation of calcium carbonate. Geochem. J., 13: 253-260.

Klein, R T. and LM. Walter, 1995. Interactions between dissolved silica and carbonate minerals: An experimental study at 25-50°C. Chemical Geology 125, p.29-43.

Langmuir Donald Aqueous environmental geochemistry, Prentice Hall, 1997.

Langmuir, D., 1978. Uranium solution–mineral equilibia at low temperatures with application to sedimentary ore deposits. Geochimica et Cosmochimica Acta 42, 547-569.

Mattus, AJ, Mattus, CH, Hunt, RD, 2002. Investigation into the control and kinetics of aluminosilicate formation on stainless steel surfaces at 100C. ORNL report ORNL/TM-2002/47

Qafoku NP, Ainsworth CC, Szecsody JE, Qafoku OS, 2003. Aluminum Effect on Dissolution and Precipitation under Hyperalkaline Conditions: I. Liquid Phase Transformations. J Environ Qual. 32, 6, pp.2354-63.

Qafoku, N.P., and J.P. Icenhower. 2008. Interactions of aqueous U(VI) with soil minerals in slightly alkaline natural systems. Rev. Environ. Sci. Biotechnol.7:355-380. doi:10.1007/s11157-008-9137-8

Qafoku, N.P., C.C. Ainsworth, J.E. Szecsody, and O.S. Qafoku. 2004. Transport controlled kinetics of dissolution and precipitation in the sediments under alkaline and saline conditions. Geochim. Cosmochim. Acta 68:2981–2995. doi:10.1016/j.gca.2003.12.017

Schlosser, F., Moskaleva, LV., Kremleva, A., Kruger, S and Rosch,N., 2010. Comparative density functional study of the complexes $[UO_2(CO_3)_3]_4^-$ and $[(UO_2)_3(CO_3)_6]_6^-$ in aqueous solution. *Dalton Trans.*, 39, 5705–5712. DOI: 10.1039/c002788j

Stefaniak E.A., Alsecz A., Frost R., Mathe Z., Sajo I.E., Torok S., Worobiec A., Van Grieken R., 2009. Combined SEM/EDX and Micro-Raman Spectroscopy Analysis of Uranium Minerals From A Former Uranium Mine. Journal of Hazardous Materials, 168: 416-423

Stumm Werner and Morgan James J Aquatic Chemistry: Chemical Equilibria and Rates in Natural Waters, New York : John Wiley & Sons, 1996.

Szecsody, J., M. Truex, L. Zhong, N. Qafoku, M. Williams, J. McKinley, et al. 2010a. Remediation of uranium in the Hanford vadose zone using ammonia gas: FY 2010 laboratory-scale experiments. PNNL-20004. Pac. Northw.Natl. Lab., Richland, WA.

Szecsody, JE, MJ Truex, L Zhong, MD Williams, CT Resch, JP McKinley, 2010b. Remediation of Uranium in the Hanford Vadose Zone Using Gas-Transported Reactants: Laboratory-Scale Experiments. PNNL-18879. Contract DE-AC05-76RL01830.

Szecsody, JE, Truex, MJ., Zhong, L., Johnson, T.CQafoku, ., N.P., Williams, MD., Greenwood, W.J., Wallin, EL., Bargar, J.D., Faurie, D.K., 2012. Geochemical and Geophysical Changes during Ammonia Gas Treatment of Vadose Zone Sediments for Uranium Remediation. Vadose Zone Journal, 11, 4. doi: 10.2136/vzj2011.0158

Um, W., Serne, R.J., Krupka, KM, 2007. Surface Complexation modeling of U(VI) sorption to Hanford sediment with varying geochemical conditions. Environ. Sci. Technol., 41, 3587-3592.

Van Waasbergen, L.G., Balkwill, D. L., Crocker, F. H., Bjornstad, B. N., and R. V. Miller, 2000. Genetic diversity among Arthrobacter species collected across a heterogeneous series of terrestrial deep-subsurface sediments as determined on the basis of 16S rRNA and recA gene sequences. Applied and environmental microbiology, vol. 66, pp. 3454.

Wellman DM, JG Catalano, JP Icenhower, and AP Gamerdinger. 2005. "Synthesis and Characterization of Sodium meta-Autunite, Na[UO2PO4] - 3H2O." Radiochimica Acta 93(7):393-399.

Wellman, DM, Icenhower, JP, Gamerdinger, A.P., Forrester, S.W., 2006. Effects of pH, temperature, and aqueous organic material on the dissolution kinetics of meta-autunite minerals, $(Na, Ca)_{2-1}[(UO_2)(PO_4)]_2 \cdot 3H_2O$. American Mineralogist, V. 91, p. 143-158.

Wellman, DM., Icenhower, JP., Gamerdinger, A.P., Forrester, S.W., 2006. Effects of pH, temperature, and aqueous organic material on the dissolution kinetics of meta-autunite minerals, $(Na, Ca)_{2-1}[(UO_2)(PO_4)]_2 \cdot 3H_2O$. American Mineralogist, V. 91, p. 143-158.

Zachara, J., C. Liu, C. Brown, S. Kelly, J. Christensen, J. McKinley, et al. 2007. A site-wide perspective on uranium geochemistry at the Hanford Site. PNNL- 17031. Pac. Northw. Natl. Lab., Richland, WA.

APPENDIX

The following reports are available at the DOE Research website for the Cooperative Agreement between the U.S. Department of Energy Office of Environmental Management and the Applied Research Center at Florida International University: http://doeresearch.fiu.edu

1. P2 Progress report on SEM_EDS_Final Draft:
   Katsenovich, Y. and R. Lapierre., *Progress Report on Morphological Changes of U-Bearing Precipitates over Time via SEM/EDS*, January 2013.
2. P2 AFM Deliverable:
   Katsenovich, Y., and P. Sepulveda, *Technical Progress Report on Atomic Force Microscopy Assessment on Bacteria Exposed to U(VI) In Bicarbonate-Bearing Solutions*, May 2013